Open Access

Advances in Environmental and Engineering Research

LIDSEN Publishing Inc.

Review

Greener Aspects of Nanoparticle Synthesis for Water Remediation: Challenges and Future Perspective

Jaspreet Kaur [1, 2], Khushveer Kaur [1], Khushwinder Kaur [1], Avtar S. Matharu [3, *], Surinder K. Mehta [1, *]

1. Department of Chemistry and Centre for Advanced Studies in Chemistry, Panjab University, 160014, Chandigarh, India; E-Mails: jas.sandhu3@gmail.com; kvbrar97@gmail.com; makkarkhushi@gmail.com; skmehta@pu.ac.in
2. School of Basic Sciences, Indian Institute of Information Technology (IIIT) Una, 177209, Himachal Pradesh, India
3. Green Chemistry Centre of Excellence, Department of Chemistry, University of York, YO10 5DD, England; E-Mail: avtar.matharu@york.ac.uk

* **Correspondences:** Avtar S. Matharu and Surinder K. Mehta; E-Mails: avtar.matharu@york.ac.uk; skmehta@pu.ac.in

Academic Editors: Gabriella Marfe and Stefania Perna

Special Issue: Waste Management and Human Health Impact

Adv Environ Eng Res
2023, volume 4, issue 2
doi:10.21926/aeer.2302027

Received: December 14, 2022
Accepted: March 31, 2023
Published: April 14, 2023

Abstract

Continued industrialization, urbanization and ecological destruction have caused significant environmental problems, particularly increased water pollution. Introducing harmful organic and inorganic effluents into watercourses has limited the supply and accessibility of safe and affordable drinking water. There is an urgent need to find green and sustainable abatement solutions for water remediation, many based on nanoparticles. The primary objective of this review is to explore and have a comprehensive discussion on the present trends, challenges and prospects for the green synthesis of nanoparticles for wastewater remediation. The connection between green chemistry and nanoparticles synthesis is articulated with many examples exploring the use of renewable or biobased resources. Energy-efficient processes (microwaves, ultrasound and laser ablation) and the use of alternative solvents (supercritical

carbon dioxide, ionic liquids and biobased solvents) are explored. The review aims to make the readers discern the mechanistic insights towards the working of various green processes. Conclusively, the adoption of green nanotechnology has the potential to veritably addresses the global water shortage issue under the domain of environmental sustainability.

Keywords
Nanoparticles; green chemistry; photocatalysis; water remediation

1. Introduction

Water has undeniably preceded as being the most vital natural resource whose accessibility is crucial for the existence of life. Ironically, human activities (anthropogenic) have polluted watercourses to such an extent that access to safe and clean drinking water has become a grand global challenge of this century [1]. According to a report by WaterAid (2018), just 10 waterless countries account for 60% of the world's population without access to clean water. It includes India at the first position with 19.33% followed by Ethiopia (7.17%), Nigeria (7.05%) and China (6.82%) [https://www.wateraid.org/The%20water%20gap-The%20state%20of%20the%20World%E2%80%99s%20Water]. Deteriorating water quality jeopardizes the state of the environment and human health. It induces chronic ailments such as gastroenteritis, cholera, amoebiasis, typhoid, giardiasis, hepatitis, fluorosis, dysentery, diarrhea, arsenicosis, jaundice, tuberculosis, etc. [2] Approximately 0.8 million people die each year from diarrhea alone and globally, it is projected that 785 million people will have a deficit of clean drinking water. According to the World Health Organization (WHO), 0.485 million diarrhoeal deaths occur yearly from drinking contaminated water By 2025, one-half of world's population will be live in water-stressed areas [3].

Besides diarrhea, several skin conditions, malnutrition, organ failure and carcinogenic effects are also linked to water contamination [4]. Therefore, Water pollution affects disease heterogeneity and clarifies the value of safe drinking water, which is crucial for achieving sustainable development goals. Regrettably, despite several genres of literature concentrate on water pollution, comprehensive analyses of the methods for mitigating water pollution are still lacking. This study focuses on the removal of water contamination, both theoretically and mechanistically, without compromising environmental concerns.

Water contaminants can be broadly categorized [5] as inorganic, organic, biological, and radiological (Figure 1), which continue to increase with time. There is a broad range of abatement technologies employed in wastewater treatment plants, namely: i. physical methods such as adsorption, nanofiltration, sedimentation, reverse osmosis and electro dialysis; ii. chemical methods like coagulation/flocculation, solvent extraction, precipitation, conventional oxidation, ion exchange, and; iii. biological methods such as aerobic and anaerobic microbial degradation, activated sludge, bioaugmentation, and the use of pure enzymes [6]. However, these processes do not offer efficient and complete removal of contaminants. It requires using non-reusable and harsh chemicals such as flocculants, has very high energy consumption, increased sludge volume generation, and has greater maintenance and operation costs [7]. Therefore, developing and

incorporating new technologies that will provide high efficiency along with multiple functionalities and generate minimum environmental hazards is pertinent.

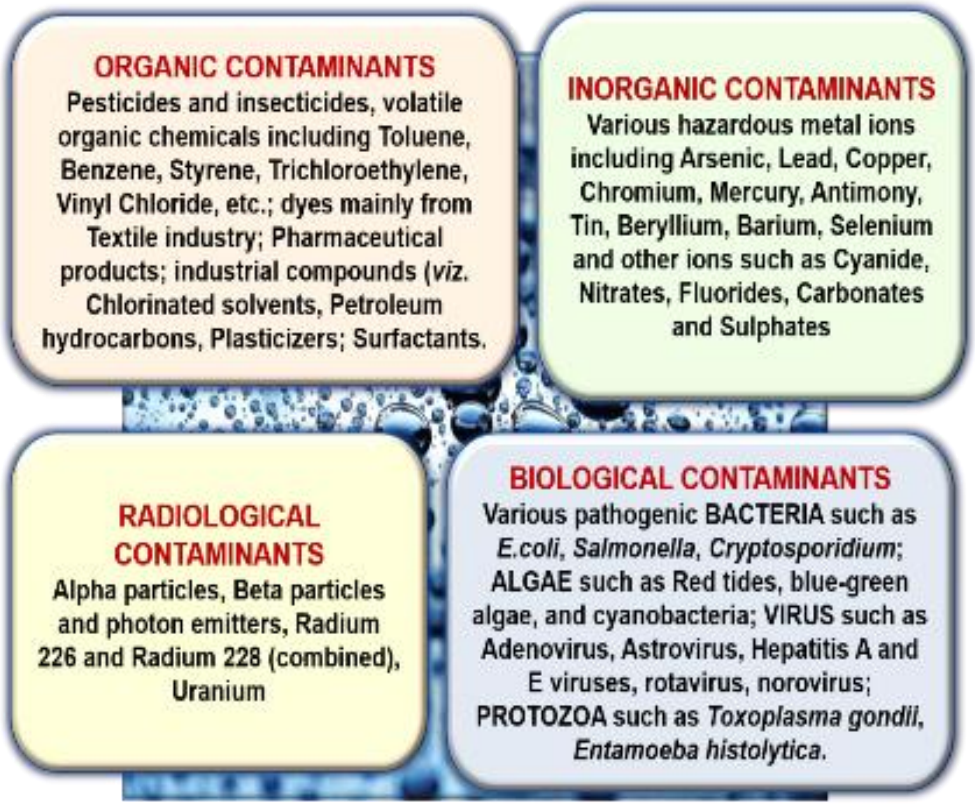

Figure 1 List of various contaminants present in Water.

Over the years, nanotechnology and its ability to provide diverse functionalities/properties to materials have led to its broad applicability in catalysis, sensing, electronics, photonics and medicine [8]. However, within nanoscience and nanotechnology, the design and synthesis (or manufacture) of nanoscale materials with tailored properties is still a major and recurring obstacle [9]. Assessment of the design of materials, processes and applications that mitigate hazards and waste will be vital as nanoscience findings move to commercialized nanotechnology-based goods [6].

Commonly, two distinct approaches *i.e.,* top-down and bottom-up are reported for the fabrication of nanomaterials. The top-down approach uses, for example, lithography [10], ball milling [11], etching [12] and sputtering [13]. While, the bottom-up method typically employs processes such as chemical vapor deposition (CVD) [14], sol-gel methodology [15], spray pyrolysis [16] and laser pyrolysis [17]. The morphological and textural properties of NPs, such as shape and size, maybe attuned by varying chemical composition and reaction parameters (e.g., temperature, solvent and pH). Thus, the judicious synthesis of NPs through controlled reduction, growth and stabilization (Figure 2) using green processes for water remediation provides a double environmental benefit [18, 19].

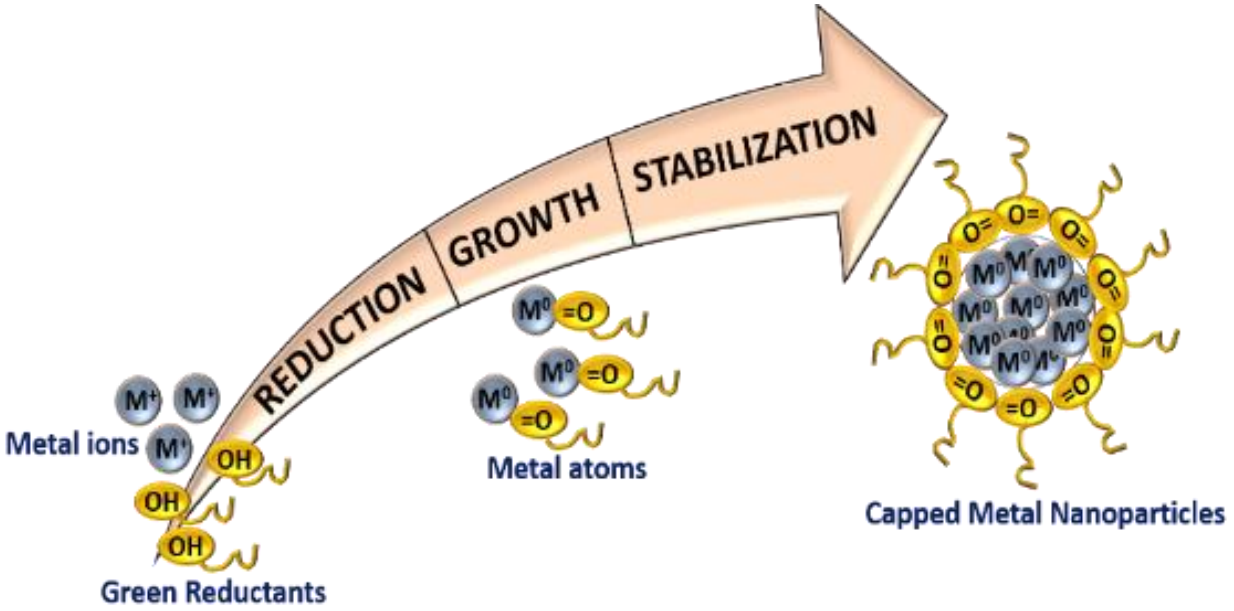

Figure 2 Schematic representation of the synthesis of NPs. Adapted from Ref [18].

This review highlights the various mechanisms utilized by NPs for the removal of effluents. It is followed by the requirement and incorporation of green chemistry in the fabrication of these NPs. Various synthesis factors such as processes, solvents and utilization of renewable resources are discussed in detail. The review also discuss key considerations of wastewater treatment, management, existing knowledge gaps and future directives.

2. Common Approaches for Using Nanoparticles in Removal of Effluents

The development of numerous nanotechnology-enabled tools and procedures, particularly in water purification, has opened up a new possible option to treat wastewater more efficiently and cost-effectively in recent years. The following are some promising water treatment techniques/tools offered by nanotechnology.

2.1 Photocatalysis/Degradation of Organic Pollutants

Photocatalysis is a viable water purification process that use a light-active nanostructured catalyst medium to break down various contaminants in water. Photocatalysis is a 'change in the rate of a chemical reaction or its initiation in the presence of a substance, *i.e.,* the photocatalyst, that absorbs the light. It is involved in the chemical transformation of the reaction partners under the action of ultraviolet, visible, or infrared radiation [20]. A typical photocatalysis system consists of a semiconductor material that acts as a catalyst medium and forms an electron-hole (e-h) pair when exposed to light with a wavelength greater than its bandgap energy [21]. Superoxides (O_2^-), hydroxyl ions (OH^-), and other highly reactive oxidizing and reducing radicals are produced in water by the photo-generated e-h pair (Figure 3). Subsequently, these radicals destroy any organic/inorganic pollutant molecules present in the contaminated water. When photo-generated electrons or holes are transmitted directly from the catalyst surface to the contaminant molecules, water pollutants can also be degraded [7].

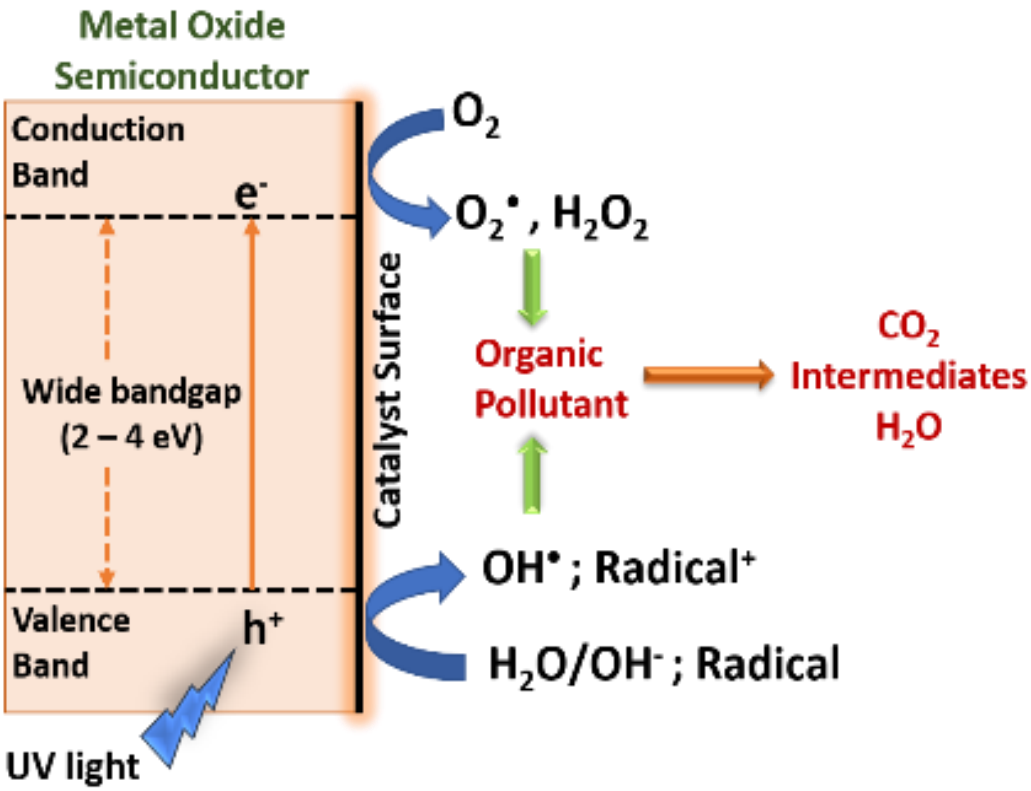

Figure 3 Schematic representation of photocatalysis process on nanostructured metal oxide photocatalyst surface. Adapted from Ref [21].

Photocatalysis is a phenomenon that occurs on the surface of a material. Its general mechanism is a complex process involving five basic steps [22]: (i) diffusion of reactants to the catalyst surface; (ii) adsorption of the reactants on the surface of the catalyst; (iii) reaction at the surface of the catalyst; (iv) desorption of the products from the surface of the products from the surface of the catalyst, and; (v) diffusion of the products from the surface of the catalyst.

The following reactions outline [23] a general course for the breakdown of organic contaminants by nano photocatalysts:

$$\boldsymbol{Catalyst} \xrightarrow{\boldsymbol{light}} \boldsymbol{h_{VB}^{+}} + \boldsymbol{e_{CB}^{-}}\ (e-h\ pair\ generation)$$

$$\boldsymbol{OP} \rightarrow \boldsymbol{OA^{-}}(\boldsymbol{aq}) + \boldsymbol{OC^{+}}(\mathbf{aq})\ (aqueous\ dissociation\ of\ the\ pollutant)$$

$$\boldsymbol{H_2O} + \boldsymbol{h_{VB}^{+}} \rightarrow \boldsymbol{OH^{\circ}} + \boldsymbol{H^{+}}(\boldsymbol{aq})\ (photo-splitting\ of\ water)$$

$$\boldsymbol{O_2} + \boldsymbol{e_{CB}^{-}} \rightarrow \boldsymbol{O_2^{-}}\ (electrophilic\ adsorption\ od\ dissolved\ O2)$$

$$\boldsymbol{H^{+}} + \boldsymbol{O_2^{-}} \rightarrow \boldsymbol{HO_2^{\circ}}\ (protonation\ of\ superoxide\ anion)$$

$$\boldsymbol{OA^{-}} + \boldsymbol{h_{VB}^{+}} \rightarrow \boldsymbol{OA^{\circ}}$$

$$\boldsymbol{OH^{-}} + \boldsymbol{h_{VB}^{+}} \rightarrow \boldsymbol{OH^{\circ}}$$

$$\boldsymbol{OA^{\circ}} + \boldsymbol{OH^{\circ}/HO_2^{\circ}} \rightarrow \boldsymbol{CO_2} + \boldsymbol{Intermediates} + \boldsymbol{mineral\ acids} + \boldsymbol{neutral\ sites}$$

$$\boldsymbol{OC^{+} + OH^{-} \rightarrow Hydroxylated\ products}$$

$$\boldsymbol{h_{VB}^{+} + e_{CB}^{-} \rightarrow catalyst + heat}\ (e - h\ pair\ recombination)$$

2.2 Adsorption of Hazardous Substances

Cationic and anionic dyes are two types of organic pollutants that are commonly utilized in different industrial applications. Organic dyes are extremely important in the paper, textile, plastic, leather, culinary, printing, and pharmaceutical industries since they are in high demand [24]. Around 60% of dyes are consumed in the textile industry during the coloring process for various materials. Nearly 15% of dye wastage, leads to significant pollution due to their low degradation [25]. These manufacturing operations' pollutants are the most significant contributors to environmental contamination. They generate undesirable turbidity in the water, which lowers sunlight penetration and leads to photochemical synthesis resistance. This leads to biomagnification and adversely affects the marine biota [26].

As a result, one of the most difficult tasks in environmental chemistry is controlling effluent-containing colours. The need for clean and safe drinking water is growing by the day. Because of this, applying metal and metal oxide semiconductor NPs for oxidizing harmful contaminants has gained much attention in recent material research domains.

2.3 Sensing/Removal of Heavy Metal Ions

Heavy metals (such as Ni, Cu, Fe, Cr, Zn, Co, Cd, Pb, Cr, Hg, and Mn) are commonly found pollutants present in air, soil, and water. Mining waste, car emissions, natural gas, paper, plastic, coal, and dye industries contaminate heavy metal. Even at trace ppm levels, several metals (Pb, Cu, Cd, and Hg ions) have increased toxicity potential [27]. As a result, identifying hazardous metals in the biological and aquatic environment has become critical for effective remediation.

In multi-element analysis, traditional techniques based on instrumental systems typically provide great sensitivity. However, the experimental setups required for such analyses are extremely costly, time-consuming, skill-dependent, non-scalable and non-portable [28]. Metallic NPs have been favored for detecting heavy metal ions in polluted water systems due to their variable size and distance-dependent optical characteristics. Simple, cost-effective, and high sensitivity at sub-ppm levels are some benefits of using metal NPs as colorimetric sensors for heavy metal ions in environmental systems/samples [29].

2.4 Anti-Microbial Activity

Various photocatalytic materials employ different interactions (*e.g.*, Van der Waals forces, electrostatic attractions, receptor-ligand and hydrophobic interactions) to come close to the bacterial cell membrane and alter the cell metabolism [30]. By causing oxidative stressors, membrane permeability imbalances. It causes a change in cell shape, protein inhibition, metabolic alterations, and DNA damage, promoting bacterial cell death. Figure 4 shows how photocatalytic NPs generate diverse reactive radicals when they receive photon energy larger than the band gap energy. These radicals penetrate the cells, affecting cell metabolism and gene expression.

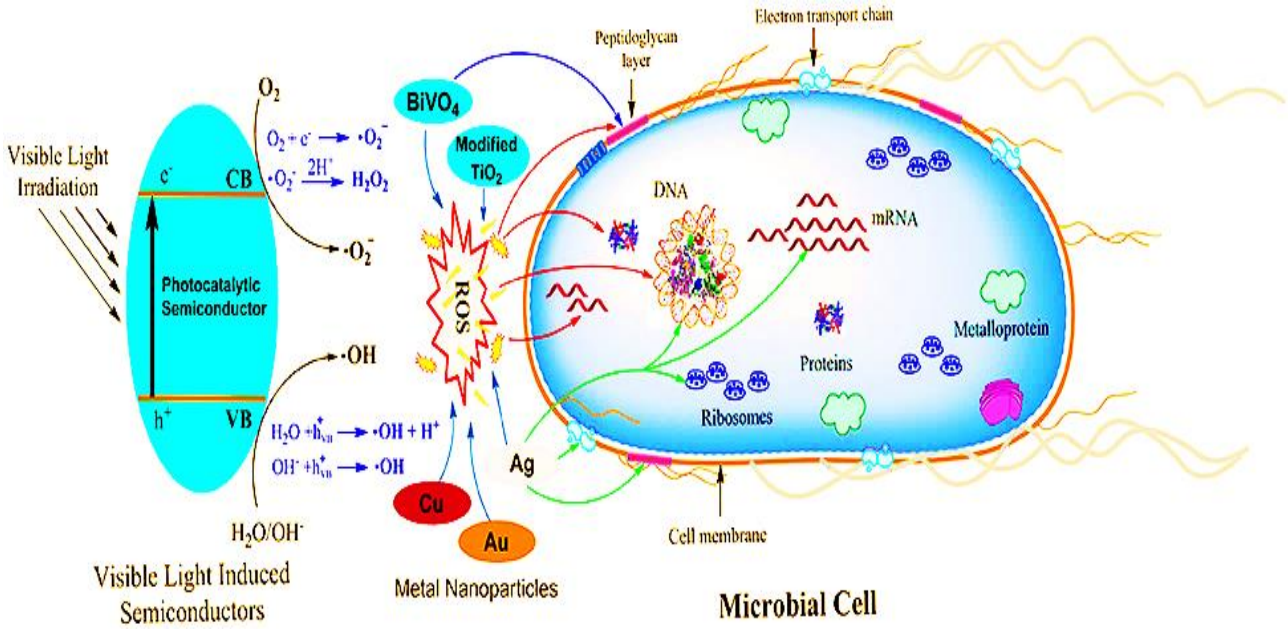

Figure 4 The possible mechanisms of antimicrobial activities exhibited by different photocatalytic semiconductors. Reproduced with permission from Ref [31].

The NP can cause stress *via* various cell routes, ultimately leads to cell death. The following sections will explore the common mechanisms of microbe killing with examples [31].

(i) Excess ROS produced due to the redox process encourages the oxidation process in the cells. This causes lipid membrane peroxidation and invades proteins and subsequently damages the DNA.

(ii) The leaching of metal ions from metal oxide semiconductors gets on the cell membrane, passes through and interacts with proteins and nucleic acid via –SH, –NH, and –COOH groups leading to cell damage.

(iii) Without inducing oxidative stress, the non-oxidative mechanism inactivates bacteria by lowering important cellular metabolisms such as protein, amino acid, nucleotide, energy, and glucose metabolism.

The first of these three putative pathways of NP antibacterial activity has gained the most interest from researchers [32]. In general, O_2 molecules are reduced by NPs generating several forms of ROS (·, ·OH, H_2O_2) which causes stress reactions in cells. It damages the peptidoglycan layer, electron transport chain system, genomic materials (DNA, RNA), proteins, and ribosomes, among other cell components. It affects the integrity of the cell membrane and disrupts it to cause the release of cytoplasmic content. Furthermore, ROS inhibits the activities of several proteins required for the cell's physiological processes [33].

3. Link between Green Chemistry and Nanoparticle Synthesis

Herein, this review explores the applicability of green chemistry principles [34, 35] to synthesizing nanomaterials concerning wastewater remediation. Several exemplary studies have already been reported on synthesizing and assembling functionalized nanoparticles (NPs). The aim is not to provide a detailed coverage of these subjects but to concentrate on aspects most important to green chemistry.

Green chemistry is "the utilization of principles that reduces or eliminates the use or generation of hazardous substances in the design, manufacture, and application of chemical products" [36]. These principles known as the Twelve Principles [34, 35] have now been implemented in the design of a broad range of chemical technologies and systems aimed at mitigating chemical health and environmental hazards, reducing waste and preventing pollution (Figure 5) [37]. Implementing these principles has minimized the use of dangerous reagents and solvents. It has improved the renewability of precursors of chemical processes and energy efficiency, and the design of end-of-life products so they may degrade and/or not pollute [38]. The development and processing of inherently safer nanomaterials and nanostructured devices will be facilitated by applying these concepts to nanoscience [39].

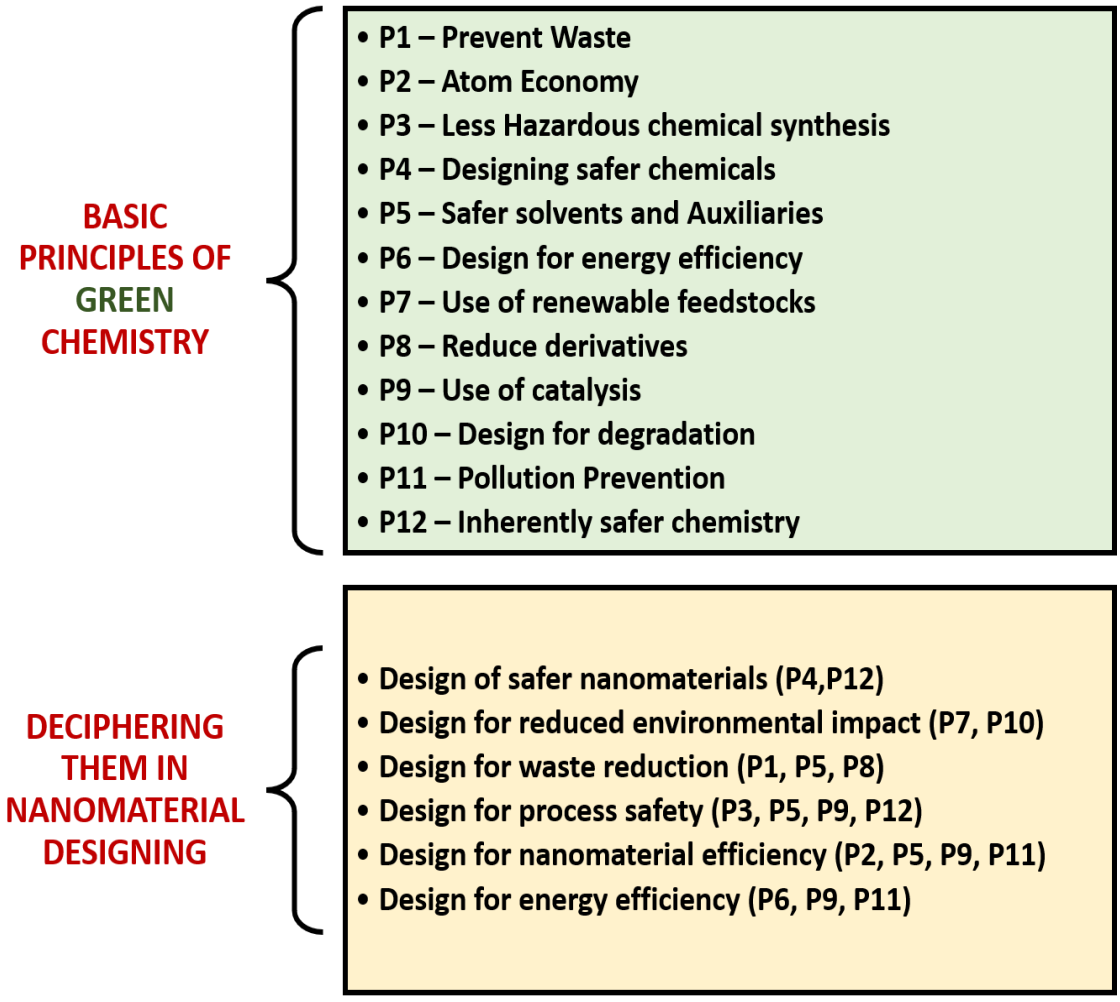

Figure 5 Connection between design of nanomaterials and the 12 Principles of Green Chemistry.

As exemplified in Figure 5, often a combination of principles is used in the design and fabrication of nanomaterials. Renewable resources are plentiful and varied, and detailed examples are given later. Also, energy-efficient processes (microwaves, ultrasound, laser ablation) and green or alternative solvents (supercritical fluids, ionic liquids, and based solvents) are gaining traction.

4. Efficient Energy Processes

Regarding energy consumption, reaction time and consistency of NPs, each synthesis route should be optimized. Researchers have been working on new energy transfer techniques such as microwave, ultrasound and laser ablation in recent years. It facilitates simultaneously minimizing reaction time and energy requirements and increasing regulation of the size and shape of NPs [40].

4.1 Microwaves

The frequency and wavelength of microwave radiation span from 0.3 to 300 GHz and 1 mm to 1 m, respectively, corresponding to the electromagnetic range between infrared and radio frequency. Since these microwaves have less energy, they do not induce distortion or break in the chemical bond with subsequently no effect on the framework of the chemical molecule [41]. Microwave-assisted nanomaterial synthesis route is a cost-effective wet-chemical process that offers several advantages such as homogeneous volumetric heating, fast reaction rates, even morphology control and energy efficiency. The creation of evenly distributed nanomaterials is attributed to the uniform heating of the reactants, which eliminates the possibility of thermal gradients and provides uniform nucleation and growth conditions [42].

Li *et al*. illustrated the comparison between conventional microwave heating, who [43] successfully prepared orthorhombic crystal of $WO_3 \cdot 0.33H_2O$ under different reaction and solvent conditions. It was found that the microwave assisted route helped in the oriented growth of crystals (*e.g.,* urchins and snowflakes) which was absent in conventional methods. This directional growth further exposed the highly acidic crystal faces, promoting better photocatalytic activity with Methylene blue (MB) dye chosen as a reference model. Microwave-based directional crystal growth along (100) direction helped in exposing the acidic (010) faces which facilitated more catalytic activity (Figure 6). The microwave-assisted NP crystal showed 100% dye degradation in 180 min which is significantly potent in contrast to 50% of dye degradation in 300 min for other crystals.

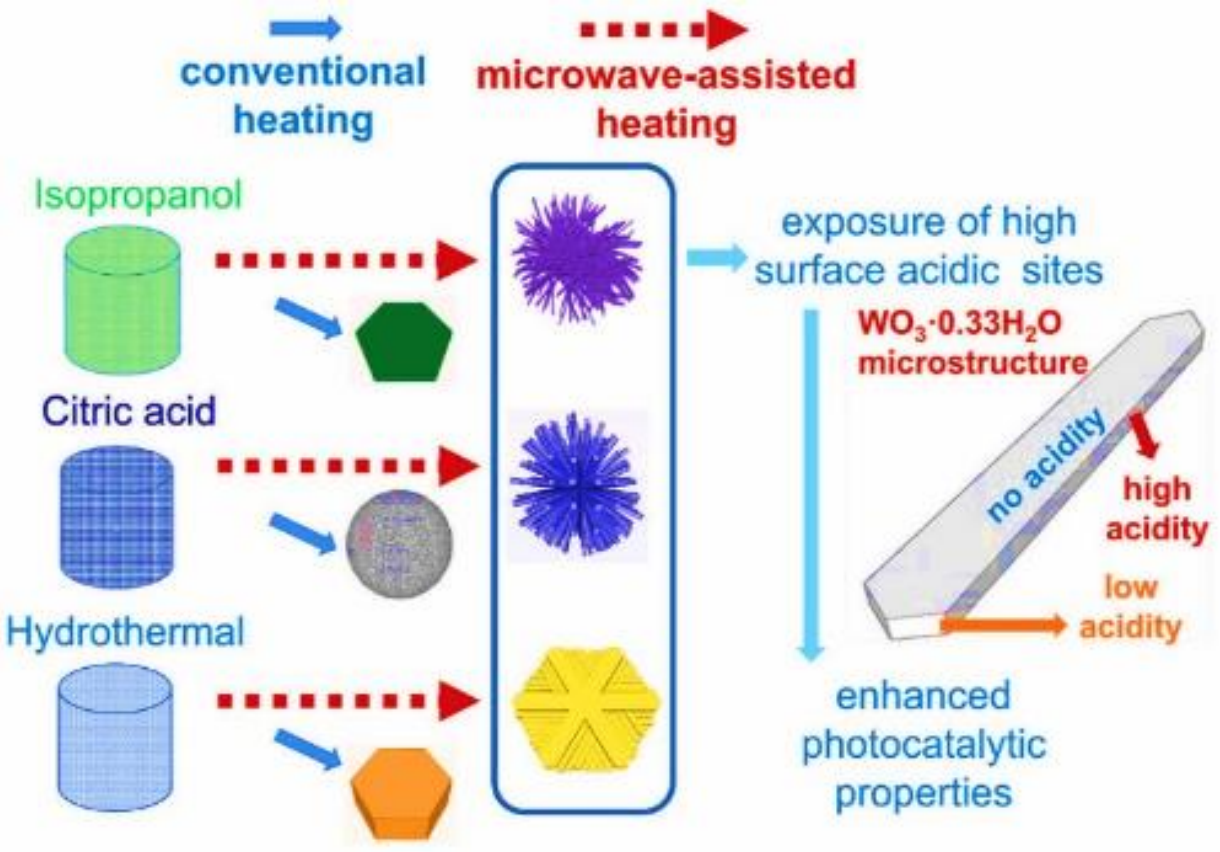

Figure 6 Illustrates the morphological changes observed in $WO_3 \cdot 0.33H_2O$ nano/microstructures synthesized under different conditions and their photocatalytic active sites. Reproduced with permission from Ref [43].

Sun *et al*. [44] used microwave irradiation to synthesise fluorescent C NPs using ammonium citrate dibasic, serving as a C and N source. The uniform heating afforded by microwave irradiation resulted in uniform growth of NPs further carbonised into nano-crystalline form. The synthesised NPs were well dispersed with a 5.5 ± 1.5 nm diameter. Also, the NPs resulted in the selective detection of PA with a quenching constant of 3.18×10^4 M^{-1}. The high selectivity and quenching efficiency are due to the synergistic effect of electrostatic interaction, photo-induced electron transfer and fluorescence energy transfer between NPs and PA molecules. Manteghain *et al.* [45] assembled MoO_3 NPs under microwave irradiation using ethylene glycol as the solvent and heating medium. The homogeneous and strong heating resulted in spherical NPs with a 50 nm average size. SEM analysis showed that the particles prepared under microwave irradiation were nano-sized with strong colloidal solution dispersion and stability, while particles synthesized by traditional heating were unstable with large diameters.

The impact of microwaves on the structural morphology of NPs was recently explored by Kaur *et al.* [46]. MoO_3 NPs tend to form rod like structures under normal temperature and pressure conditions. However, any distortion of the morphology could only be obtained under harsh reaction conditions. Kaur *et al.* demonstrated the use of microwaves for homogenous heating of precursor solution and incorporating surfactant molecules. The activation of reactant molecules under microwave allowed the reaction to complete under 10 mins at 100°C and prevented the directional

growth of NPs. This facilitated the formation of spherical-shaped NPs with a size of nearly 10 nm (Figure 7).

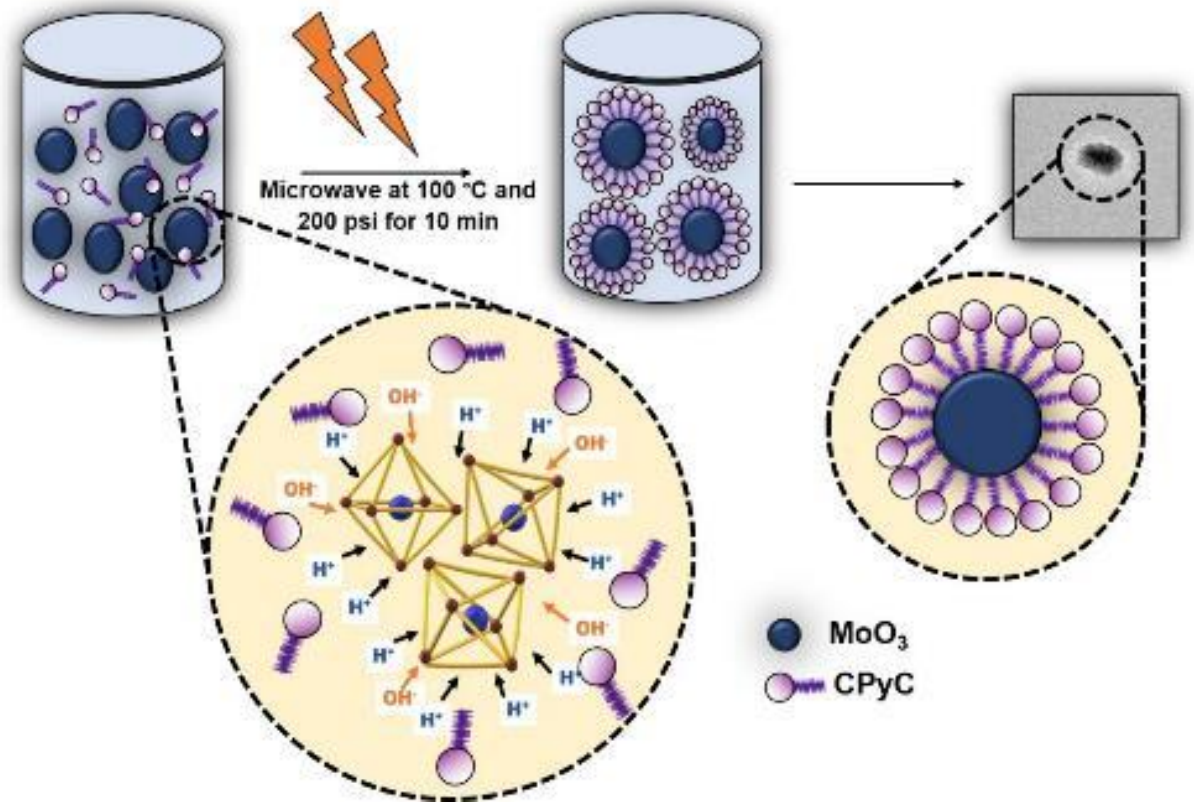

Figure 7 Schematic representation of the formation of spherical-shaped MoO_3 NPs using microwaves. Reproduced with permission from Ref [46].

Hence, microwave synthesis has been used in nanoparticle production because it combines the advantages of speed and homogenous heating of the precursor materials. Microwave irradiation has a penetrating feature that allows for uniform heating of the reaction fluid. Compared to other traditional procedures, synthesis by microwave irradiation has the benefit of a rapid response time. It is attributed to the combined forces generated by the MW's electric and magnetic components which undergo vibration, producing friction and generation of heat.

4.2 Ultrasound and Sonochemistry

Sonochemistry is derived from the severe transitory waves caused by ultrasound, which leads to the formation of hot spots with temperatures reaching nearly 5000 K, pressures surpassing 1000 ATMs, along with heating and cooling speeds exceeding 1010 K/s. The wavelength of ultrasonic waves ranges from 10-100 mm which exceeds the molecular size scale [47]. Hence the synthetic reaction is caused by the physical process of acoustic cavitation produced due to ultrasound energy. It involves the production, development, and collapse of bubbles creating active sites for reaction. Hence these ultrasounds promote chemical reactions and have been used for NPs fabrication without high bulk temperatures, high pressures, or long reaction times. Several phenomena [48] like acoustic cavitation (the formation, growth, and implosive collapse of bubbles) are responsible

for the production and modification of NPs. As shown in Figure 8, acoustic cavitation facilitates the formation of hot spots for the formation of Au FCC nanostructures.

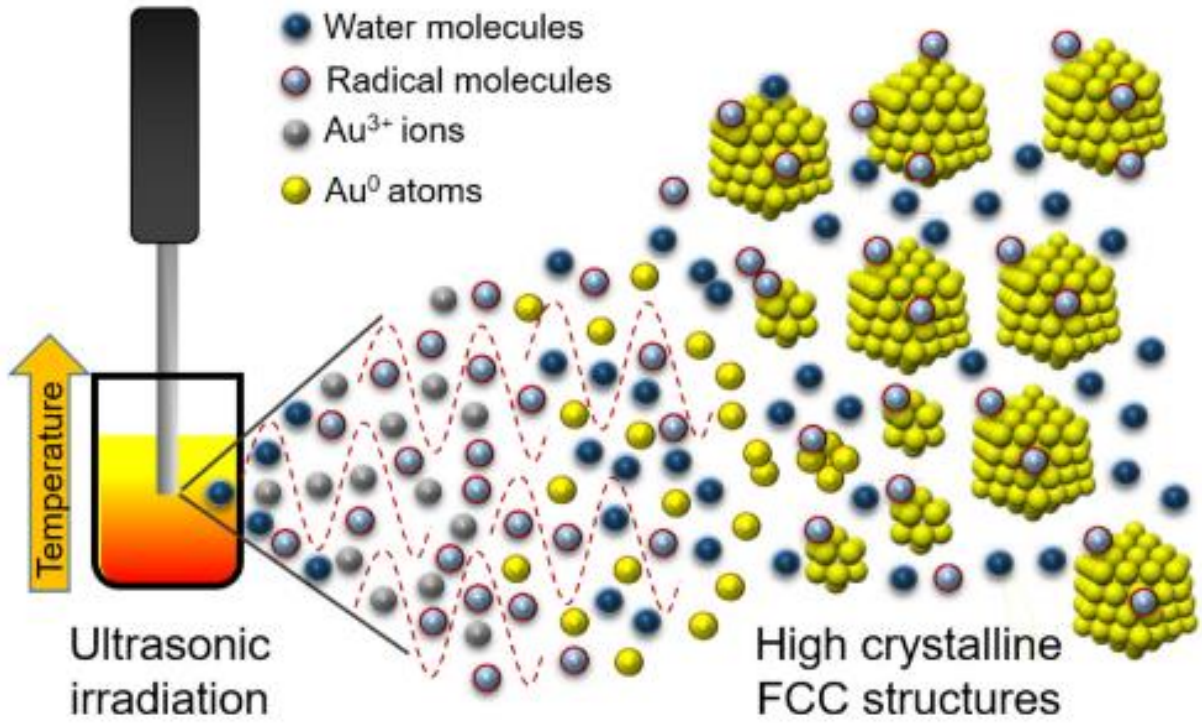

Figure 8 Working mechanism of Sonochemical energy via bubble formation leading to the formation of Au nanostructures. Reproduced with permission from Ref [47].

Green synthesis of 3D hexagonal-like zero-valent Cu NPs was documented by Kamali *et al.* [49] *via* the oncolysis of copper (II) acetate in ethylene glycol/ethanol (1:1). The low vapor pressure and extremely high temperature in the bubbles of solvent created due to acoustic cavitation led to the decomposition of the precursor and formation of NPs. The resultant high purity (>99%) zero-valent Cu nanostructured materials (99 percent) showed excellent ability to remove nitrates (90% removal in 30 mins) from contaminated water.

Yasuda *et al.* [50] used ultrasound irradiation to create ultrafine bubbles (UFBs) within an aqueous solution of $HAuCl_4$ aqueous solutions to obtain size-controlled Au NPs. The addition of air-UFBs greatly lowered the diameter of the spherical Au NPs due to the air-UFB's accelerated sonochemical reduction of Au(III) ions. Since Au nanospheres were electrostatically adsorbed on those UFBs with a long water life, of more than two months, the substance was homogeneously dispersed in an aqueous solution. In addition, the NP's diameter could be further decreased by pulsed ultrasound supplied with the same time-averaged power as continuous irradiation.

Furthermore, chitosan/activated carbon/iron NPs bio-composite was synthesized by Sharififard *et al*. [51] *via* the sonochemical method. The ultrasonic approach provided adequate temperature and pressure conditions, resulting in increased mass transfer rate and better uniformity in particles size with decreased reaction time. The novel composite had excellent adsorption potential for removing cadmium from polluted water (344 mg of Cd removed in approximately 20 mins).

Hence, the Sonochemical synthesis of NPs has a high potential in synthetic chemistry. This approach is reasonably powerful yet simple for manufacturing nanomaterials. Just tuning the

ultrasonic process parameters can form diverse NPs with many characteristics. It provides an unconventional path to existing materials without needing high bulk temperatures, pressures, or extended reaction periods.

4.3 Laser Ablation

As the laser beam in the atmospheric medium (gas or liquid) is centered on the surface of a solid target material, the temperature of the irradiated spot increases exponentially, vaporizing the target material. Collisions between the evaporated species (atoms and clusters) and the intervening molecules contribute to electron state excitation combined with light emission and generation of electrons and ions, forming a laser-induced plasma generation. The advantages of this method include- does not require a high vacuum, gives high yields, and avoids using chemicals.

Altuwirqi *et al*. [52] fabricated Cu and Cu_xO spherical NPs via a green method using Pulsed Laser Ablation in Liquid (PLAL) technology from spinach leaf extract. The ablation experiment was performed using a pulsed Q-Switched Nd: YAG laser with a wavelength of 532 nm, laser energy of 200 mJ/pulse having a repetition rate of 10 Hz, and a pulse width of 6 ns. The beam was further reflected downward perpendicular to the sample using a 90° prism. A 50 mm focal length lens focused the laser on the target containing Cu powder mixed with spinach extract. The laser ablation method enhanced the nanoparticles'dispersion, purity and stability and allowed size and shape-controlled synthesis by changing the irradiation time. The average size of the NPs obtained was 5 nm, which have huge potential to act as sensors.A comparative synthetic analysis of CuO-ZnO nanocomposite using the laser ablation method versus the anodization method was performed by Rashid *et al.* [53]. It was reported that homogeneous NPs with smaller diameters (74 nm) were prepared using laser energy without any aggregation. However, the nanoparticles formed by the other method were aggregated and had greater diameters. Also, the laser ablation method was energy efficient as less time was required. The authors aimed to solve the water pollution problem in the Diyala River (Iraq) due to different contaminants. It was found that laser ablation composite needs less than 60 mins to treat broad-spectrum water pollutants. In contrast the anodization composite water sample is still polluted even after 90 minutes observed by changes in water sample absorbance.

In a vortex fluidic system (VFD), Cu_2O NPs were selectively prepared in high yields under continuous flow by irradiating a Cu rod with a pulsed laser operating at 1064 nm and 600 mJ [54]. The plasma plume was formed inside a glass tube interacting with the enclosed air inside the microfluidic chamber. This led to a large mass transfer of material into a flexible thin film of water (Figure 9). Obtained Cu_2O NPs were of 14 nm and under subsequent heat treatment formed CuO NPs of 11 nm at 50°C in 10 hrs.

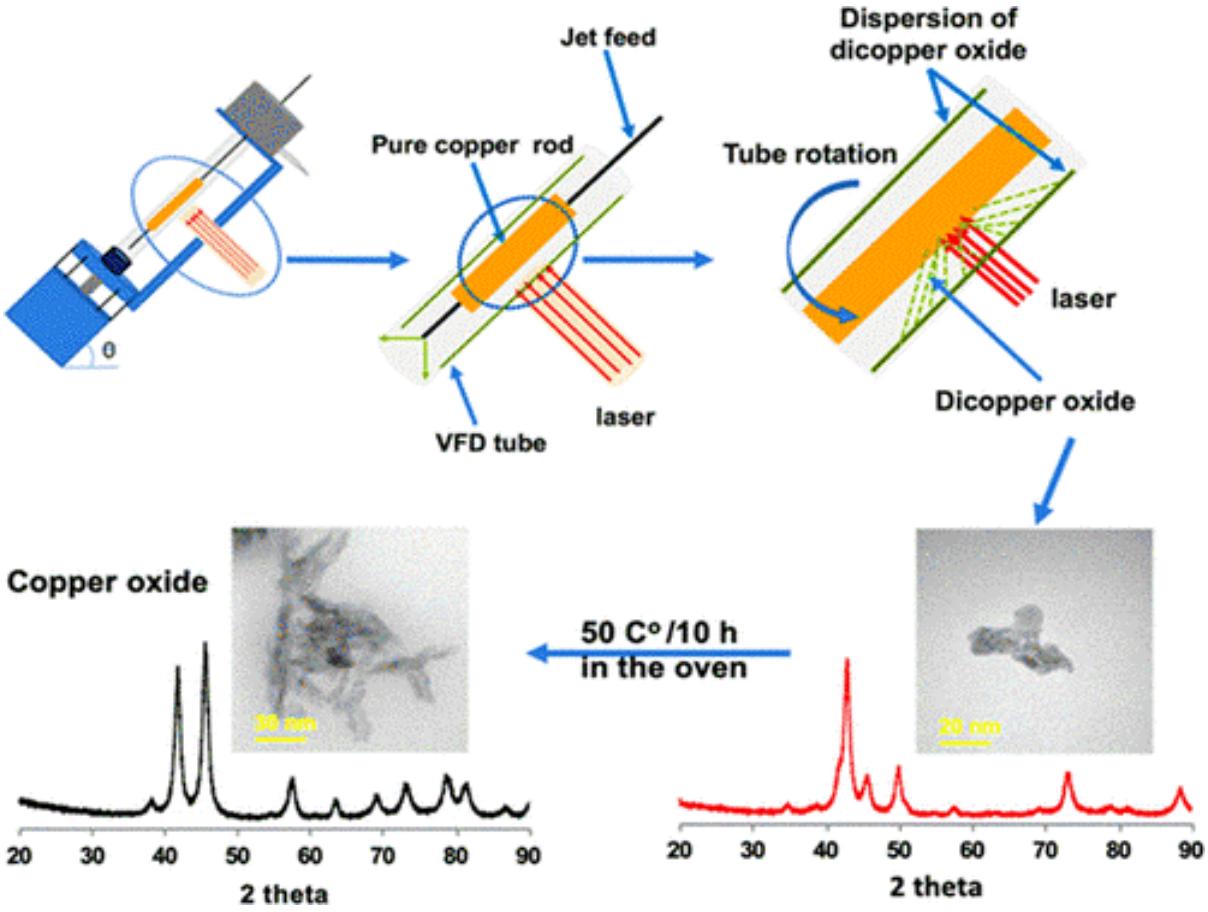

Figure 9 VFD shows the position of the pure Cu rod as the laser target with the arrangement of the tube for the formation of Cu_2O NPs and further formation of CuO NPs. Reproduced with permission from Ref [54].

Luo *et al.* [55] selectively synthesized magnetite NPs using laser ablation of bulk Fe metal at 1064 nm in a VFD with Nd: YAG pulsed laser. The superparamagnetic single-phase magnetite NPs were hexagonal and spheroidal-shaped, with an average size of 15 nm. This method can selectively monitor phase composition and the size and shape of the particles compared with traditional processes. It minimizes the generation of chemical waste and avoids time-consuming purification steps. The magnetite phase selective synthesis assists in the magnetic retrievability of the NPs which is usually an issue in heterogeneous water treatment systems.

Furthermore, Jaleh *et al.* [56] reported the deposition of Pd NPs on carbon cloth using liquid laser ablation as the fabricating technique. The experiment exploited the significant characteristics of the laser method such as laser wavelength, energy per pulse, power density and a combination of solvents which led to the synthesis of nanoparticles with the required shape, size and crystallinity. The nanoparticles proved to be an efficient catalyst for the degradation of 4-NP, CR, MB and hexavalent Cr ion in 390 s, 120 s, 3 s and 4 min respectively at ambient room temperature. Also, the nanocatalyst could be reused for over 9 cycles without any change in catalytic capacity.

Overall, the major advantage of using this vapor phase laser ablation route is the formation of high-purity NPs using a continuous flow reactor. However, the process suffers from dispersed size and morphology sometimes leading to agglomeration. Therefore, the process is less prominently used than the microwave or sonochemical route.

5. Alternative Green Solvents

In a wider range of reaction media/solvents, new transformations and reagents that are more reliable, safer, and efficient will inevitably provide access to greener media. Recent progress in using alternative solvents has opened up new arenas for the green synthesis of NPs and minimizing waste generation.

5.1 Supercritical Fluids

Supercritical fluids such as CO_2 have density, viscosity and solvent properties that are intermediate between the vapor and liquid phases at temperatures and pressures above the critical point of liquid vapor equilibrium. Their strength [57] could be easily tuned by changing pressure or temperature in a supercritical state. Liu *et al.* [58] obtained β-D-glucose-stabilized Au NPs of 6.9 nm processed into low-defect, wide-area thin films using carbon dioxide instead of traditional organic solvents. CO_2-expanded liquid and supercritical CO_2 ($scCO_2$) methods prevented the adverse dewetting effects and interfacial pressures in traditional solvent evaporation techniques. This CO_2-based approach also allows for much greater concentration on NPs deposition since the particles settle directly on the substrate without being transported by the liquid/vapor interface to undesired locations. Hence synthesis of NPs is facilitated without any leaching or handling loss.

Highly crystalline and pure-phase anatase TiO_2 NPs were synthesized by Wang *et al.* [59] in supercritical water (SCW) with a diameter of around 10 nm. Water serves as both a medium for reaction and a reagent. In the first stage of the reaction, metal salts of water solution such as $Ti(SO_4)_2$ can be hydrolyzed with alkaline solution (KOH for example) or pure water in SCW condition to $Ti(OH)_2$; immediate dehydration of $Ti(OH)_2$ follows to obtain particles of TiO_2. Due to increased temperature and pressure, the NPs adsorb less water as confirmed by FTIR.

5.2 Ionic Liquids

Salts with low melting points (less than 100°C) are known as ionic liquids. Due to their high thermal and chemical stability, they comprise anionic and cationic components and can be utilized in high-temperature operations up to 300°C. Temperatures greater than just this induce decomposition [60]. In general, ionic liquids are salts of asymmetric and massive ions with fewer attractive cation-anion attractions than traditional salts like table salt. It allows them to be liquids at various temperatures, including the ambient temperature in most situations (Figure 10) [61].

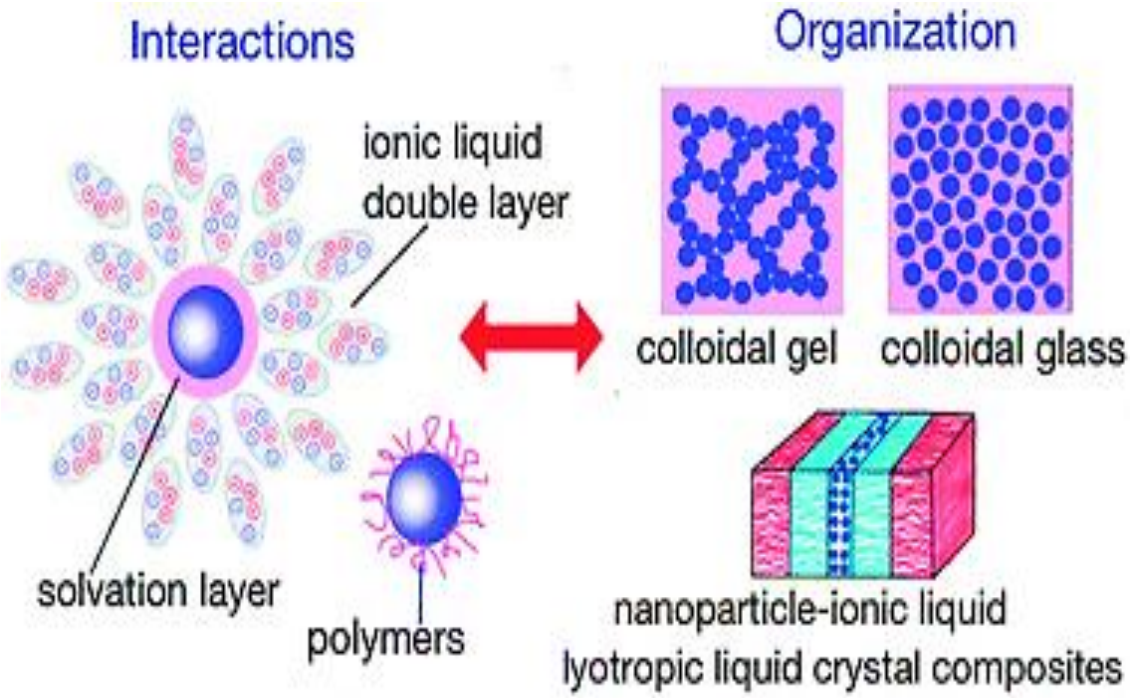

Figure 10 Schematic of ion clusters surrounding NPs. The clusters form a protective electrical double layer. Reproduced with permission from Ref [61].

Corrêa *et al.* [60] synthesized Ag NPs using in a homogeneous phase constituted of different ionic liquids based on the 1-alkyl-3-methylimidazolium cation- tetrabutylammonium borohydride ($TBABH_4$) as reducing agent and silver(I) bis(trifluoromethane sulfonyl)imide ($AgTf_2N$) as a salt precursor. The four imidazolium ionic liquids used were 1-butyl-3-methylimidazolium bis(trifluoromethane sulfonyl)imide, 1, 2-dimethyl-3-butyl imidazolium bis (trifluoromethane sulfonyl) imide, 1-butyl-3-methyl imidazolium tetrafluoroborate, 1-octyl-3-methylimidazolium bis(trifluoromethane sulfonyl)imide. The PVP stabilized the resultant NPs for one month. The electric double layer provides necessary electrostatic interactions which prevent the agglomeration of NPs and increase their shelf life.

Ahmed *et al.* [62] reported the synthesis of α-Fe_2O_3 rhombohedral quantum dots using ionic liquid (1-butyl-3-methylimidazolium tetrafluoroborate) under microwave irradiation. The NPs showed excellent photocatalytic activity for the degradation of Methyl orange (MO) with quantum dots having maximum efficiency for 100% dye removal from water in 240 mins.

5.3 Biomass-Derived or Bio-Based Solvents

Glycerol and its acetals, some low melting carbohydrate mixtures, esters of lactic acid and gluconic acid, 2methyl tetrahydrofuran (2MeTHF), Cyrene (Cyr), limonene (Lim), payment (Cym), and valerolactone are some of the most common biomass-derived or biobased solvents used in organic synthesis today. Unfortunately, the advancement in biomass-derived solvents has been limited to organic transformation reactions and very few are used as a substitute for NPs synthesis.

Rizk *et al.* [63] were successfully able to utilize polyol media *i.e.,* ethylene glycol (EG) or diethylene glycol (DEG) for the fabrication of Magnetite NPs (MNPs) *via* the reverse co-precipitation method. The NPs were highly crystalline and spherical with a mean diameter of 18.8, 14.45 and 10.49 nm for Fe_3O_4, DEG-MNPs and EG/MNPs, respectively. Compared to DEG-MNPs, EG/MNPs

exhibited remarkable efficiency for Pd(II) uptake from aqueous medium, attributed to a higher OH group on EG than on DEG. It follows the pseudo-second-order rate equation (k_2 = 0.00337 g/mg min at 288 K). The Langmuir equation gives a monolayer adsorption capacity of 26.32 mg/g, higher than other traditional models. The sorption is spontaneous and endothermic (ΔH° = 25.93 kJ/mol) due to the presence of electrostatic interactions between sorbent and sorbate species. EG-coated MNPs demonstrated good efficiency and selectivity in separating Pd(II) from different metal ions with good reusability.

Cyrene (dihydrolevoglucosenone) is a biodegradable and bio-derived green solvent with interesting properties for many applications [64]. Poon and Zhitomirsky [65] used this bio-derived solvent to produce multi-walled carbon nanotube (MWCNT) suspensions. The fabricated MWCNT were durable, devoid of surfactants and stable for more than two months even at high concentrations of 1-3 g/L. For the manufacturing of Polymethylmethacrylate (PMMA) binder solutions, Cyrene was uncovered to be a sustainable replacement for harmful substances. In Cyrene, the interactions of soluble PMMA with Mn_3O_4 NPs led to strong colloidal dispersion and the development of stable suspension. It is suggested that PMMA macromolecules adsorbed on NPs in Cyrene solvent provided steric dispersion of the particles. The electrodes had a high capacitance of 3.79 F/cm^2 and 4.15 F/cm^2 from cyclic voltammetry results, as well as good cyclic stability.

Hence, green solvents have become very lucrative as a replacement of conventional organic solvents, which usually demonstrate high volatility, flammability and toxicity. Taking advantage of these new solvatis' solvation properties and synthetic versatility, a wide variety of applications can be plausible in environmental decontamination.

6. Green Synthesis of Nanoparticles for Water Remediation Using Renewable Resources

The use of biological matter or renewable resources, for example, bacteria, fungi, algae, plant extracts, *etc* in the green synthesis of metallic nanoparticles is reported widely. Using these extracts or living species is a fairly convenient and straightforward method of generating NPs on a large scale. These materials are collectively known as NPs of biogenic origin [66]. NPs synthesis mediated through biomolecules has gained interest because of their inherent non-toxicity and the involvement of harsh synthetic methods. Biomolecules such as polyphenols, flavonoids, terpenoids, proteins, amino acids, carbohydrates, polysaccharides, and sugars act as reducing, stabilizing, capping and templating agents during NPs synthesis. This process also allows the shape and size-controlled synthesis during NP formation [67].

Herein, the current state of research on green metal/metal oxide NPs synthesis using biomass and their biomolecules within is reviewed coupled with approaches that are energy efficient or use green solvents, where appropriate.

6.1 Terrestrial Plant (And Their Residues)-Mediated Synthesis

Gardea-Torresdey *et al.* [68] first reported the synthesis of icosahedral Ag NPs from the root extract of *Alfalfa sprouts* with a diameter of 2-4 nm. Alfalfa roots are capable of absorbing silver as Ag(I) ions and reducing them to Ag(0) which are then translocated into the shoots in the same oxidation state. TEM/SEM analysis suggested that the Ag atoms accumulate inside the alfalfa plant tissue undergoing nucleation and NPs formation concurrently.

Nadagouda and Varma [69] could fabricate face centered cubic Ag and Pd NPs (20-60 nm diameter, Figure 10) using coffee- and tea-leaf extract without any external surfactant, caping or templating agent. Organic moieties such as polyphenols and caffeine were responsible for capping the metal NPs, leading to apparent inter-particle separation, as shown in Figure 11 (A). Further, the reduction potential of caffeine is sufficient to simultaneously reduce Ag and Pd metals and provide the capping of oxidised polyphenols/caffeine. A control experiment was also carried out on Au which yielded wire-like structures in the presence of pure caffeine (Figure 11 (B)).

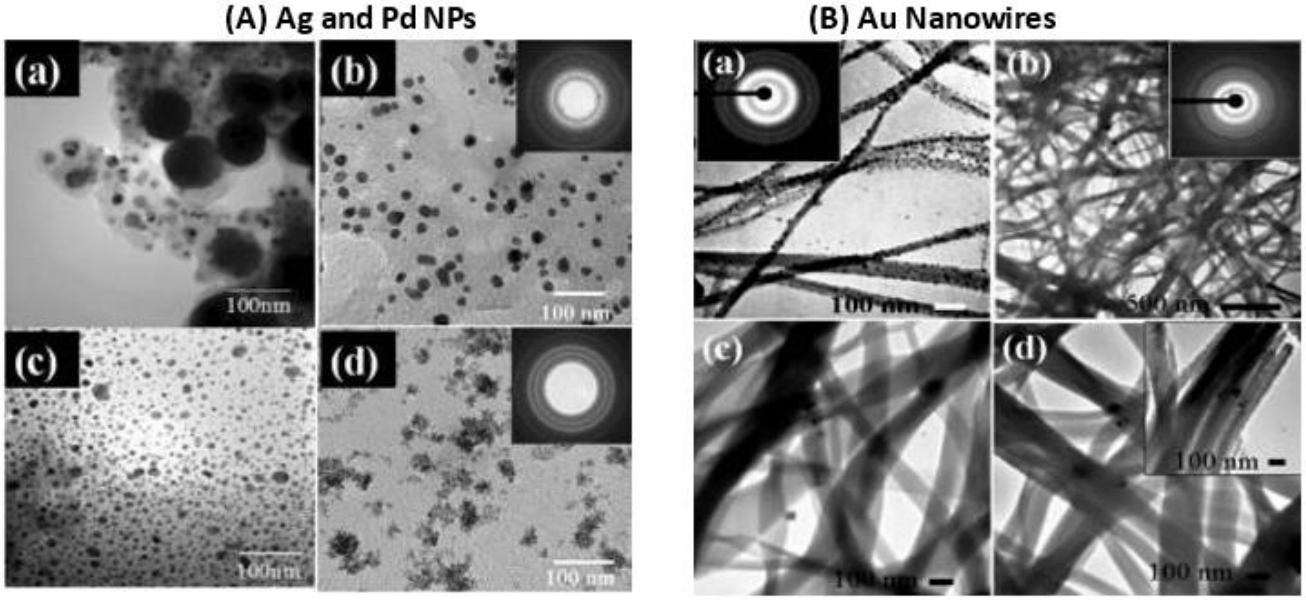

Figure 11 (A) TEM images of (a, b) Ag NPs prepared using coffee and tea extract respectively, (c, d) Pd NPs from coffee and tea extract respectively. (B) TEM images of Au nanowires (2 mL of 0.01 N) fabricated with (a) 25 mg (b) 100 mg (c) 200 mg and (d) 300 mg of pure caffeine. [Inset shows the corresponding diffraction area]. Reproduced with permission from Ref [69].

Hatamifard *et al*. [70] carried out the green synthesis of Ag/zeolite nanocomposite using the leaf extract of Euphorbia prolifera. The presence of phenolic acid and flavonoids in the leaf extract facilitated the formation of nanocomposite by reduction of Ag(I) ions. Ag/zeolite composite demonstrated effective catalysis for ligand-free hydroxylation of phenylboronic acid. It was also potent at room temperature of 4-nitrophenol (4-NP), methyl orange (MO), Congo red (CR), methylene blue (MB) and rhodamine B (RhB). Similarly, Ag NPs (5-15 nm diameter) derived from *Ruta graveolens* leaves [71] extract acting as a reducing and stabilizing agent have been immobilized on the surface of a waste almond shell. The catalytic performance of the synthesized catalyst was analyzed for the reduction of 4-NP, RhB and MB at ambient temperature. AgNPs/almond shell composite demonstrated good recyclability up to seven times with the minimum loss of catalytic activity.

Doan *et al.* [72] demonstrated the significance of OH groups present in the phytochemicals for the synthesis of Au NPs using fruit extract of *Litsea cubeba*. The extract is rich in alkaloids, flavonoids, lignans and steroids, and was responsible for reducing Au metal ions and capping of Au NPs. The formed NPs catalytically reduced 4-NP to 4-AP in the presence of NaBH4. Similarly, *Momordica*

charantia leaf extract was used for the green synthesis of Gold@Silver@Silver chloride (Au@Ag@AgCl) core-double shell NPs. These NPs were used for photocatalytic degradation of pharmaceuticals such as clofibric acid (CA) and ibuprofen (IBP), and 2, 4, 6-trinitrophenol (2, 4, 6-TNP). Likewise, Nasrollahzadeh *et al.* [73] prepared a Pd/bentonite nanocomposite using *Gardenia triteness* leaf extract. The catalytic activity of the prepared nanocatalyst was evaluated in the ligand-free hydroxylation of phenylboronic acid to phenol and reduction of chromium (VI) and nitro-compounds such as 4-NP and 2, 4-dinitrophenylhydrazine (2, 4-DNPH).

Ghosh *et al.* [74] successfully synthesize Cu NPs using leaf extract of *Jatropha curcas* (JC). The existence of flavonoids, tannins, glycosides, and alkaloids acted simultaneously as reducing, stabilizing and capping agents. The average particle and crystal sizes of the JC-CuNPs were 10 ± 1 and 12 ± 1 nm, respectively. The JC-CuNPs showed potential photocatalytic activity against MB with a rate constant (k) value of 2.30×10^{-4} s^{-1} compared with other dyes in sunlight (Figure 12).

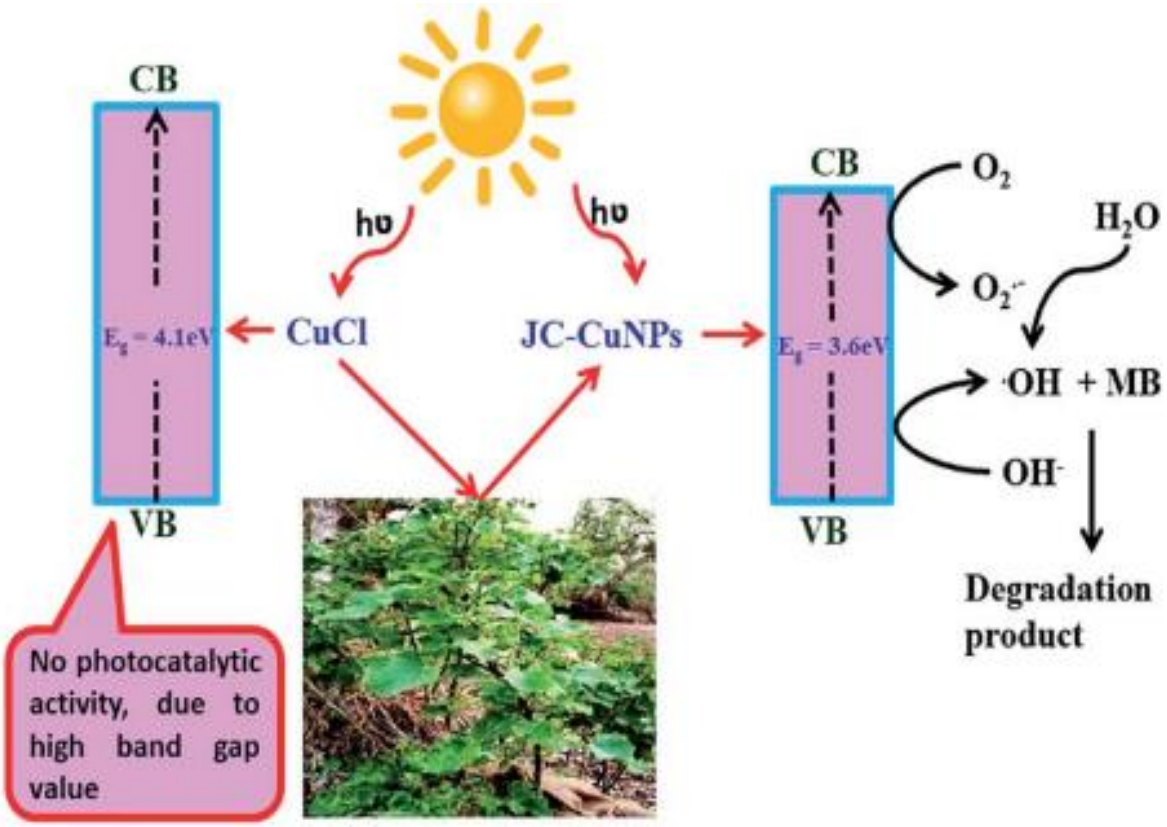

Figure 12 Proposed mechanism of the utility of Jatropha curcas-based CuNPs in degradation of MB. Reproduced with permission from Ref [74].

Song and Yang [75] explored bamboo shoots as a readily available and renewable form of biomass for NPs synthesis. They fabricated Pd NPs immobilized on *N*, *O*-dual doped porous carbon derived from bamboo shoots by wet chemical impregnation and reduction. The Pd NPs were found to be homogeneously distributed throughout *N*, *O*/carbon support with an average diameter of 11.9 nm. The synthesized Pd/*N*, *O*-porous carbon was utilized for selective hydrogenation of functionalized nitroarenes to form anilines, imines, and formamides, offering a perspective for a nitro compound reduction in wastewater remediation.

Sharma *et al*. [76] reported the green synthesis of magnetically retrievable Fe_3O_4 NPs using starch-rich potato extract. Starch comprises amylose and amylopectin, which differ in the regiochemistry of the glycosidic bond, i.e., 100% alpha (1-4) and, a mixture of alpha (1-4) and alpha (1-6), respectively. The OH groups within amylopectin through H-bonding form cavities acting as templates for the growth of NPs and facilitating the complexation of metal ions. The synthesized Fe_3O_4 NPs (10 mg) showed promising results for the 100% degradation of RhB dye from wastewater in 30 mins. The magnetic properties of the NPs allowed their easy separation after use in 20 secs.

Intriguingly, Devi *et al*. [77] demonstrated the use of a Jute stick (waste material) to form activated carbon which was impregnated with Ag NPs derived from peel extract of *Coccinia grandis* (commonly known as ivy gourd, scarlet gourd, tindora or kowai fruit). The Ag-activated carbon nanocomposite showed antimicrobial activity towards gram-negative (*E. coli*, *P. aeruginosa*) and positive (*B. subtilis* and *S. aureus*) bacteria, and had great potential for photocatalytic degradation of toxic malachite green oxalate dye (98%) and active pharmaceutical compound, Clofibric acid (97%) under solar irradiation under 90 mins.

Thi *et al.* [78] used orange peel waste to synthesize ZnO NPs whose size and morphology significantly depended on physicochemical parameters such as annealing temperature and pH. Samples annealed at 400, 700, and 900°C gave a random particle size distribution from 35-60, 70-100 and 200-230 nm, respectively. The flavonoids, limonoids, and carotenoids in the orange peel ligate with the Zn precursor leading to stabilization, nucleation and formation of ZnO NPs. The NPs showed strong antibacterial properties against E. coli and S. aureus due to ROS produced by ZnO NPs in water at a low concentration of 0.025 mg/ml.

Kaur *et al.* [79] explored MoO_3 NPs embedded in a carbonaceous mesoporous material derived from corn starch known as Starbon™ for their efficacy as catalysts in reducing 4-NP to 4-AP (Figure 13). TEM and SEM analysis revealed homogeneous dispersion of the MoO_3 NPs (average diameter 2 nm within the Starbon™ matrix. The NPs had excellent catalytic activity for reducing 4-NP to 4-AP in the presence of $NaBH_4$ ($k = 11.2 \times 10^{-2}$) proving its worth for waste-water remediation. This material also showed superior DPPH radical quenching activity with a low IC_{50} (1.006 mg/ml) value compared concerning to other green synthesized composites and NPs.

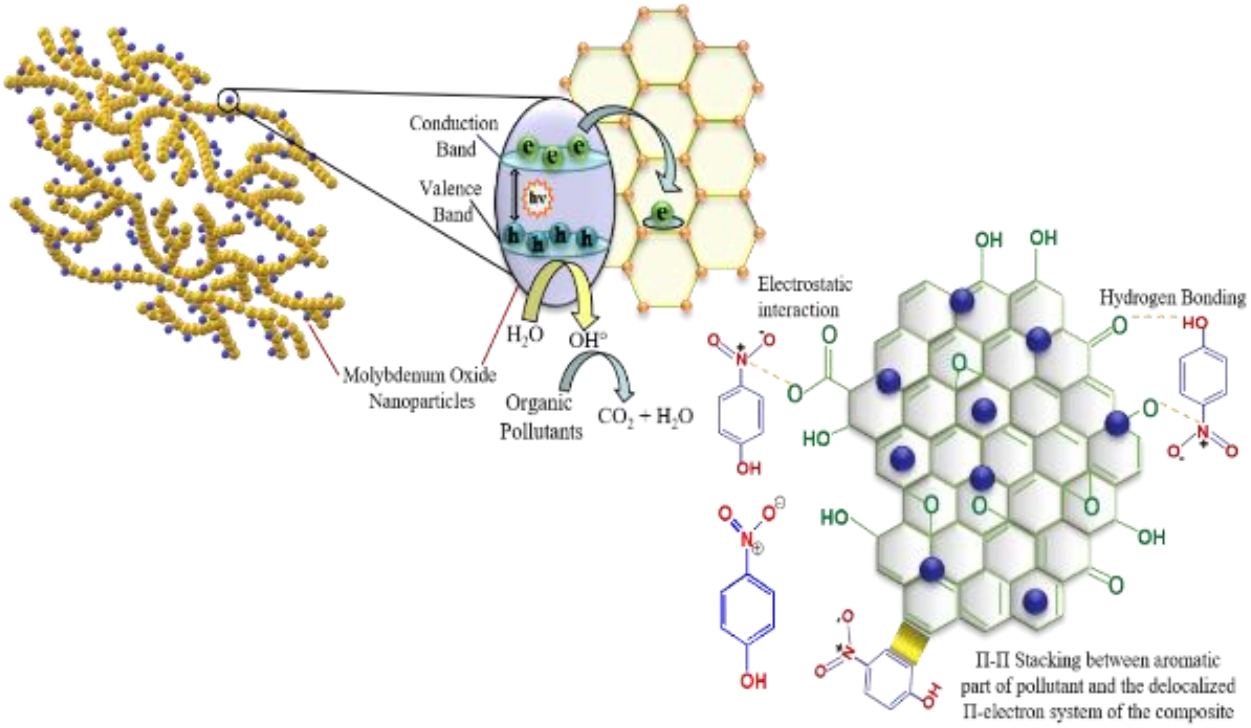

Figure 13 Schematic representation of the use of Biomass-derived NPs in 4-NP reduction. Reproduced with permission from Ref [79].

Li *et al*. [80] synthesized Ag NPs using rice straw at room temperature concerning light intensity, biomass concentration, time, and $AgNO_3$ concentration. Rice straw is a significant waste stream in rice-growing regions that are often burned. The rice straw acted as both a reducing and stabilizing agent and XRD data showed the Ag NPs had a tetrahedral centripetal crystal structure. The synthesized Ag NPs had good antimicrobial activity against *E. coli, P. aeruginosa, B. subtilis,* and *S. aureus.*

Han *et al.* [81] utilized lentinan (LNT) as both a reducing and stabilizing agent for synthesizing Pd NPs. LNT is a polysaccharide with the composition of one β-(1→6)-D-glucopyranoside branch for every three β-(1→3)-glucopyranoside linear linkages (Figure 14). LNT is reported to possess antiviral and anticancer properties [82, 83]. The Pd_n-LNT NPs formed were spherical with of 25-29 nm hydrodynamic radii and no cytotoxicity. The synthesized NPs showed great potential for the 90% reduction of 2, 4-NP to 4-AP in 21 mins.

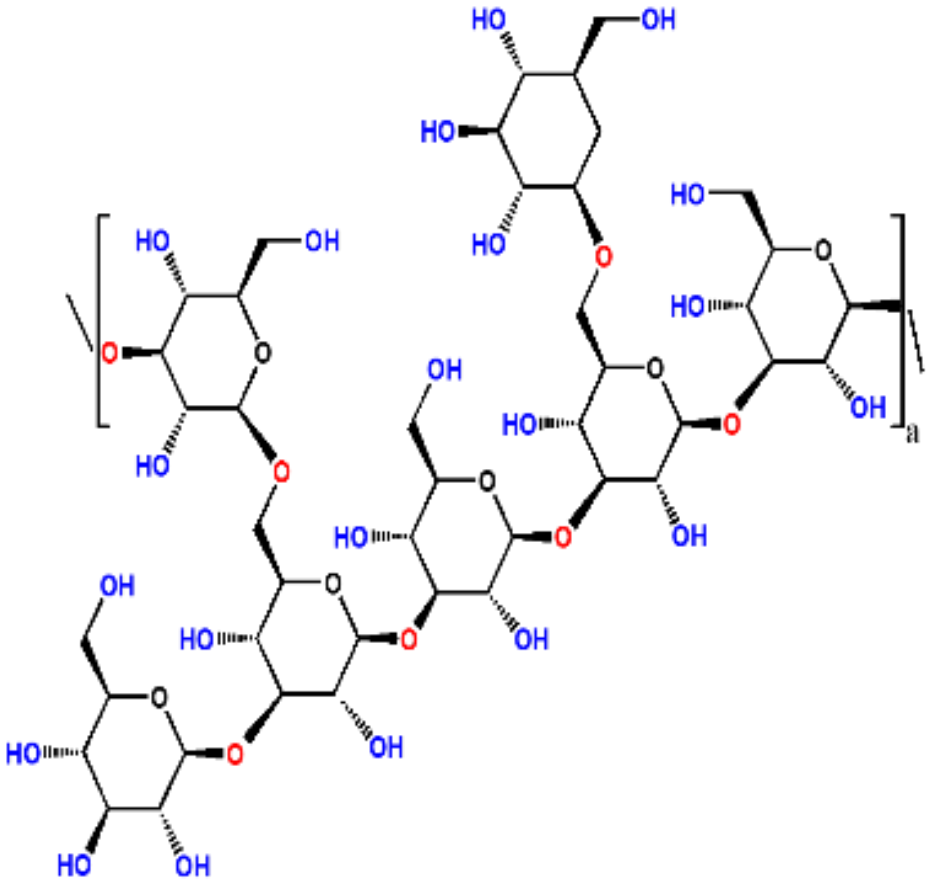

Figure 14 Chemical structure of Lentinan.

Kahrilas *et al.* [84] explored the use of different biomolecules such as starch, arabinose, and dextrose, for the microwave-assisted green synthesis of Ag NPs (diameter <30 nm). Microwave methodology allowed for selective size control of NPs as compared to traditional methods. Further, the high microwave energy output in small time helped expand the amylose content of starch, which controlled the NPs morphology. The synthesized NPs showed activity against biofilms and were active against various bacteria (*E. coli* (MG1655), *B. subtilis*, *K. pneumoniae*, *P. aeruginosa*, *S. aureus*, and *Janthinobacterium lividum*).

Saponin, a terpenoid (Figure 15), was used as a biosurfactant and shape-controlling agent by Sundar *et al.* [85] for the morphological controlled synthesis of anisotropic Fe_2O_3 NPs. Saponin-enriched aloe vera extract was utilized in the selective growth of different polymorphs of Fe_2O_3 nanostructures such as Fe_2O_3 nanospheres, γ-Fe_2O_3 nanoribbon and α-Fe_2O_3. The formation mechanismof nanospheres and thus nanoribbons was described as nucleation, surface regularity, growth and oriented attachment of the NPs to saponin. The NPs displayed biosensing properties towards pharmaceutical products like uric acid and dopamine, thus giving us a perspective for removing pharmaceutical waste from water sources.

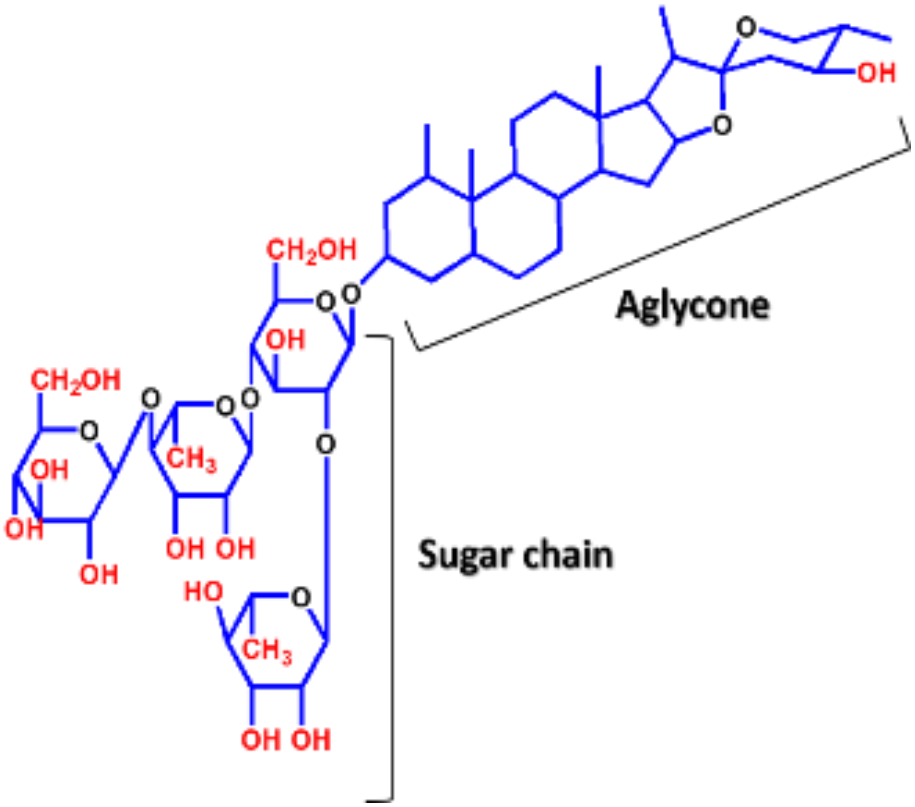

Figure 15 The chemical structure of steroid Saponin.

Zein protein is an alcohol-soluble plant protein found in corn and manufactured from corn gluten meal. Mahal *et al.* [86] incorporated zein protein to prepare bioconjugated Zein-Au NPs. Here the unfolding of zein in aqueous phase helps provide stabilizing and reducing properties. The surface plasmon resonance (SPR) of Au NPs activated the adsorption of zein on the NP's surface and thus resulted in the unfolding of the protein. This exposed the reducing amino acids such as cysteine that reduced of Au (III) to Au (0) and simultaneously formed Au NPs. The adsorption of zein further helped control the crystal growth of Au NPs, which directly correlated with the degree of unfolding and fusogenic behavior *i.e.,* cell fusion of zein due to its hydrophobic nature. The latter property triggered a significant blue shift in the SPR rarely encountered in the growing NPs during nucleation (Figure 16). A deeper unveiling of was essential in inducing zein-coated faceted NPs assigned to their haemolytic response for subsequent use as drug release vehicles.

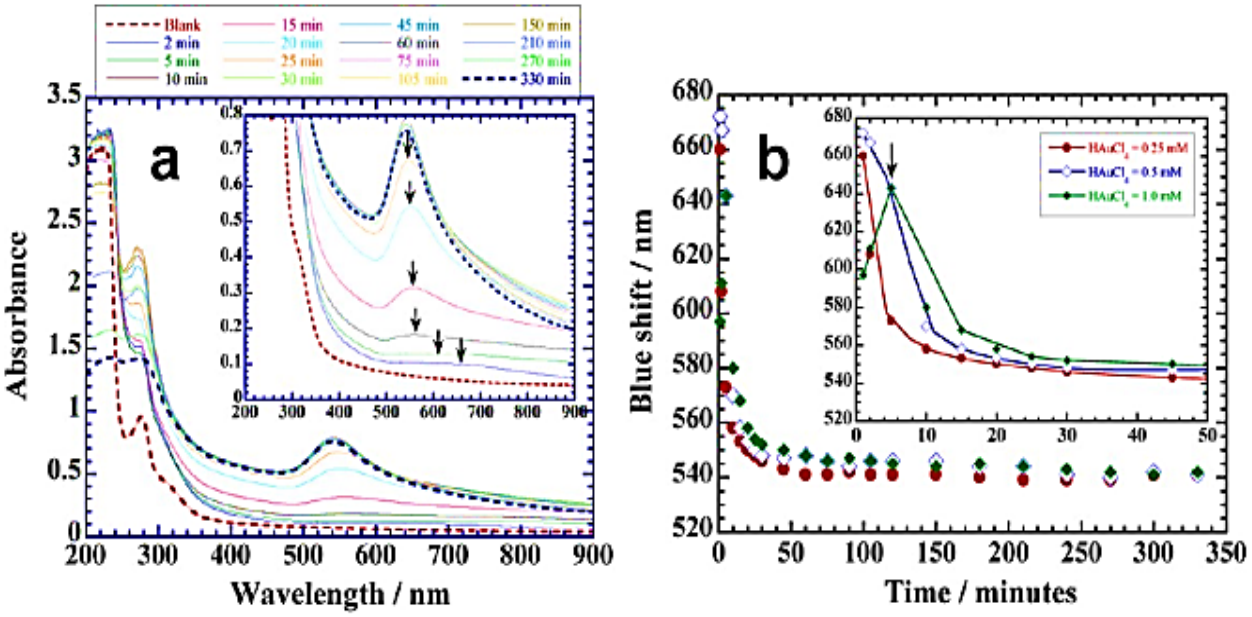

Figure 16 (a) The UV-Visible time study of the interaction of 0.25 mM $HAuCl_4$ and 0.1% zein solubilized in 24 mM aqueous SDS. The inset signifies the blue shift with an increase in time. (b) Plots of time variation in absorbance at 540 nm (blue shift) with change in $HAuCl_4$ concentration. Reproduced with permission from Ref [86].

Rice husk and Sugarcane waste (bagasse and ash) are agricultural waste products having high silicon content. Rovani *et al*. [87] synthesized highly pure SiO_2 NPs from sugarcane waste ash. Sodium silicate was extracted from the sugarcane ash waste by heating it to 400°C in the presence of NaOH. For SiO_2 NPs synthesis, the sodium silicate was hydrolysed and condensed using sulfuric acid in a biphasic medium in the presence of cetyltrimethylammonium bromide (CTAB). This CTAB surfactant controlled the size of the NPs and stabilized them. No definitive form was observed for the NPs; however, TEM analysis showed the size to be less than 20 nm and the NPs produced were pure without any organic matter. BET analysis represented the specific surface area to be 131 $m^2 g^{-1}$. The produced SiO_2 NPs proved an excellent adsorbent for acid orange 8 dye with an adsorption capacity of 230 mg g^{-1} (90% adsorption). The adsorbent could be effectively reused for over 5 cycles (Figure 17).

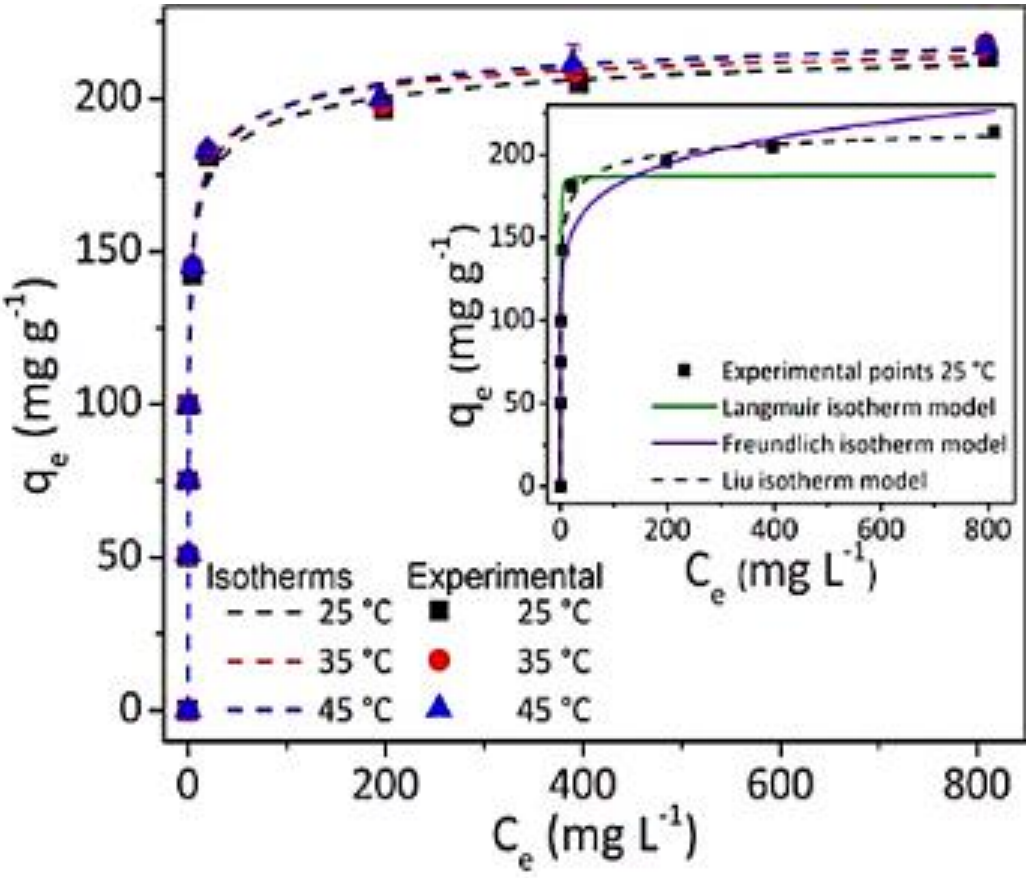

Figure 17 Adsorption Liu Isotherms for Acid Orange 8 (AO8) dye adsorbed by SiO_2 NPs. Reproduced with permission from Ref [87].

Further, another approach was explored by Peres *et al*. [88] for SiO_2 NPs using microwave leaching of rice husk. During the microwave synthesis, no bonds were broken or formed; only physical transformation occurred. Using the microwave for rice husk leaching increased surface area, pore volume, porosity and high purity with a particle size of 93 nm. With these properties SiO_2 NPs acted as excellent adsorbents for removing MB from aqueous media with an adsorption capacity of 679.9 mg g^{-1} in 240 mins.

Microwave-assisted of nanoscale zero-valent iron nanoparticles (nZVI-NPs) using leaf extracts of *Mentha piperita* was reported by Shad *et al*. [89]. The use of microwave irradiation reduced reaction time to only 3 mins at 48°C and resulted in spherical NPs in size range of 5-10 nm. The resultant nZVI-NPs were efficiently used for the removal of five major agricultural pollutants within 24 h from canal water, namely: phosphate 85.01%); ammonia (99.51%); nitrate (86.33%); lead (79.33%), and; chloride (83.04%), respectively.

Banana fruit waste extract was utilized by Deokar and Ingale [90] for green synthesis of Au NPs by reduction of hydrogen tetrachloroaurate(III) hydrate ($HAuCl_4.3H_2O$). FTIR analysis showed that biomolecules present in fruit waste reduced Au metal ions by oxidizing aldehydes to carboxylic acids. At the same time, pectin and carbohydrates in the extract acted as capping agents to stabilize the NPs (predominantly spherical with 20 nm diameters).

Gurrola *et al.* [91] reported the ultrasound-assisted formation of corn starch esterified with 2-octen-1-yl succinic anhydride (OSA) NPs. The NPs were from oval to spherical shape with sizes less than 100 nm and their morphologies depended on sonication time. The strong mechanical forces

produced by acoustic cavitation during ultrasound treatment gradually disintegrated starch granules into smaller particles resulting in the breakage of amylopectin branches into amylose blocks as confirmed by FTIR data. The time required for the formation of non-esterified NPs was optimized to 80 mins (Figure 18) and one-pot synthesis of esterified NPs was done by subsequent addition of OSA.

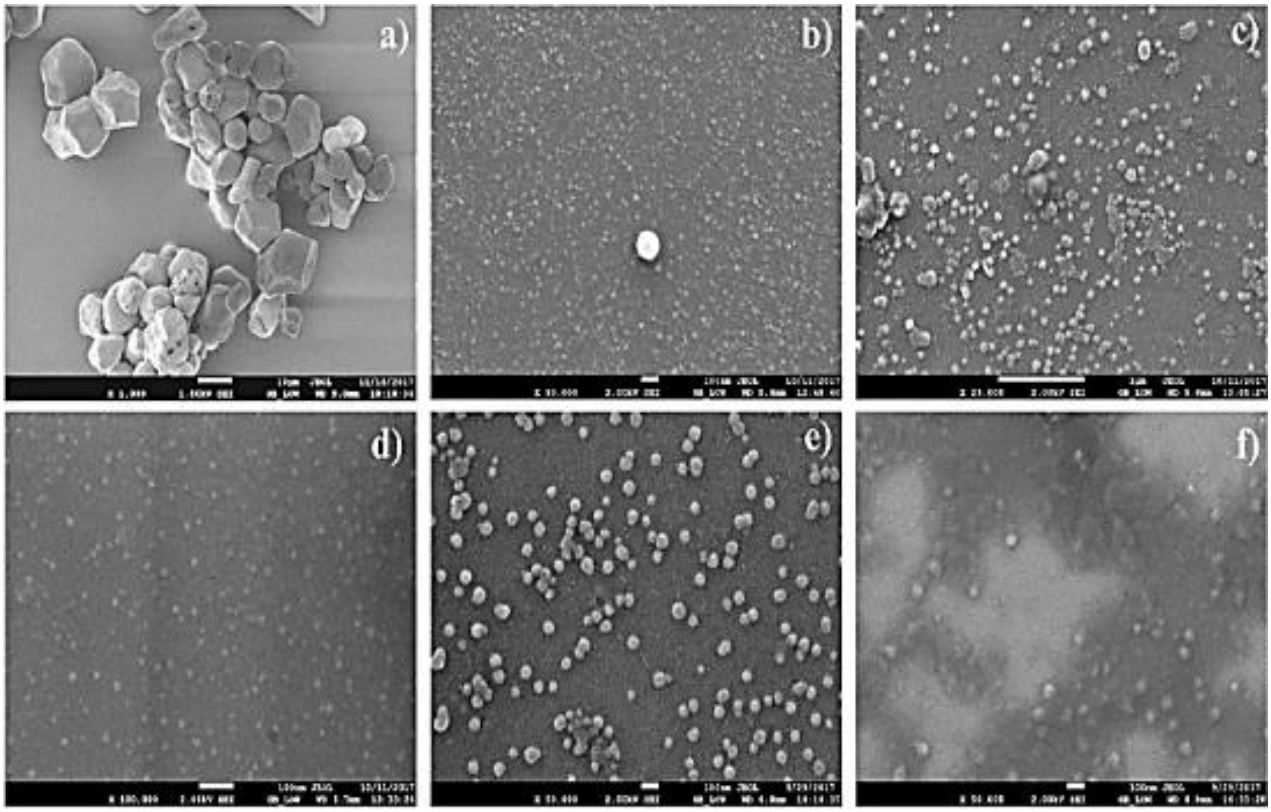

Figure 18 FE-SEM studies of non-esterified starch NPs obtained at different ultrasonication times: (a) native waxy starch; (b) 20 min (63 nm); (c) 40 min (53 nm); (d) 60 min (58 nm); (e) 80 min (48 nm), and (f) 100 min (48 nm). Reproduced with permission from Ref [91].

The biosynthesis of Ag immobilized on the ZrO_2 surface using *Ageratum conyzoides L.* extract has been documented as a green and *in-situ* strategy by Maham *et al*. [92]. To promote Ag(I) reduction, the phytochemicals present in the *Ageratum conyzoides L.* extract acted as reducing and stabilizer agents. The NPs could effectively degrade 100% 4-NP in 6 min in the presence of $NaBH_4$ with good reusability as high as five times without losing significant catalytic activity. Because of the synergistic interaction and immobilization of Ag NPs on the ZrO_2 surface, it resulted in better catalytic efficiency and less propensity for Ag NPs to agglomerate during the reaction. The proposed reduction mechanism consists of two stages: first, the target analyte and $NaBH_4$ adsorption on the nanocatalyst surface followed by electron transfer from BH_4 to the target analyte with subsequent desorption of the products from the catalyst surface.

Aksu *et al.* [93] utilized green synthesized iron oxide NPs (gINPs) to eliminate the beta-lactam antibiotic amoxicillin (AMX) from carob pods (*Ceratonia siliqua*) in an aqueous solution. The NPs were spherical with 7 ± 5 nm diameter and a surface area of 7.67 m^2/g. At a molar ratio of 1:50 AMX/gINPs, 99% of AMX was reduced in 200 mins at pH 2. Kinetic tests for adsorption and

degradation processes were used to study the removal of AMX. The kinetic analysis revealed that adsorption is a physical process with a 30 kJ/mol activation energy. Due to the high activation energy of 87 kJ/mol, the removal efficiency followed a pseudo-first-order reaction with a surface-controlled chemical reaction. It was discovered that initially AMX was physically adsorbed on the gINPs, then diffused to the metallic surface, and eventually reduced to several degradation products as detected by HPLC/MS analysis (Figure 19).

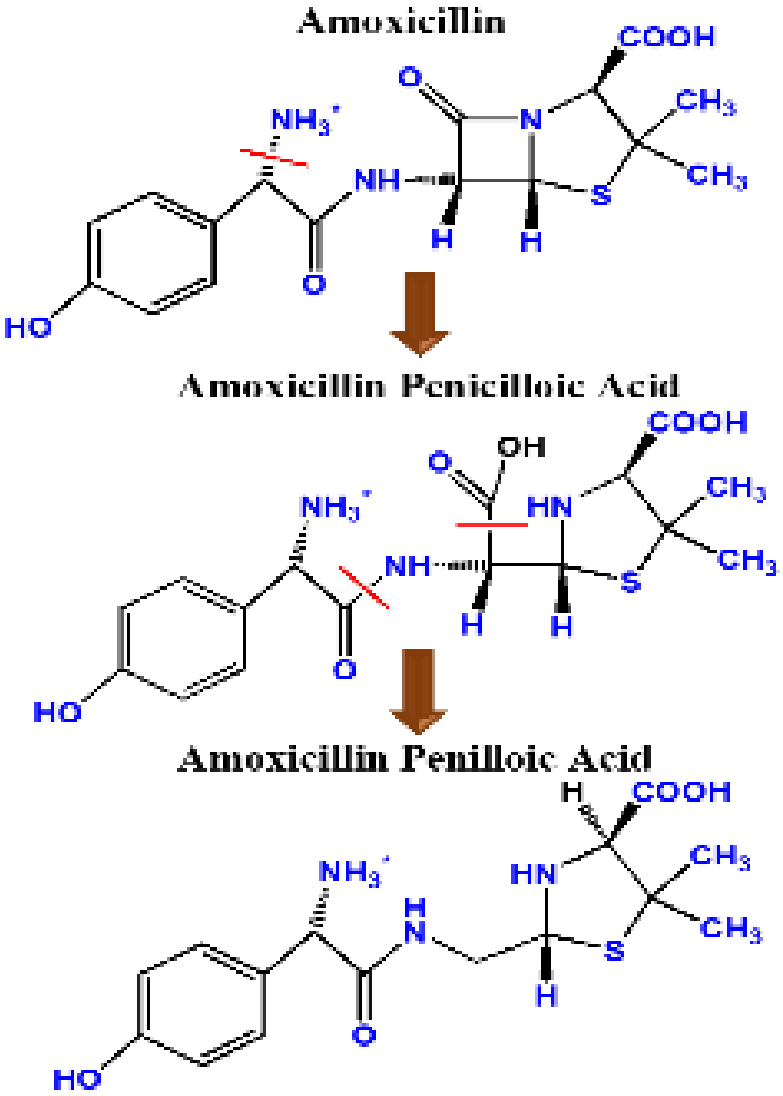

Figure 19 Degradation pathway of AMX. Adapted from Ref [93].

Isoimperatorin, a natural furanocoumarin found in several plant species, is a reducing reagent for producing Ag NPs (iso-AgNPs) with excellent photocatalytic activity [94]. Spherical-shaped iso-AgNPs were formed in a size range of 79-200 nm. They displayed catalytic activity for the degradation of New Fuchsine (96.0%), MB (96.5%), Erythrosine B (92%), and 4-chlorophenol (95%) in 60 min under visible light in 60 mins. It showed good reusability up to 4th cycle with a small decline in photo-degradation performance, i.e., 96% to about 88%. The photocatalytic mechanism involves the generation of HO$^{\bullet}$ radicals *via* a series of reactions (Figure 20). When a photon is irradiated, Iso-AgNPs absorb the photons (h*v*) and produce e-h pairs due to their high SPR effect. Under the light, the adsorbed dye molecule is excited and donates its photo-generated e^- to the CB of Iso-AgNPs.

The photo-generated electrons rapidly convert O_2 adsorbing on the photo-catalyst surface to $O_2^{-\bullet}$ and $^{\bullet}OOH$ radicals. The holes could directly oxidize adsorbed dye molecules, or react with surface adsorbed H_2O or OH^- to produce $HO^{\bullet}$ radicals which aid in the photo-degradation and mineralization of dye molecules.

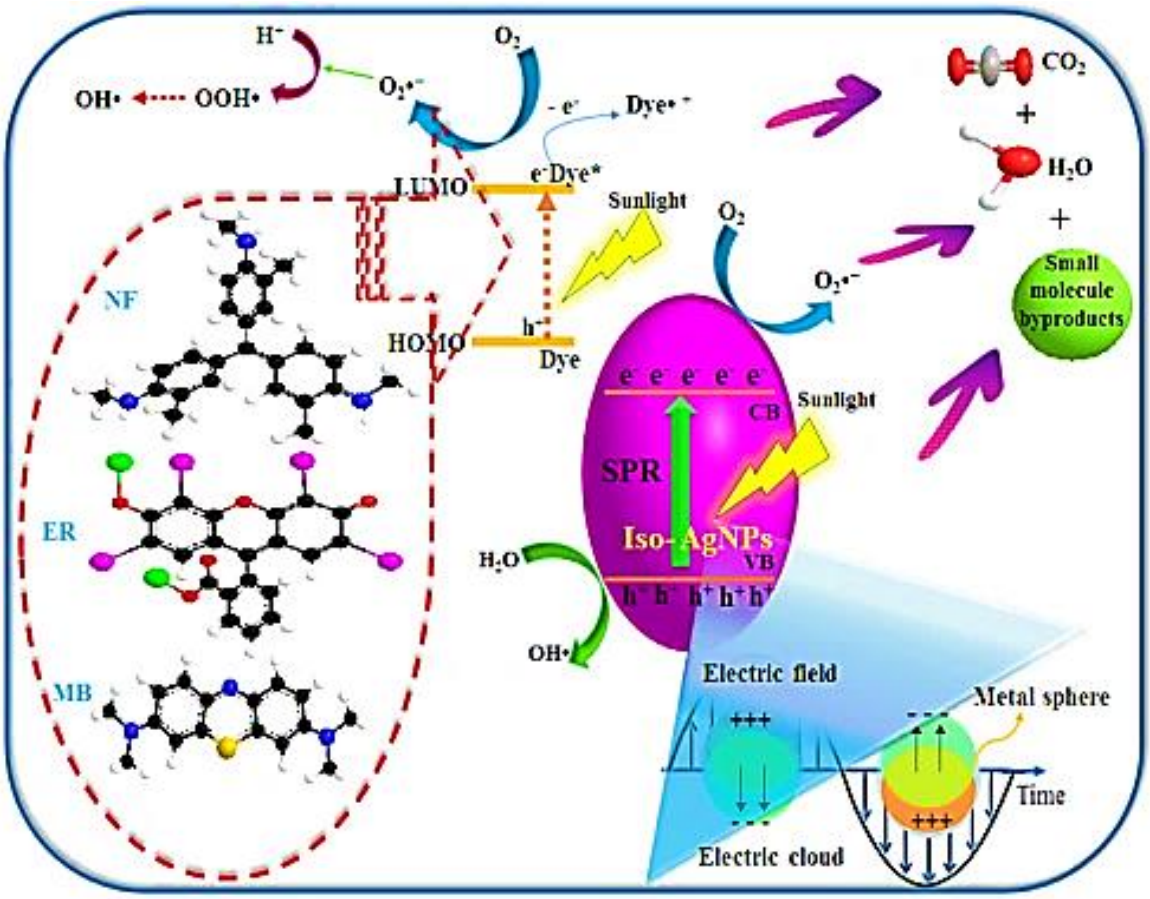

Figure 20 The photo-degradation pathway of dye pollutants in the presence of Iso-AgNPs under sunlight irradiation. Reproduced with permission from Ref [94].

Adsorption of arsenic on green-fabricated amorphous Fe NPs (with a specific surface area of 51.1368 $m^2\ g^{-1}$) has been evaluated for removing highly toxic and carcinogenic arsenic (As) from polluted resources [95]. The NPs were fabricated using a hybrid of *Eucalyptus urophylla* and *Eucalyptus grandis* leaves which acted as stabilizing agents and prevented agglomeration. This helped in the homogeneous adsorption of arsenate on the iron NP's surface. The XPS analysis revealed the presence of As(V) which predominantly formed the FeOAs bond which facilitated the adsorption as shown by FTIR evaluation. Hence it can be inferred that the iron NPs interact with arsenate to form a monodentate chelating ligand which leads to the formation of the bidentate binuclear complex. The adsorption efficiency was maximum in the pH range of 4-6, followed by Langmuir adsorption isotherm (RL^2 = 0.9903) with the highest adsorption capacity of 14.617 mg g^{-1}. It validated Chemisorption and the adsorption efficiency fitted the pseudo-second-order kinetic model well.

Akpomie and Conradie [96] successfully impregnated Ag NPs into pristine *Solanum tuberosum* peel (STpe) to create a hybrid adsorbent (STpe-AgNP) for the elimination of bromophenol blue from

water bodies. Various functional groups on the surface of the hybrid facilitated more efficient bromophenol blue adsorption. The best match for Freundlich isotherm revealed that the pristine and hybrid adsorbents were heterogeneous, confirmed by an independent focused site study. The intraparticle diffusion and pseudo-first order models better match the kinetic analysis. Thermodynamic research revealed that bromophenol blue adsorption is endothermic and spontaneous. The ion interference study in simulated wastewater decreased bromophenol blue accumulation in the order Pb (II) > Ni (II) > Cd (II) > Zn (II), with Zn (II) ions causing the least interference. The overall uptake potential of pristine Solanum tuberosum peel increased marginally from 8.157 to 9.604 mg/g after AgNP impregnation. H-bonding, hydrophobic, electrostatic, and – interactions were discovered to be involved in bromophenol blue adsorption onto pristine STpe and STpe-AgNP hybrids. When using NaOH as an eluent, STpe and STpe-AgNP showed BB desorption of 91.3% and 88.5%, respectively (Figure 21).

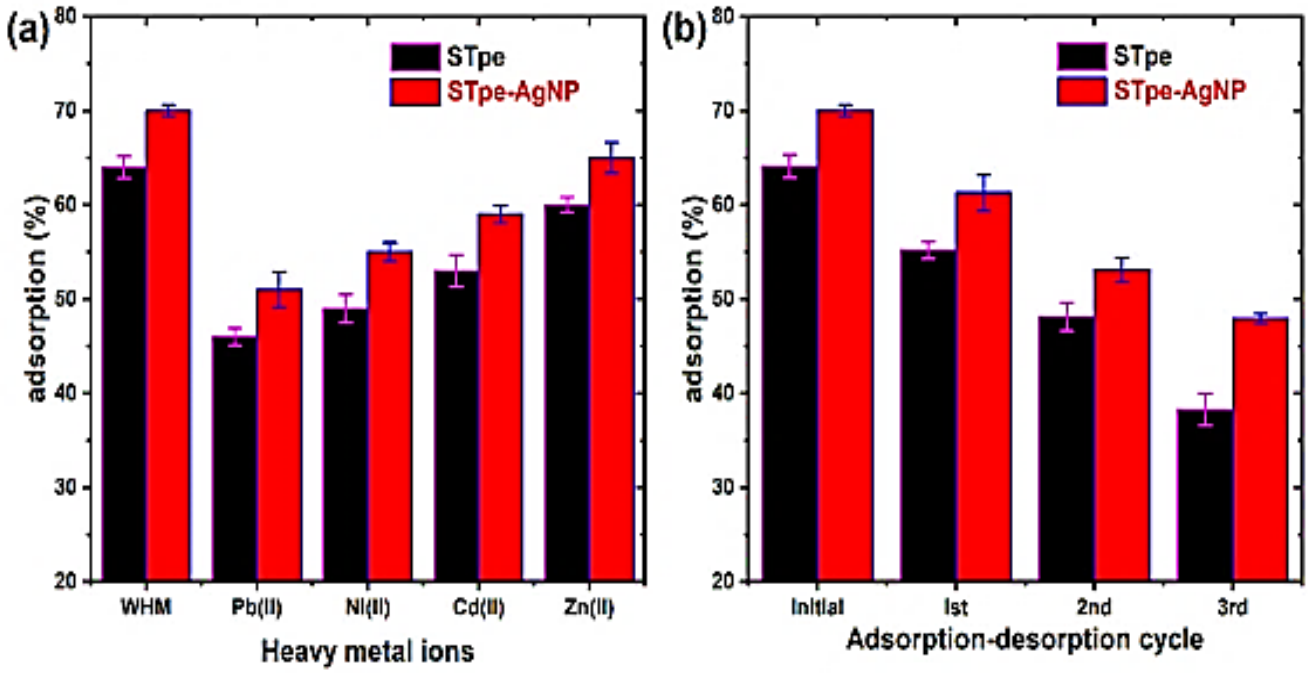

Figure 21 (a) Metal ion interfering study on the adsorption of BB dye (WHM represents the absence of heavy metal ions), and (b) recyclability study of BB adsorption (0.5 M NaOH used as an eluent for desorption). Reproduced with permission from Ref [96].

Jain *et al*. [97] depicted a non-toxic and simple process for making Fe_2O_3 NPs using *Syzygium aromaticum* bud extract (clove). Both Fe_2O_3 NPs (16.5 nm) and calcined-Fe_2O_3 NPs (25 nm) were investigated for their use in the removal of methylene blue (MB) dye from aqueous solution to see whether plant extract affected adsorption efficiency. When calcined Fe_2O_3 at 700°C was compared to biosynthesized Fe_2O_3 NPs, biosynthesized Fe_2O_3 NPs had a higher removal percentage (92%) than calcined Fe_2O_3 at 700°C (88%) against MB. The most critical topic in adsorption research is understanding the mechanism of adsorption. The dominant mechanism for the synthesized NPs is surface complexation via electrostatic interactions between cationic dyes and negatively charged Fe_2O_3 NPs, as confirmed by zeta potential measurements. The dye molecules ionized at the adsorbent surface, and these charges were stabilized by hydroxyl groups (OH^-), which aided the

adsorption process. Since MB is a cationic dye, it separates into MB^+ and Cl^- ions in an aqueous solution. The MB^+ ion interacts with the OH groups on the surface of Fe_2O_3 NPs through electrostatic interaction.

Similarly, clove bud extract was also used to make Fe_2O_3-Dy_2O_3 NPs that effectively removed the antibiotic ciprofloxacin (CIP) [98]. The NPs were nano-rice in c-FD, with a width of 55.6 nm and a length of 176 nm. The magnetic counterpart c-Fe_2O_3-Dy_2O_3 (c-FD) was generated by calcining FD at 700°C and then evaluated for CIP elimination. The FD and c-FD had BET surface areas of 112 and 41 m^2g^{-1}, respectively. For FD and c-FD, maximum adsorption capacities of 125 and 328 mg/g were obtained, respectively. For 40 ppm initial concentration of CIP, the maximum percentage removal of CIP was found to be 70% for FD and 53% for c-FD at an adsorbent dose of 1 g/L within 90 minutes (Figure 22). Furthermore, considering their robustness, nano adsorbents regeneration and recyclability NPs demonstrated excellent stability up to 5 cycles, which is beneficial for further application in water purification and treatment.

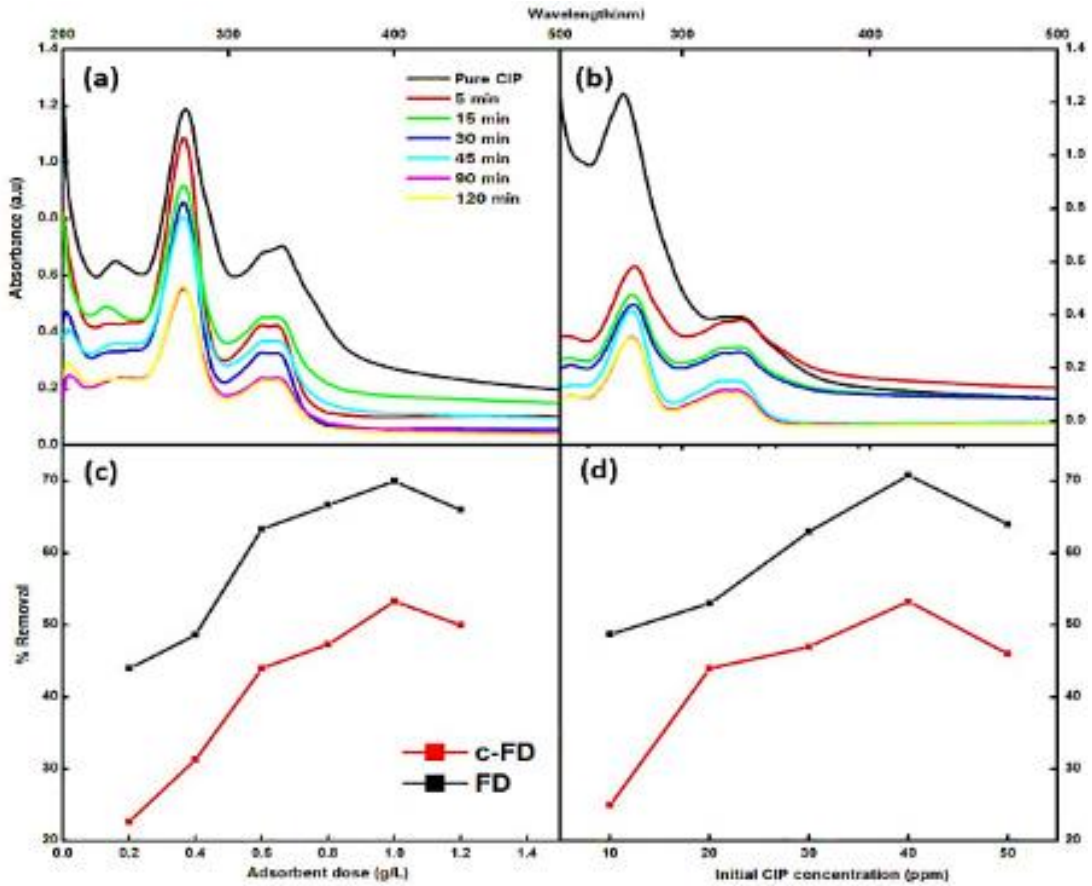

Figure 22 The effect of various parameters on CIP adsorption-(a) c-FD, (b) FD, (C) adsorbent dose and (d) initial CIP concentration. [Initial CIP Conc: 40 ppm, contact time: 90 min, adsorbent dose: 1 g/L, Temp: 298 K, pH: 7]. Reproduced with permission from Ref [98].

Jain *et al.* [99] demonstrated clove (*Syzygium aromaticum*) bud extract-mediated synthesis of Dy_2O_3 NPs for the selective detection of PA. TEM analysis revealed 16.5 ± 0.28 and 37.2 ± 0.24 nm size of Dy_2O_3 (amorphous) and calcined Dy_2O_3 (cubic crystal structure) NPs, respectively. These findings revealed that *Syzygium aromaticum* bud extract is important in reducing and stabilizing the

NPs. With a limit of detection (LOD) of 431.5 nM, the synthesized NPs showed excellent sensitivity and selectivity towards PA. The high Stern–Volmer constant (K_{sv}) of 4.19 × 104 M indicates that Dy_2O_3 NPs have a high PA selectivity. The sensing principle elucidates the quenching of Dy_2O_3 NPs' FL emission by PA as a consequence of electron transfer via electrostatic interactions among electron-rich PA molecules and electro-rich NPs (Figure 23). Because of the three $–NO_2$ groups on the benzene rings, PA is a heavy acid. Dy_2O_3 NPs, on the other hand, have a lot of –OH groups in an aqueous solution, so they're convenient to protonate. As a result of the addition of PA, Dy_2O_3 NPs got protonated in an aqueous solution.

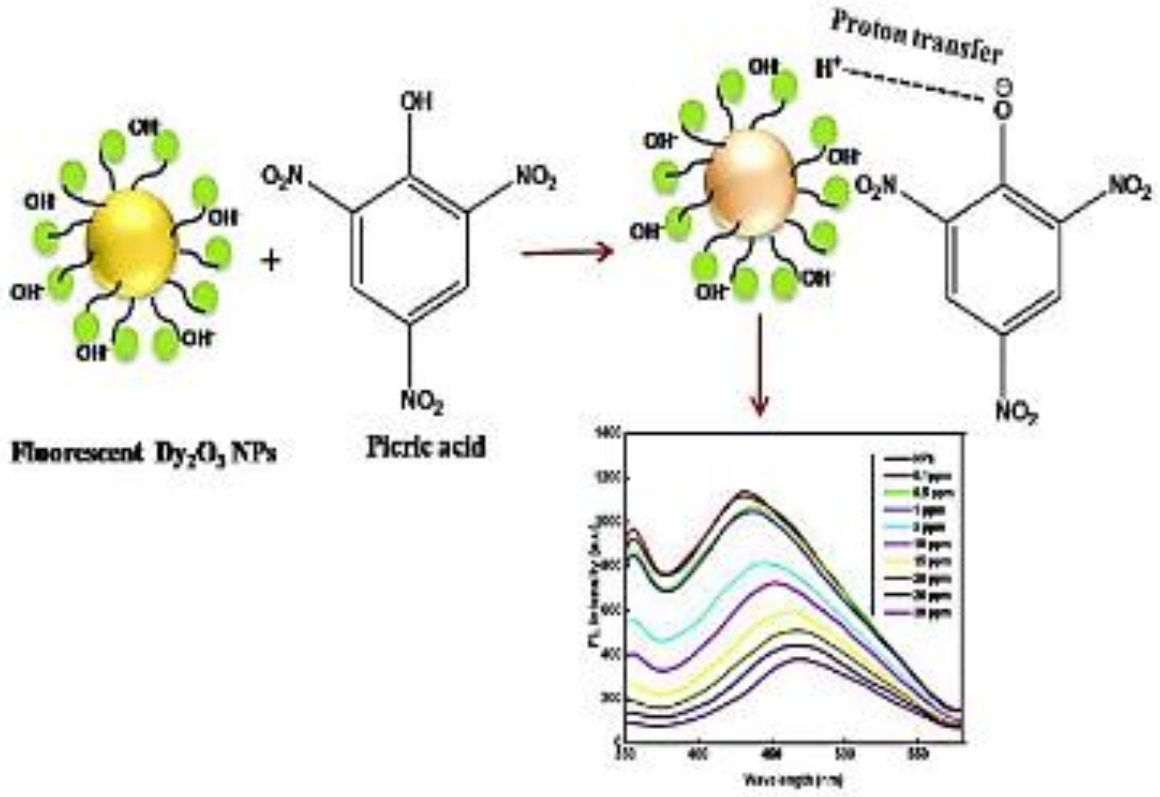

Figure 23 Schematic representation of PA sensing by Dy_2O_3 NPs. Reproduced with permission from Ref [99].

Citrus fruit extracts *i.e.,* Citrus limon (Cl-1), were used to demonstrate the green and environmentally sustainable syntheses of crystalline Ag NPs [100]. Only in the presence of sunlight does Cl-1 reduce Ag^+ ions into AgNPs. These green synthesized Cl-1–AgNPs demonstrated selective sensing of the toxic Hg^{2+} ion in water at micromolar concentrations. Specifically, sensor systems based on green synthesized Cl-1–AgNPs detected Hg^{2+} ions in water over a broad pH range (3.2 to 8.5). The electrochemical differences between Ag^+ and Hg^{2+} ions are crucial in sensing. The standard reduction potential for Ag is +0.80 V. In contrast, the standard reduction potential for Hg^{2+} is +0.92 V, and metals with higher reduction potentials serve as stronger oxidizing agents, according to the electrochemical sequence. Colorimetric sensing tests of Cl-1–AuNPs with various metal ions, including adding Hg^{2+}, revealed no major differences. In order to reveal the mechanistic role of citric acid in metal ion sensing, commercial citric acid was employed as a stabilizer in NPs synthesis in the presence of $NaBH_4$. It developed an AgNPs solution that was very light yellow (Figure 24). There was

no preferential sensing of any metal ions in the colorimetric experiments. These findings suggest that the synergistic influence of different chemical species present in the juice extract, rather than citric acid–citrate alone, is responsible for selective Hg^{2+} sensing of Cl-1–AgNPs at lower and higher pH.

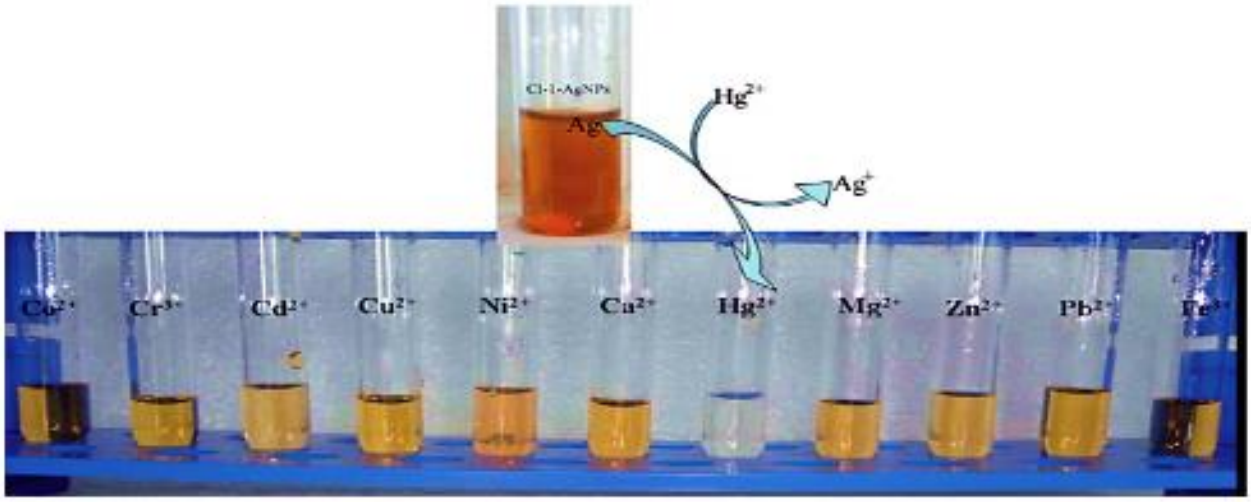

Figure 24 Cl-1–AgNPs selective sensing of Hg^{2+} in aqueous solution. Reproduced with permission from Ref [100].

Gold–palladium core–shell nanoparticles (Au@PdNPs) have been successfully synthesized *via* orange peel extract (OPE) which acted as a reducing as well as stabilizing agent [101]. The core AuNPs were first synthesized with OPE; then, the Pd shell was generated by reducing $PdCl_2^{4-}$ solution. According to TEM images, the Au@PdNPs had a core–shell configuration, with an average Au core diameter of 40 nm and a Pd shell thickness of 7 nm. By reducing the $AuCl^-_4$ and $PdCl_2^{4-}$ excess to produce more and bigger Au@PdNPs in the presence of HCHO, the Au@PdNPs performed a sensitive colorimetric detection against the HCHO sample. The UV–Vis specific absorbance of the solution increased as the concentration of HCHO increased, as did the color change of the solution from light to dark brown, which was visible to the naked eye. With an average LOD of 304.9 mM, linearity of the absorbance responses from the formaldehyde concentration range of 36.3 mM to 3.63 M (R^2 = 0.991) was achieved.

Aqueous leaf extract of Eucalyptus globulus (ELE) as a reducing, dispersing, and stabilizing agent is demonstrated for the biosynthesis of CuO NPs [102]. Terpineols, 2,6-octadienal-3,7-dimethyl, benzamidophenyl-4-benzoate, and β-eudesmol were found to be associated with the CuO NPs as ELE-capping, and are most likely involved in the nucleation and stabilization of ELE-CuO NPs. The intracellular uptake propensity of terpenoids encapsulated ELE-CuO NPs was significantly increased, as was the accumulation of intracellular reactive oxygen species, according to flow cytometric results. Compared to bare surface commercial nano-CuO and bulk sized CuO, ELE-CuO NPs killed planktonic cells of E. coli-336, P. aeruginosa-621, and methicillin-resistant *Staphylococcus aureus*-1 (MRSA-1) clinical isolates (Figure 25).

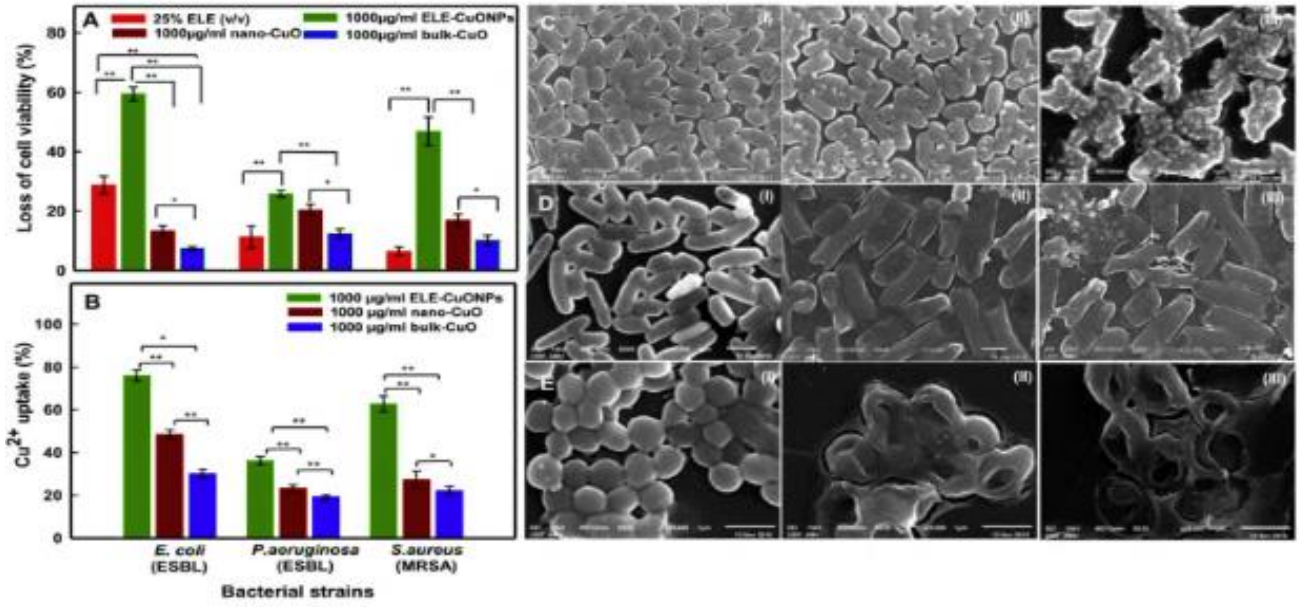

Figure 25 (A) The percentage cell viability loss in ESβL producing E. coli, P. aeruginous and MRSA isolates against ELE, ELE-CuONPs, bare nano-CuO and bulk-CuO (n = 6); (B) Graph showing the% of intracellular Cu^{2+} (1000 µg/ml) after exposure on the treated bacteria cells (n = 3); C, D and E depict the SEM images of the bacteria in the absence (I) and presence of 1000 µg/ml of bare surface nano-CuO (II) and ELE-CuONPs (III), respectively. Reproduced with permission from Ref [102].

The simple synthesis and differential bio-nano interface activities of terpenoid-capped bio-inspired CuO NPs with bacterial ELE surface and cell wall composition were demonstrated. CuO NPs-induced intracellular oxidative stress disrupts proteins involved in adhesion and biofilm formation, resulting in potent antibacterial and biofilm inhibition. Compared to commercially available nano CuO and bulk-CuO, indigenous terpenoids-capped bio-inspired CuO NPs are more stable and efficient antibacterial and antibiofilm agents.

Haroon *et al.* [103] fabricated Ag NPs that were environmentally friendly, stable, inexpensive, and possessed antimicrobial activity. *Azadirachta indica* leaf extract was used to conduct and optimize the green synthesis of AgNPs. When screened for antifungal activity, the green synthesized AgNPs showed significant growth destruction of *Penicillium sp., Fusarium sp.,* and *Aspergillus sp. Penicillium sp.* (92%), *Fusarium sp.* (89%), and *Aspergillus sp.* (89%) were the most sensitive to AgNPs among the test fungi (69%) after 6 days. Damaged cellular envelopes, bulging cells, and pit formation were observed after Ralstonia solanacearum was exposed to AgNPs (MIC/MBC 200/400 lg ml^{-1}). Powerful interactions of AgNPs with the cell wall affect the high surface energy and mobility of nanoparticles. It alters cellular respiration and metabolic activities in the process. Furthermore, the rapid attachment of AgNPs to bacterial surfaces increases ROS output and the release of other superoxides. This leads to increased porosity of cell membranes and allows nucleic acid to be released from the cell. According to the findings, the AgNPs synthesized in this study had sufficient anti-pathogenic potential and could be used as a cost-effective and safe alternative to non-toxic agrochemicals.

Bio-inspired NPs fabricated using various medicinal plant extracts achieved significantly greater antibacterial effects than bare surface micro- and nano-sized inorganic analogs and pure extracts.

Cherian *et al.* [104] demonstrated an exhaustive involvement of *M. fragrans* bio-actives in the dynamics of bio-synthesis of flower-shaped ZnO NPs (48.32 ± 2.5 nm) and their antibacterial and antibiofilm efficiency against MDR E. coli-336, MRSA-1, and MSSA-2 clinical isolates. MFLE-ZnO NPs substantially increased the zone of growth inhibition of E. coli-336 (17.0 ± 0.5 to 19.25 ± 1.0 mm), MSSA-2 (16.75 0.8 to 19.0 0.7 mm), and MRSA-1 (16.25 1.0 to 18.25 0.5 mm) in E. coli-336, MSSA-2 (16.75 ± 0.8 to 19.0 ± 0.7 mm), and MRSA-1 (16.25 ± 1.0 to 18.25 ± 0.5 mm), respectively. The minimum inhibitory concentrations (MIC) and minimum bactericidal concentrations (MBC) for E. coli-336, MRSA-1, and MSSA-2, were found to be 1500, 1000, and 500 µg/ml and 2500, 2000, and 1500 µg/ml. Respectively (Figure 26). The presence of pits and cavities in MFLE-ZnO NPs-treated strains led to loss of native rod and coccoid shapes (SEM images), resulting in cellular damage. At their MICs (1500 and 1000 µg/ml), E. coli-336 and MRSA-1 strains decreased biofilm generation by 51 and 24%, respectively. Internalization of MFLE-ZnO NPs is thought to increase oxidative stress, producing intracellular reactive oxygen species and eventually caused cell death.

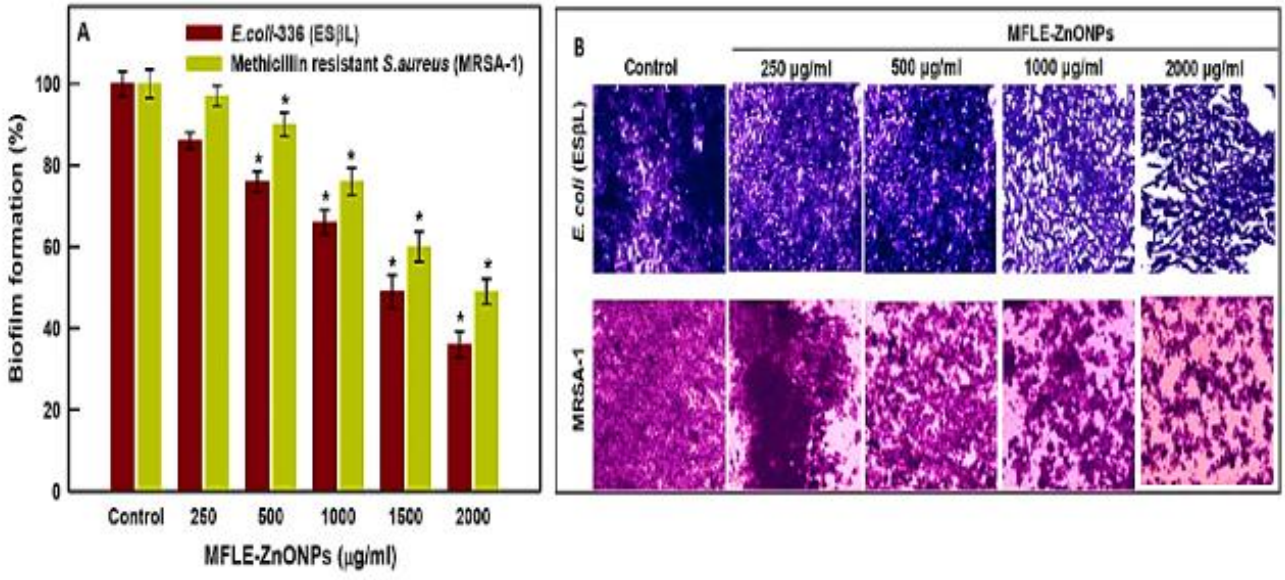

Figure 26 (A) Graph representing the decrease in biofilm formation with variation in MFLE-ZnONPs concentration (n = 3, *p < 0.05 vs control) and (B)Photomicrographs of the effect of MFLE-ZnONPs on biofilm formation of E. coli-336 and MRSA-1 at various concentration of control (i.e., absence of NPs), 250, 500, 1000 and 2000 µg/ml. Reproduced with permission from Ref [104].

6.2 Microbe-Mediated Synthesis

Microbial synthesis is an environment-friendly green route for the synthesis of NPs using microorganisms, such as, bacteria, actinomycetes, viruses, fungi, yeast, and algae [105]. It mainly requires an aqueous medium, minimal energy utilization and chemical-free routes. Microorganisms besides synthesizing NPs also act as templates for directional growth leading to multifaceted nanostructures [106].

6.2.1 Bacteria-Actinomycetes Mediated Synthesis

Bacteria can be conveniently sculpted and genetically engineered for the biomineralization of metal ions. They have inherited the name 'Nano factories' for NPs synthesis because of their higher yields, easy handling and convenient scaling-up process [107]. When bacteria are exposed to high-stress conditions in the surroundings, they develop various defense mechanisms which play a vital role in the synthesis of NPs. Intracellular sequestration, efflux pumps, change in metal ion concentration and extracellular precipitation facilitate the NPs fabrication [108].

The bacterial-mediated synthesis of NPs was first reported in 1980 by Beveridge and Murray [109]. They deposited Au NPs in the cell wall of *B. subtilis*. Carboxylic groups on the cell wall offered major sites for the deposition of NPs.

Recently, Singh *et al.* [110] demonstrated the synthesis of Ag NPs from the cell-free aqueous extract of the cyanobacterium *Leptolyngbya sp.* WUC 59, which was isolated from wastewater. The NPs formed were crystalline with a size range of 2-0-35 nm (Figure 27). The mechanism was not established but it was assumed that the biomolecules present in the cell extracts of cyanobacteria, such as sugars, proteins, peptides, polysaccharides, and pigments acted as reducing agents for the reduction of metal ions to form NPs. The Ag NPs suppressed the activity of *B. subtilis* and *E. coli* bacteria to a great extent.

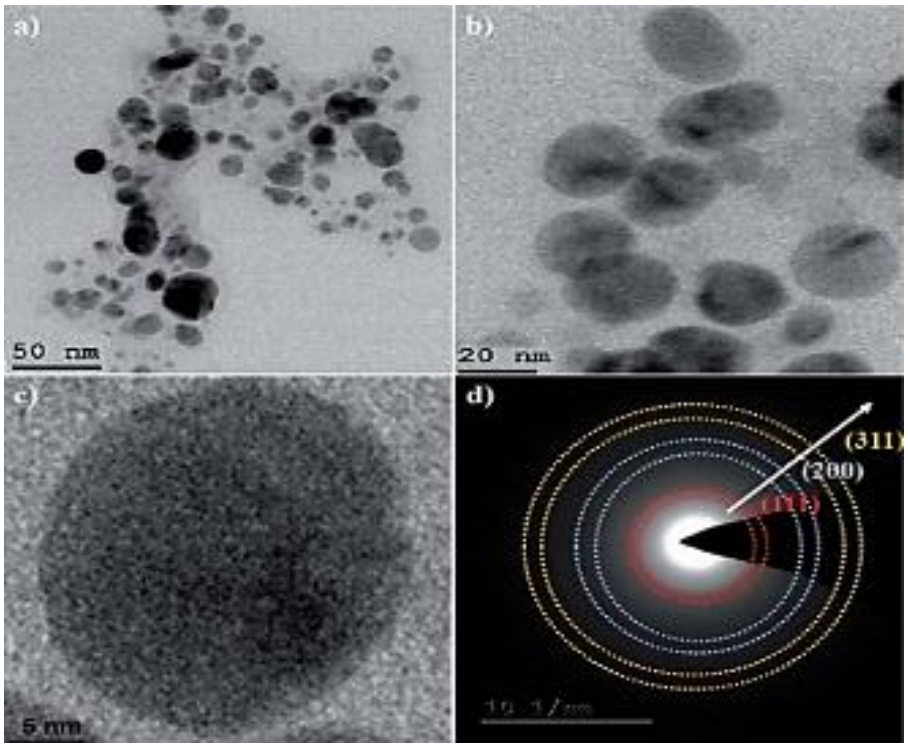

Figure 27 HRTEM images of Ag NPs at: (a) 50 nm; (b) 20 nm; (c) 5 nm bar scale and (d) SAED pattern of Ag NPs. Reproduced with permission from Ref [110].

While, Eadi *et al*. [111] have utilized the cyanobacterium *Nostoc* sp. EA03 (CEN) in the biogenic synthesis of ZnO NPs. Replacing carboxylic groups of bacterial cell extract with hydroxyl and methyl groups was responsible for the synthesis and stabilization of NPs. The synthesized NPs destroyed 24 hr old biofilm by up to 90% and had antibacterial activities against gram-positive and gram-negative bacteria. Further, Raj *et al.* [112] explored the extracellular polymeric substances (EPS) of the marine bacterium *P. aeruginosa* JP-11 for green synthesis of cadmium sulfide (CdS). EPS provided binding

sites for the metal ions and stabilized them to form NPs in size range of 21.54-38.28 nm. The CdS NPs displayed good adsorption potential for Cd^{2+} ions which is a harmful effluent in water.

Arsenopyrite ashes from the industrial site have been used to isolate Ochrobactrum sp. MPV1 bacteria. For example, Zonaro *et al.* [113] used this bacterium to reduce selenite and tellurite ions to their elemental state in different conditions along with forming NPs. The authors propose that the bioreduction of SeO_3^{2-} and TeO_3^{2-} ions was affected by glutathione (GSH) and NADH-based enzymes, respectively. Ahmed *et al.* [114] reported the synthesis of ultra-small Pd and Pt NPs from *Shewanella loihica (S. lochia)* PV-4 bacteria strain with the help of electrochemically active *S. logician* biofilms. The NPs were formed in size range of 2-3 nm and demonstrated great catalytic activity for the degradation of methyl orange dye.

Buszewski *et al.* [115] divulged the synthesis of Ag NPs from *Streptacidiphilus durhamensis* HGG16n actinomycete strain isolated from acidic forest soil. The NPs synthesized were formed in size range of 8 to 48 nm (Figure 28). They suggested that proteins from the bacteria strain were responsible for the synthesis of NPs. The formed biogenic NPs had great antimicrobial properties against *P. aeruginosa, S. aureus, and P. mirabilis,* followed by *E. coli, K. pneumonia, and B. subtilis.*

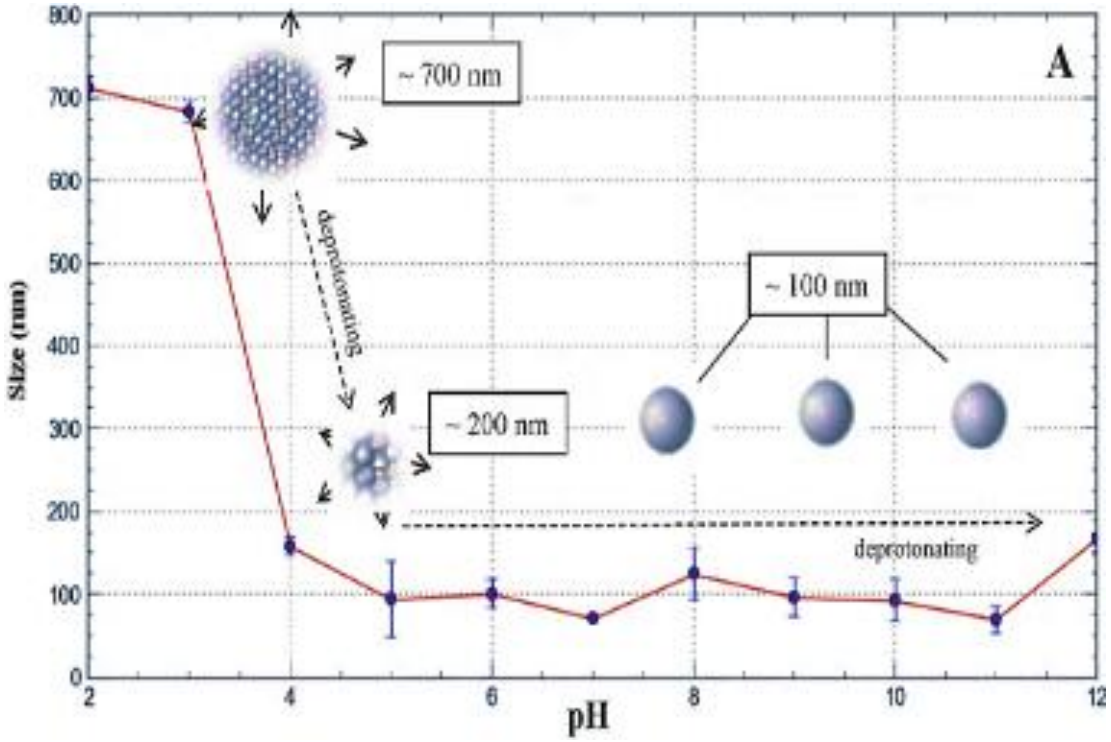

Figure 28 Size of the bio AgNPs and their activity according to pH value. Reproduced with permission from Ref [115].

Ag NPs were also fabricated from two marine-derived actinomycetes isolates-*Streptomyces* sp. 192ANMG (F2) and *Streptomyces* sp. 17ANMG (F7) including both the bacterial supernatant (F) and their cell filtrate (C) [116]. It was a safe, efficient and energy-conserved synthesis for NPs. The synthesized NPs showed the potential to o eradicate bacterial biofilm formation of four pathogenic bacteria (S. aureus, P. aeruginosa, B. subtilis, and E. coli). They had antimicrobial properties against yeast, gram-positive and gram-negative bacteria.

Hassan *et al*. [117] reported an endophytic actinomycete Streptomyces capillispiralis Ca-1, isolated from a healthy medicinal plant (*Convolvulus arvensis*), for its synthetic activity. They synthesized monodisperse and spherical Cu NPs in size range of 3.6-59 nm. The biosynthesized NPs demonstrated activity against infectious microorganisms and biocontrol of phytopathogenic fungi that represent the hopeful uses of Cu NPs in wastewater treatment.

6.2.2 Fungi- and Yeast-Mediated Synthesis

Fungi are a better biological agent than bacteria and viruses for the production of monodispersed NPs having well-defined surface morphologies with higher productivities because of the presence of a variety of active metabolites such as enzymes, organic acids, proteins or reducing components on the cellular surfaces or inside the fungal cell [118]. Fungi possess higher bioaccumulation ability towards metal ions, making the synthesis of NPs a cost-effective, efficient and easy-to-handle process. Enzymatic reduction on the cellular surfaces or within the cell is specifically involved in the plausible explanations for NPs formation. The production of NPs through the reduction of enzymes (reductase) present in the cell wall, in the cytoplasmic membrane, and on the inner surface of the fungal cell involves intracellular biosynthesis [119].

Venkatesh *et al.* [120] demonstrated nanoceria (CeO_2) formation using the plant pathogenic fungus *F. solani.* The spherical-shaped NPs lay under the size range of 20-30 nm. The FTIR data indicated that various proteins, amino and other heterocyclic compounds were responsible for reducing metal ions. The NPs exhibited antibacterial activities against various bacteria in the order *P.aeruginosa* > *K.pnemoniae* >*E.coli* > *S. aureus*, inhibiting the bacteria's respective biofilm formation.

Reaction parameters such as pH, salt concentration, reaction time and temperature greatly influence the size and yield of fungi-mediated synthesized NPs. For example, Bhargava *et al.* [121] synthesized Au NPs using *C. oxysporum* fungal species reporting that the maximum yield of NPs was obtained when the salt concentration was 1 mM with biomass to water ratio of 1:5 at pH 7. The synthesized NPs showed excellent catalytic activity for degrading rhodamine dye within 7 mins.

Mishra *et al.* [122] used *Trichoderma viride* (*T. viridian*) and *Hypocrea li xii fungus* to synthesize Au NPs as triangular, rods and hexagons with an average size of 60 nm within 10 mins. The NPs were a great biocatalyst for reducing 4-NP to 4-AP and had antibacterial activities. More fungal strains like *F. oxysporum sp. cubense* JT1, *Botrytis cinerea*, *Nigrospora oryzae, and Rhizopus oryzae* were used for the green fabrication of Au NPs.

Gudikandula *et al*. [123] synthesized Ag NPs from *Schizophyllum radiatum* also called as white rot fungus. The NPs were well dispersed with size range from 15-20 nm. The extracellular biomineralization stabilized the NPs. The NPs showed excellent antibacterial activities against gram-positive and gram-negative bacteria. Tyagi *et al.* [124] divulged the extracellular synthesis of Ag NPs using an entomopathogenic fungus (*Beauveria bassiana)* (Figure 29). The NPs formed had different shapes-triangular, circular, and hexagonal with sizes ranging from 10-50 nm. These small NPs showed antibacterial activity. Similarly, various other fungal strains can be used for Ag NPs syntheses such as *Trichoderma harzianum, F. oxysporum, Curvularia lunata, Metarhizium anisopliae, Neurospora crassa, Trichoderma reesei, Aspergillus niger, Penicillium brevicomaactum* and *Aspergillus flavus* CR500 [125].

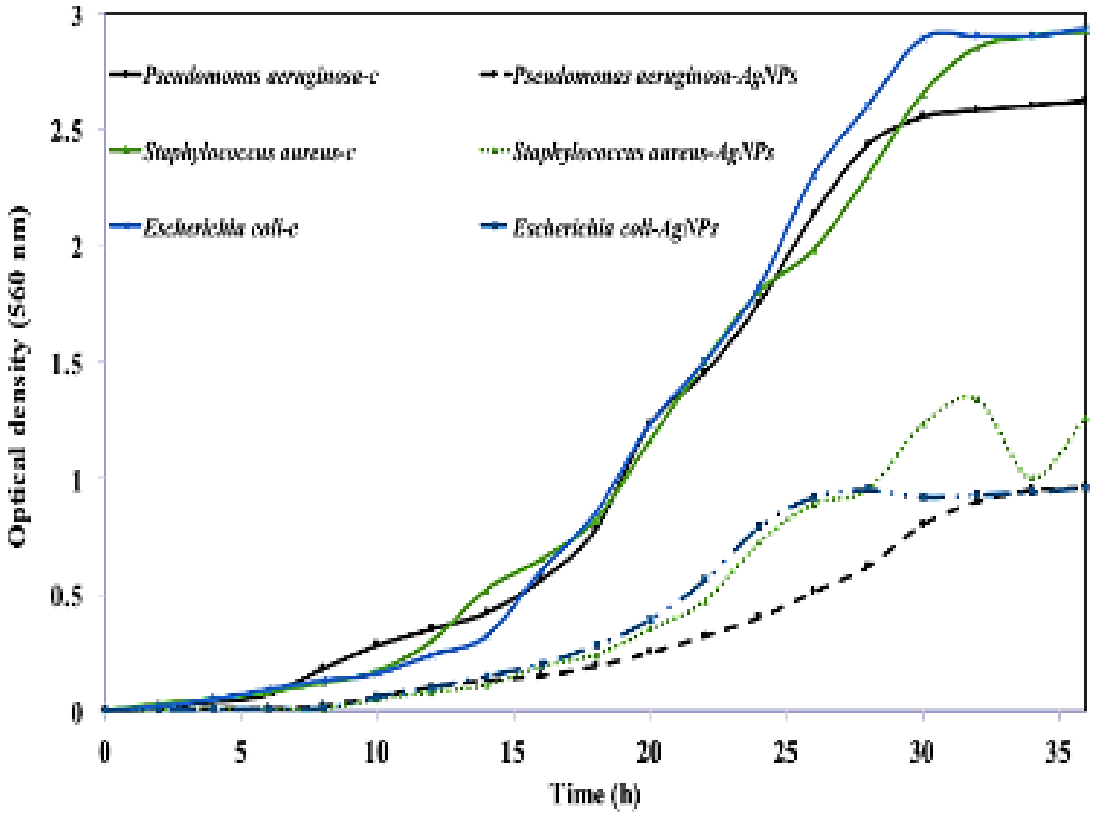

Figure 29 Growth kinetic of bacterial species without and with AgNPs synthesis from B. bassiana at 560 nm. (c: control and AgNPs: in the presence of Ag NPs). Reproduced with permission from Ref [124].

Bhadwal *et al.* [126] used *Trichoderma harzianum* fungal strain for the green synthesis of CdS NPs. The NPs were formed in a 4-5 nm size range with crystalline nature and spherical morphology. The amine groups of the fungal protein interacted with the CdS NPs which stabilized the NPs to a great extent. Their photocatalytic activity to degrade MB dye was evaluated to be 37.15%. Baskar *et al*. [127] reported a nano-composite comprising ZnO NPs and L-asparaginase metalloproteins, both produced by *Aspergillus terreus* fungus. The nano-composite was formed in size range of 28-63 nm. The proteins released by fungus were responsible for the reduction of metal ions along with the production of L-asparaginase.

Yeast is a single eukaryotic-celled organism belonging to the kingdom of fungi. It is easy to control yeast in laboratory circumstances and the ability of yeast to accumulate and adsorb toxic metal ions from their surroundings. Yeast deploys various mechanisms like bio-precipitation, chelation and intracellular sequestration for detoxification, which various researchers have utilized for NPs synthesis [128].

Seshadhari *et al.* [129] synthesized PbS NPs from a marine yeast, *Rhodosporidium diobovatum* using lead nitrate as a precursor. Crystallite size as determined from TEM was estimated in the 2-5 nm range with a lead to sulphide ratio 1:10. *R. diobovatum* yeast presented a favorable parameter compared to terrestrial yeast such as *Schizosaccharomyces pombe* and *Torulopsis*. It facilitated the fabrication of PbS NPs even when Pb2p was introduced simultaneously with the inoculum, contrary to injecting metal ions in the mid-log growth phase. Thus, the *R. diobovatum* method does not require growth phase monitoring, making it appropriate for bulk PbS NP production.

In a recent study, Elahian *et al.* [130] synthesized Ag NPs using a genetically modified yeast, *Pichia pastoris (P. pastors)*. To reduce metal ions into NPs, an engineered *P. pastoris* strain overexpressed a metal-resistant gene, cytochrome b5 reductase enzyme, obtained from *Mucor racemosus*. This enzyme helped form stable and homogenous Ag and Se NPs wihtin the size range of 70-180 nm.

6.2.3 Algae-Mediated Synthesis

Algae are a large and diverse group of photosynthetic eukaryotic organisms that are abundant in secondary metabolites, proteins, and peptides; and are easy to cultivate, have fast growth, and are scalable. Over the recent years, Algae has been exploited as nano factories for NPs synthesis with the exceeding use of brown, red, blue-green, micro and macro green algae [131]. Algae have huge potential for metal take up, making the synthesis process rapid and cost-effective.

Sargassum bovinum, a brown seaweed qenus, was utilized to fabricate monodispersed octahedral Pd NPs in size range of 5-10 nm [132]. The FTIR data elucidated the importance of polyol and polysaccharides extracted from the *Sargassum* alga in reducing and capping the Pd NPs. Further, they successfully developed Pd NPs modified carbon ionic liquid electrode (PdNPs/CILE) for the sensing of H_2O_2 with high selectivity, high sensitivity (of 284.35 mA mM^{-1} cm^{-2}) and sensing in the range of 5.0-15.0 mM.

Ramakrishna *et al*. [133] explored two brown algae *Turbinaria conoides* and *Sargassum tentorium, to synthesize* Au NPs using aqueous algal extracts. Brown algae are a rich source of polysaccharides with inherent reduction capacity. The OH groups of the secondary metabolites interact with the metal NPs, thereby capping and stabilizing them. The size of polydispersed NPs was near 35 nm. These NPs acted as an efficient catalyst for the degradation of nitro compounds (4-NP to 4-AP) and various dyes such as RhB and Sulforhodamine 101 (Figure 30).

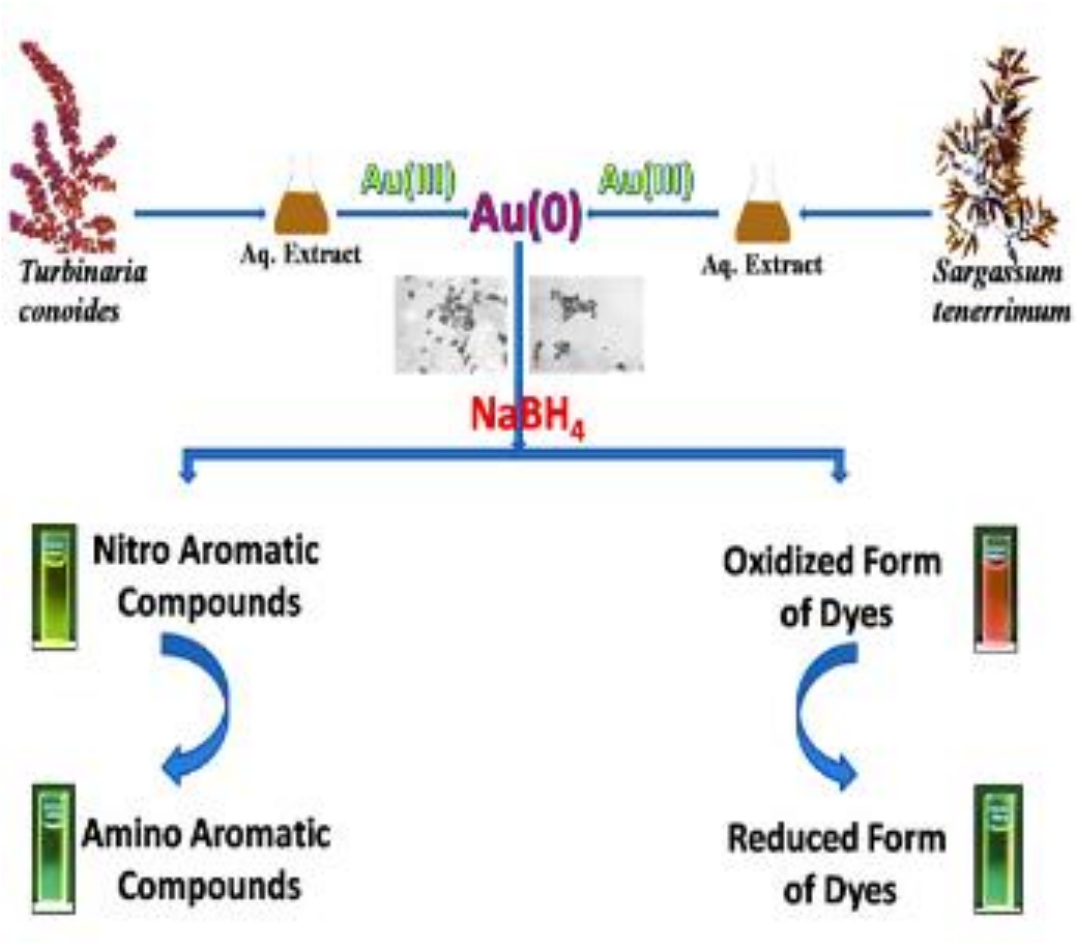

Figure 30 Green synthesis Au NPs from Turbinaria conoides from Sargassum tentorium and its Catalytic application. Reproduced with permission from Ref [133].

Pugazhendi *et al.* [134] used marine red algae *Gelidium mansion* to synthesize spherical-shaped Ag NPs within the size range of 27-54 nm. The carbonyl groups of the amino acids of algal proteins had a strong affinity towards Ag NPs. They acted as capping agents to avoid agglomeration and stabilize the NPs. The Ag NPs showed significant activity against biofouling in gram-positive and gram-negative bacteria with a 99% reduction of the microfouling film.

Salem *et al*. [118] were able to successfully synthesize Fe_3O_4 NPs using brown (Colpomenia sinuosa) and red (Pterocladia capillary) seaweed aqueous extracts. The SEM images elucidated the size of 11.24-33.71 and 16.85-22.47 nm for two types of Fe_3O_4 NPs samples synthesized by C. sinuosa and P. capillary aqueous extracts, respectively. The FTIR results confirmed the involvement of the (NH)C=O group of cyclic peptides in the biosynthesis and stabilization of NPs. The NPs showed antibacterial activity against gram-positive and gram-negative bacteria and possessed excellent antifungal properties.

6.2.4 Virus-Mediated Synthesis

A virus is a small collection of genetic code, either DNA or RNA, surrounded by a protein shell requiring a host body to replicate. The outer thick surface coating of multifunctional proteinaceous shell-capsid surrounds the genomic material. It provides a surface for interacting with metallic ions for size and shape-controlled synthesis of desired nanostructured material [135].

Viruses hold great promise in assembling and connecting novel nanosized components, enabling organized NPs assemblies to be created. They make a good scaffold for molecular assembly into nanoscale devices due to their size, monodispersity, and diversity of chemical groups available for alteration [135]. Tobacco mosaic virus (TMV) [136] was used as a model for synthesizing iron oxides by oxidative hydrolysis, co-crystallization of CdS and PbS, and synthesizing SiO_2 by sol-gel condensation. This was achieved on the external surface of the virus with the aid of external glutamate and aspartate groups. TMV consists of helically arranged protein subunits that generate a hollow protein tube as a prototype for various nanotube fabrications.

In the crystalline capsid of the virus, M13 bacteriophages, peptides like A7 and J140, which can nucleate ZnS and CdS nanocrystals, were expressed as pVIII fusion proteins. Using a pVIII phage monitor, these structured template peptides (A7/J140-pVIIIM13) were selected and exposed to semiconductor precursor solutions. It was observed that ZnS nanocrystals assembled on the viral capsid were hexagonal wurtzite of around 5 nm or CdS assembled as 3-5 nm nanowires. With a dual peptide virus designed to express A7 and J140 inside the same viral capsid, hybrid nanowires (ZnS-CdS) were also achieved [137, 138].

6.2.5 Enzyme-Mediated Synthesis

Enzymes have become very attractive in a wide range of industrial processes over the last few decades, including biocatalysis, bioremediation, biomedical applications and biosensors, with the articulated goal of reducing the consumption of energy and raw materials, as well as the production of waste and toxic by-products. In addition, enzymes may also be used to functionalize the formation of different NPs and stabilize them [105].

García *et al.* [139] reported the green synthesis of Cu nanohybrids such as Cu(0), Cu(II) or $Cu_3(PO_4)_2$ using *Candida antarctica lipase* B enzyme (CAL-B). The NPs formed could be tailored by changing various conditions like pH, incubation time, or enzyme concentration. In the final formulation of NPs, the enzyme plays an important function, both enabling the good dispersion of the NPs and deciding their size, which was demonstrated by decreasing the size of the NPs upon using a higher amount of protein. Out of all the nanohybrids, the Cu-CALB-PHOS-NR $Cu_3(PO_4)_2$ NPs which comprised 70% Cu(I) in the form of Cu_2O and 30% of Cu (0) showed the best catalytic performance for the conversion of carcinogenic benzene to phenol.

Shi *et al.* [140] probed into the mechanistic approach of Fe_3O_4 NPs morphological growth including nanosheets, nanorods, and nanospheres using the Urease enzyme (Figure 31). Urease is a hydrolytic enzyme that acts as a catalytic and templating reagent. It induced the nucleation of Fe_3O_4 NPs as it catalyzes the hydrolysis of urea, thereby increasing the pH slowly and providing the appropriate mild reaction conditions for forming Fe_3O_4 NPs with different morphologies. The morphologies of Fe_3O_4 NPs are controlled by simply adjusting the reaction temperature with no addition of any other organic reagent or polymer dispersant. The synthesized NPs were used for the adsorption of CR dye from water with the maximum adsorption percent of 87.08%, 78.46% and 68.14% for nanosheets, nanorods and nanospheres, respectively.

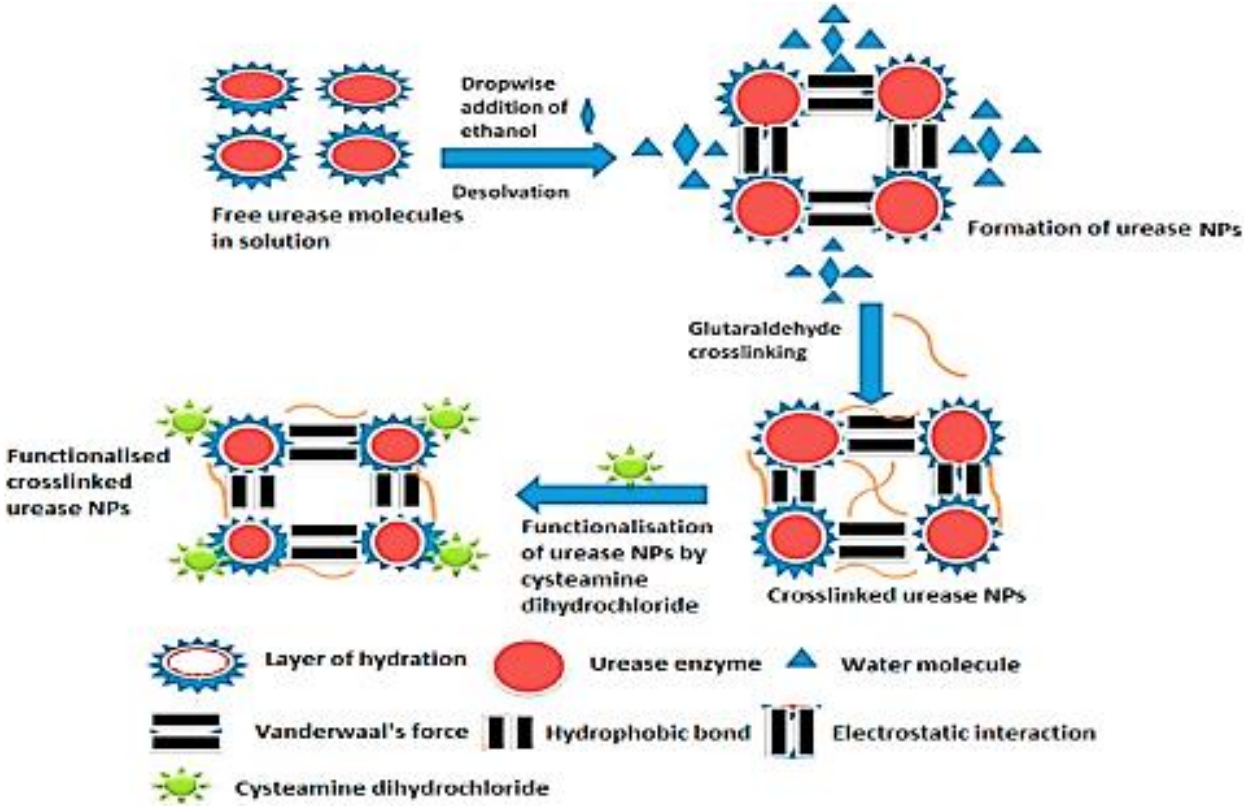

Figure 31 Schematic representation of Crosslinked urease NPs aggregates formation by desolvation process. Reproduced with permission from Ref [140].

Khan *et al.* [141] explored the green synthesis of Au NPs using purified SDS-resistant sulfite reductase enzyme. The NPs formed were monodisperse, spherical with 2-6 nm diameters. The enzyme catalyzed the reduction of Au^{3+} to Au^0 when NADPH donates electrons to sulfite reductase to reduce sulfite to hydrogen sulfide and water. The proteins capped the NPs stabilizing them and preventing agglomeration. The enzyme which acted as a reducing agent for forming Au NPs and the protein for the capping of NPs are derived from the same source *i.e., Thermomonospora sp.*

As discussed above the biogenic synthesis of NPs has gained a trend that promotes environmental sustainability. It exhibits improved characteristics than physical or chemical synthesis routes such as high costs, greater energy consumption, complex reaction conditions and toxicity. Hence the gained momentum of these bio-inspired approaches can be utilized in various aspects to provide multiple functionalities, and dimensions to the fabrication of NPs for wastewater treatment. Some of these aspects are enlisted in Table 1 which depicts the various approaches for some metal NPs synthesis.

Table 1 Various routes for green synthesis of metal NPs and their application in Water Remediation.

S. NO	METAL	GREEN METHOD FOR SYNTHESIS	MORPHOLOGICAL CHARACTERISTICS	APPLICATION IN WATER REMEDIATION
		Plant mediated synthesis		
1.	**Gold (Au)**	*Abelmoschus esculentus (seed extract)* [142]	Spherical (45-75 nm)	Antifungal activity against *P. graminis, C. albicans*

Crinum latifolium (leaf extract) [143]	Multi-shaped including spherical, triangular, and octagonal structures (17.6 nm)	Degradation of 4-NP, Dyes-MO and Rh B; Antibacterial properties
Croton sparsiforus (leaf extract) [144]	Spherical (16-200 nm)	Antibacterial properties against *S. epidermidis* and *E. coli*
Citrus maxima (fruit extract) [145]	Rod and Spherical (25 ± 10 nm)	Catalytic reduction of 4-NP
Litsea cubeba (fruit extract) [72]	Spherical (8-18 nm)	Catalytic reduction of 4-NP
Bacteria mediated synthesis		
Actinomycete *Gordonia amarae* [146]	Spherical (15–40 nm)	Detection of Cu ions
Streptomyces fulvissimus [147]	Spherical (10-50 nm)	Antifungal activity
Staphylococcus epidermidi [148]	Spherical (20-25 nm)	MB degradation
Nocardiopsis sp. MBRC-48 [149]	Spherical (11.57 ± 1.24 nm)	Antimicrobial against-*S. aureus* and *Calbicans;* and antioxidant property
Streptomyces griseoruber [150]	(5-50 nm)	Dye degradation
Yeast mediated synthesis		
Candida parapsilosis ATCC 7330 [151]	Cubic (10-20 nm)	Reduction of nitroarenes and substituted nitroarenes to amino-arenes
Magnusiomyces ingens LHF [152]	Spherical and pseudo-spherical (20.3-28.3 nm)	Reduction of nitrophenols (*i.e*., 4-NP, 3-NP and 2-NP)
Algae mediated synthesis		
Galaxaura elongate [153]	Rod, triangular, truncated triangular and hexagonal shapes (3.85–77.13 nm)	Antibacterial activity against ***E****. coli*, *K. pneumoniae* and MRSA, *S. aureus* and *P. aeruginosa*
Blue green alga *Spirulina platensis* [154]	Spherical (2-8 nm)	Antibacterial efficacy against Gram positive organisms-*B. subtilis* and *S.aureus*
Virus mediated synthesis		
Bacteriophage [155]	Varied shaped viz., spheres, hexagons,	Antibiofilm activity against *P. aeruginosa*

			triangles, rhomboids and rectangular (20-100 nm)	
		Fungi mediated synthesis		
		Cladosporium cladosporioides [156]	100 nm	Antibacterial and antioxidant activities
		Trichoderma harzianum [122]	Spherical (26-34 nm)	MB degradation; antibacterial activity
		Aspergillus terreus IF0 [157]	Elongated, triangular and rod shaped (10-19 nm at pH 10)	Antibacterial activity against gram positive bacteria
2.	**Silver (Ag)**	***Plant mediated synthesis***		
		Salt-marsh plant *Sesuvium portulacastrum L.* (leaf extract) [158]	Spherical (20-90 nm)	Antimicrobial and antibacterial
		Morinda tinctoria (leaf extract) [159]	Spherical and rod shape (79 to 96 nm)	Degradation of MB
		Zanthoxylum armatum (leaf extract) [160]	Spherical (36 nm)	Degradation of Safranine O, MR, MO and MB
		Citrus sinensis (peel extract) [161]	Spherical (10-35 nm)	Antibacterial activity against *E. coli*, *P. aeruginosa* and *S. aureus*
		Azadirachta indica (leaf extract) [162]	(38-42 nm)	Adsorbents for azo dye
		Bacteria mediated synthesis		
		Cyanobacteria [163]	Spherical (140 nm)	Photodegradation of MB and antibacterial activity against *B. subtilis, E. coli* and *S. aureus*
		Leuconostoc lactis [164]	Spherical (30-60 nm)	Degradation of azo dye and antibacterial activity
		Bacillus licheniformis Dahb1 [165]	Spherical (18.69 to 63.42 nm)	Antibiofilm activity against *P. aeruginosa* and *S. epidermidis*
		Yeast mediated synthesis		
		Dry baker's yeast [166]	Spherical (13.8 nm)	Antibacterial activity against *E. coli*
		Saccharomyces cerevisiae [167]	Spherical (10 nm)	Photodegradation of MB
		Algae mediated synthesis		
		Spirogyra varians [168]	Quasi spheres (17.6 nm)	Antibacterial activity against *S. aureus, B.*

				cereus, L. Monocytogenes, S. typhimurium, E. coli, P. aeruginosa and *Klebsiella*
		Red algae-*Gracilaria corticate* [169]	Spherical (100 nm)	Photocatalytic degradation of MG
		Pithophora oedogonia [170]	Cubic and hexagonal (25-44 nm)	Antibacterial activity against *E. coli, P.aeruginosa, V.cholera, Shigella flexneri B. subtilis, S. aureus* and *M. luteus*
		Hypnea musciformis (a red alga) [171]	Cubic and spherical (2–55.8 nm)	Photocatalytic degradation of MO
		Fungi mediated synthesis		
		Arthroderma fulvum [172]	Spherical (20.56 nm)	Antifungal activity against *Candida* spp., *Aspergillus* spp. and *Fusarium* spp.
		Endophytic fungal extract of *Pestalotiopsis versicolor* [173]	Spherical (Variable size)	Azo dye-degrading against CR, Rh B and Orange G and antibacterial activity against gram positive and gram-negative bacteria
		F. oxysporum [174]	Spherical (24 nm)	Anti-bacterial activity against *E. coli*
		Rhodotorula glutinis [175]	Spherical (15.45 ± 7.94)	Antifungal activity; degradation of nitrophenol and MB
		Trichoderma spp. [176]	pH dependent size	Anti-bacterial activity against gram negative bacteria
		Plant mediated synthesis		
3.	**Platinum (Pt)**	*Quercus glauca* (leaf extract) [177]	Spherical (5-15 nm)	Detection and Electrochemical oxidation of hydrazine
		Pinus resinosa (bark) [178]	Irregular shape (6-8 nm)	Catalytic oxidation of alcohols and reduction of 4-NP to 4-AP
		Coffea Arabica (seed extract) [179]	Spherical (2 nm)	Catalytic reduction of 4-NP and MB and their mixture
		Taraxacum laevigatum [180]	Spherical (2-7 nm)	Antibacterial activity against *P. aeruginosa* and *B. subtilis*

		Boswellia serrata (gum extract) [181]	Spherical (4.4 ± 0.5 nm)	Selective sensing of mercuric ions
		Bacteria mediated synthesis		
		Shewanella loihica (*via* biofilm) [114]	Spherical (2-7 nm)	Degradation of MO dye
		Desulfovibrio vulgaris [182]	Irregular shape	Removal of Pharmaceutical products-ciprofloxacin, sulfamethoxazole, ibuprofen and 17β-estradiol
		Algae mediated synthesis		
		Green alga *Botryococcus brauni* [182]	Cubical, spherical, and truncated triangular (86.96 nm)	Antimicrobial potential against bacterial and fungal species and antioxidant efficacy
		Fungi mediated synthesis		
		F. oxysporum [183]	(25 nm)	Antioxidant, antimicrobial activity against bacteria and algae and degradation of MO
		Penicillium oxalicum [184]	Spherical (4 nm)	Degradation of MB
4.	**Palladium (Pd)**	***Plant mediated synthesis***		
		Sapium sebiferum (leaf extract) [185]	Spherical (5 nm)	Photocatalytic degradation of MO and antibacterial activity against *S. aureus* , *B. subtilis* and P*. aeruginosa*
		Pinus resinosa (bark) [178]	Spherical shape (16-20 nm)	Catalytic oxidation of alcohols and reduction of 4-NP to 4-AP
		Cotton boll peels [186]	Spherical (4-20 nm)	Degradation of toxic azo-dyes
		Pimpinella tirupatiensis (plant extract) [187]	Spherical (12.25 nm)	Degradation of CR dye
		Prunus yedoensis tree (gum extract) [188]	Spherical and oval (10-50 nm)	Antifungal activity against *C. acutatum and C. fulvum* phytopathogenic fungi
		Bacteria mediated synthesis		
		Shewanella loihica [114]	Spherical (2-7 nm)	Degradation of MO dye
		Shewanella oneidensis MR-1 [189]	Spherical (200-250)	Electrocatalysts
		Yeast mediated synthesis		

Saccharomyces cerevisiae [190]	Cubic structure hexagonal shape (32 nm)	Photocatalytic degradation of direct blue 71
Algae mediated synthesis		
Sargassum bovinum [132]	Octahedral (5 nm)	Detection and electrocatalytic reduction of H_2O_2
Green alga *Botryococcus brauni* [191]	Cubical, spherical, and truncated triangular (4.89 nm)	Antimicrobial potential against bacterial and fungal species and antioxidant efficacy

7. Current Challenges and Future Perspective

The emerging paradigm of Green Nanoscience is confronted by significant research challenges to deliver efficient water solutions while minimizing the risk to individuals and ecology. The implementation of Green Chemistry principles provides a pedestal for the development of synthetic methodologies and nanomaterial framework. The demand for large-scale production of homogeneous and functionalized NPs requires intensive insights to evolve green nanoscience from the discovery stage to the production level. However, carefully scrutinizing the examples described in this review suggests much to learn in green synthesis. Small steps must be taken to overcome the synthetic challenges for smooth transitioning towards green nanosynthesis. The key factors that need to be addressed are:

7.1 Greener Design and Modification

Designing NPs with low ecological impact and desired physical properties is a prerequisite for the budding arena of green nanoscience. The task of fabrication of NPs with high uniformity, purity, robustness and homogeneous nature is enormous. A deep understanding of the green synthetic approaches along with their mechanistic studies using enhanced nano-enabled analytical methods is important. Understanding the fabrication methodology will help develop activity-specific NPs, as material science has developed a deep relationship between nanomaterial structure and a specific activity. However, a lack of comprehension of fundamental mechanisms and modeling factors creates hurdles in developing more flexible and precise microanalysis and detection methods. Optimized analytical methods and trained manpower will allow NPs to be routinely analyzed for composition, structure, and purity. Pertinently, there is a need for analytical methods and technologies real-time, *in-situ* monitoring to optimize manufacturing processes. This will facilitate minimized waste generation and energy costs and provide mechanistic evidence. The mechanism of the utility of NPs in remediation can be understood via active site accessibility, surface tuning and understanding the adsorption kinetics [192]. Various analytical tools can be employed in elucidating the effect on the removal efficiency of NPs.

Design efficient routes of purification that provide access without producing significant quantities of solvent waste to pure nanomaterials. The existence of pure NPs samples or those with well-defined impurity profiles for applications will be needed as nanoscience transitions from the discovery stage to commercialization. Furthermore, for research dedicated to developing structure-

activity relationships it is required to predict the physical properties and reactivity of metals. The complexity of integrating and structuring systems requires metrics or other frameworks for comparing the greenness of competing approaches. This will consider the potential risks and efficiencies of the immediately applicable conversion and the relative impacts of each process within a wider life cycle. Along with it, it is pertinent to adopt fundamental R's *i.e.* recycling/reuse/regeneration. Such metrics continue to be developed, but will become enormously helpful in determining the selection of strategies, notably during the scale-up of reactions and the emergence of new, greener approaches to NPs synthesis. Hence, it is desirable in the real world that the properties, behavior, and types of nanomaterials should be enhanced to meet the points outlined above.

7.2 Lab to Field Scale

Currently, laboratory nanomaterial syntheses are only capable of delivering small quantities of products and are plagued by batch-to-batch deviations. This restricts the scaled-up development of nanomaterials and contributes to ambiguity in key features such as size and shape. Therefore, the design of scalable synthesis schemes is a key challenge facing the practical application and industrialization of nanomaterials. One of the recent problems that emerged in water pollution is oil spillage. Several methods have been employed for oil removal at the lab scale such as using graphene NPs with excellent oil recovery [193]. However, the upscaling of the NPs for large-scale commercial use is an extremely tedious task.

Further a compelling need for consistent, efficient and scaled-up synthesis strategies is of utmost importance. On the other hand, costly reagents and strict reaction conditions have hampered the production of many nanomaterials on a large scale using conventional technologies. However, the use of a continuous flow system allows costly solvents and surfactants to be recycled through properly engineered separation and purification schemes. Therefore, it can therefore be used for low-cost, high-throughput commercial nanomaterial manufacturing.

7.3 Nanotoxicity

Nanotoxicity is the toxicity of NPs dealing with the threat they pose to humans and the ecosystem [194]. The toxicity of NPs is attributed to their shape, size and greater surface area to volume ratio. We can say that NPs enter our ecosystem in two steps, once when their manufacturing occurs and the next when they are used in the treatment plant and get released into the water. Hence they enter our drinking lines, thereby entering our bodies. Nanotoxicology is an attention-seeking field these days and we need to have measures to prevent it so that we can incorporate nanomaterials in real life in wastewater treatment at a large scale. Minimizing public and environmental health risks could be achieved by decreasing the potential exposure through NPs immobilization onto reactor surfaces or support media. It is important for NPs that release toxic metals to control their dissolution by using stabilizing coatings or optimizing NPs' shape and size. The use of safer nanomaterials whose constituents are inherently non-hazardous should be considered [195].

To project the effect of AG NPs on aquatic fauna, Kakakhel *et al.* [196] studied *C. carpio (*freshwater fish) when it was exposed to blood-mediated Ag NPs for toxicity, mortality, bioaccumulation, and histological alterations. No behavioral changes were observed at a high concentration of 0.09 mg/ml, but bioaccumulation occurred in different fish organs. The liver had

the highest level of Ag NP bioaccumulation, followed by the intestine, gills, and muscles. The results revealed that Ag NP bioaccumulation resulted in histopathological changes, including compromised gill tissue structure and necrosis (Figure 32). Hence direct contact with metal NPs induce toxicity which can be overcome by using green synthesis methodology such as capping to prevent direct contact with the living tissues.

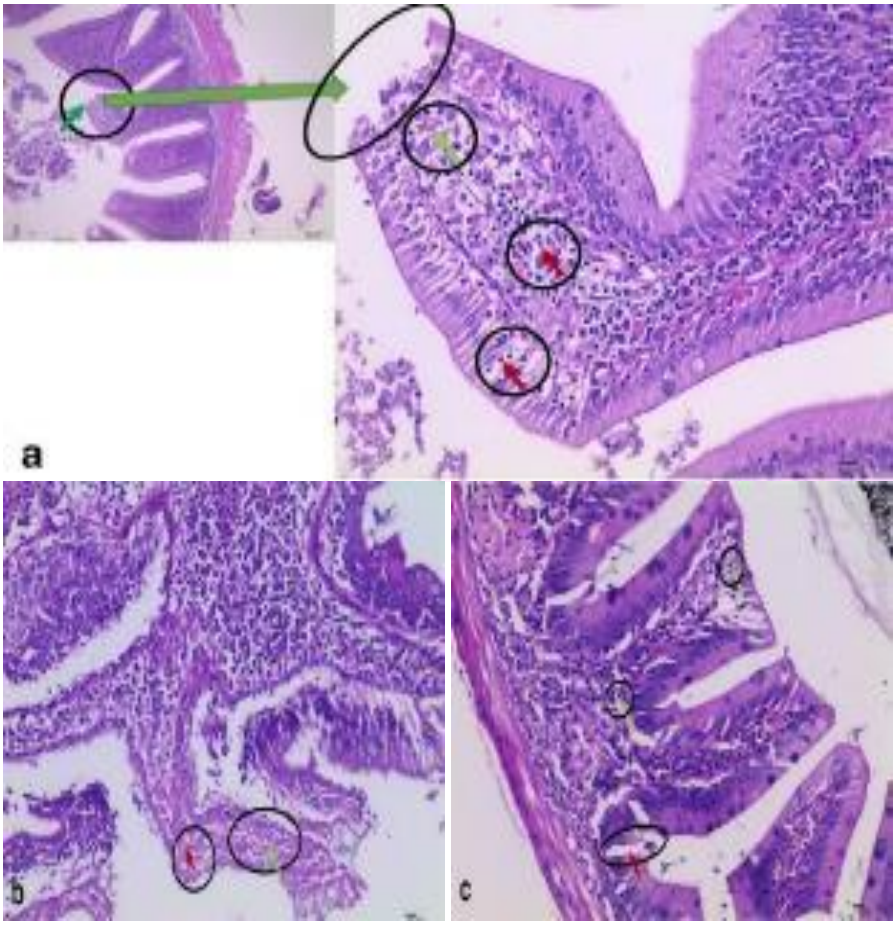

Figure 32 The effect of exposure of AgNPs on the histopathology of the common carp fish intestine at (a) 0.03 mg/ml (Necrosis with increased lymphocytes), (b) 0.06 mg/ml (Necrosis accompanied by the disintegration of lamina propria into the mucosal cells) and (c) 0.09 mg/ml (Prominent necrosis with lysis in the intestinal villi). Reproduced with permission from Ref [196].

Janani *et al.* [197] studied the effect of BSA as a capping agent in bare and capped ZnO NPs. The difference in toxicity of bare ZnO and BSA interaction was studied in different environmental models such as *P. aeruginosa and S. aureus (bacterial systems), C. pyrenoidosa* (algal system), *Daphnia sp.* (crustacean system) and A. cepa root cells (plant model). ZnO NPs therapy, increased cytotoxicity, chromosomal aberrations, and micronuclei (MN) index in *A. cepa* but was decreased in the presence of BSA. The bare NPs showed the following toxicity order *P. aeruginosa* (LC50-0.092 mg/L) > *S. aureus* (LC50-0.33 mg/L) > *Daphnia sp.* (LC50-0.35 mg/L) > *C. pyrenoidosa* (LC50-8.17 mg/L). While in the presence of BSA, LC50 was determined to be 18.45, 26.25, 17.27 and 53.97 mg/L for *P. aeruginosa, S. aureus, Daphnia sp.* and *C. pyrenoidosa* respectively. As a result, the study indicates that BSA-stabilised ZnO NPs are more suitable for environmental remediation.

7.4 Alternative Precursors to Renewable Resources

In the future, alternatives to the use of renewable resources for production may be considered. This is an interesting point because although it goes against green chemistry principle 7, it does obey principle 1 (waste minimization). Two major non-renewable waste streams include petroleum-derived, non-biodegradable plastic waste and electronic or E-waste.

7.4.1 Plastic Waste Mediated Synthesis

The positive effect on the environment has made upcycling plastic waste one of the fascinating topics in science. Chaudhary *et al.* [198] illustrated a safe method for converting plastic waste such as bottles, used cups, and polyethylene bags into fluorescent C-dots (5-30 nm) by simply heating them. For C-dots formed from plastic polybags (P-CDs), cups (C-CDs), and bottles (B-CDs) showed excellent emission properties with peak positions around 422 nm and quantum yield (QY) values of 62, 65, and 64 percent, respectively. The optimized C-dots have also emerged as excellent nanosensors for the fluorescence detection of Cu^{2+} ions, one of the most common heavy metal ion contaminants (Figure 33). The limit of detection for P-CDs, C-CDs, and B-CDs sensors was found to be 0.24 mm, 0.15 mm, and 0.43 mm, respectively.

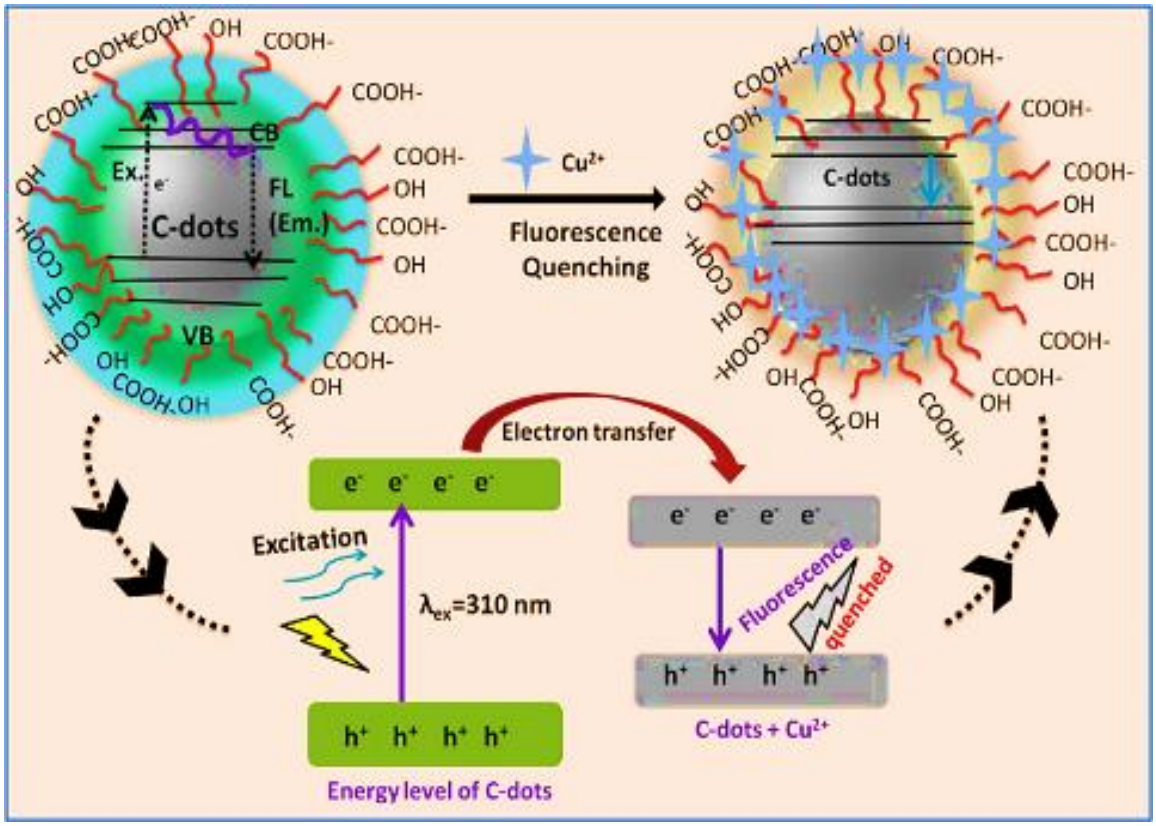

Figure 33 Schematic illustration showing the mechanistic behavior of C-dots towards copper metal ions. Reproduced with permission from Ref [198].

In addition, Roy *et al.* [199] identified a simple and cost-effective method for recycling waste polyethylene terephthalate (PET) scraps, which can help to reduce pollution. Using scrap PET bottles as raw materials, an electrospinning process created a three-dimensional (3D) nanofiber-based

aerogel that is extremely smooth, flexible, fluffy, and structurally robust. Under ideal experimental conditions, it can act as an adsorbent with extremely high capability in removing various heavy metals such as Pb(II), Hg(II), and Zn(II) from polluted water, with an adsorption capacity ranging from 94.5 to 98.3%.

7.4.2 Electronic Waste-Mediated Synthesis

El-Nasr *et al.* [200] published an easy and effective method for producing Cu NPs from the leach solutions of old computer waste printed circuit boards (WPCBs). To avoid the drawbacks of acid leaching, they utilized ammonia/ammonium salt leaching to selectively extract Cu from WPCBs with high extraction yields (>90%). Cu NPs can be extracted from leaching solutions in an eco-friendly way by reducing copper salts with L-ascorbic acid as a reductant and CTAB as a stabilizer. Cu NPs were found to be in a single crystalline phase with a 5 to 32 nm.

The elimination of benzene, toluene, ethylbenzene, and xylene (BTEX) is gaining popularity due to its negative effects on human health such as neurological damage. Mohan *et al.* [201] analyzed the effectiveness of a magnetic zinc–ferrite/V_2O_5 (ZFV) nanocomposite for photocatalytic degradation of BTEX isomers in an aqueous solution. A solvothermal process was used to make the ZFV nanocomposite, which consisted of V_2O_5 (extracted from treated E-waste) and zinc–ferrite (produced via a chemical co-precipitation method). Maximum BTEX degradation of 95% was achieved at acidic pH with high robustness even after the fifth cycle. Due to the prevention of electron–hole recombination, the presence of H_2O_2 increased the degradation efficiency to 98%. In contrast, the hydroxyl scavenging properties of NaCl, Na_2CO_3, $NaNO_3$ and Na_2SO_4 decreased the degradation performance by 60%, 63%, 80% and 72%, respectively.

Every effort has been made to introduce the readers to this field of green nanochemistry. However, this field is ever-expanding and evolving, and it is difficult to incorporate each aspect into a single review. Hopefully, the review will be able to engage the researchers in deciphering the varied aspects of green nanochemistry in water remediation.

8. Conclusions

The quality of drinking water plays a significant impact on human health. Several water-borne infections such as diarrhea, gastrointestinal illness, dysentery and many more are linked to the sub-standard drinking water condition. The negative health of water contamination is linked to increased morbidity and mortality in developing countries. Therefore, green methodologies are advocated in this review to mitigate environmental concerns without compromising the efficiency of the environmental remediation process.

Green nanotechnology research and engineering are progressing toward new awareness dimensions and crossing visionary limits. The future advancement of science and academic rigor lies with nanotechnology or green nanotechnology. This review has shown the importance of the link between green chemistry and the fabrication of NPs for water treatment applications. Unlike previous research reviews which focus on either one or two parameters of water decontamination; this article focuses on the comprehensive analysis of mechanism, use of greener synthetic routes and renewable resources, all encompassed into a single work. Further, a detailed analysis of future outlook and advancement has also been done.

Thus, forthcoming research and development of the prospective synthesis of 'green' materials/NPs should be designed to expand laboratory-based research to an industrial level by considering the challenges above, especially health and environmental implications. With better control over nanomaterial synthesis, chemists can make the world of nanomaterials more exquisite.

Overall, the precise understanding of the greener reaction pathways, their mechanism and the choice of reaction conditions will allow the researchers to modulate the existing routes to optimize fabrication routes. Further will encourage them to utilize green chemistry over conventional methodologies to promote environmental sustainability.

Acknowledgments

SKM and JK are thankful to CSIR for open SRF Fellowship and for CSIR project grant (Ref No. 01(2951)/18/EMR-II). ASM, SKM and JK also wish to acknowledge the Commonwealth Scholarship Commission in the UK for the award of Commonwealth Split-Site Scholarship to JK (Ref No. INCN-2018-75). KK would like to thank the DST for funding and INSPIRE faculty award.

Author Contributions

Jaspreet Kaur did the conceptualization, data analysis, interpretation and drafting. Khushveer Kaur did data collection and interpretation. Khushwinder Kaur did the overall supervision of the layout and drafting. A.S. Matharu did the co-supervision, proof reading and review designing. S.K. Mehta conceptualized the review, supervised and did the proof reading.

Funding

CSIR project grant (Ref No. 01(2951)/18/EMR-II) and Commonwealth Split-Site Scholarship to JK (Ref No. INCN-2018-75).

Competing Interests

The authors have declared that no competing interests exist.

References

1. Hu M, Liu Y, Yao Z, Ma L, Wang X. Catalytic reduction for water treatment. Front Environ Sci Eng. 2018; 12: 3.
2. Lu H, Wang J, Stoller M, Wang T, Bao Y, Hao H. An overview of nanomaterials for water and wastewater treatment. Adv Mater Sci Eng. 2016; 2016: 4964828.
3. WHO. World health day – 7 April [Internet]. 2023. Available from: https://www.who.int/.
4. Lin L, Yang H, Xu X. Effects of water pollution on human health and disease heterogeneity: A review. Front Environ Sci. 2022; 10: 880246.
5. Sharma S, Bhattacharya AJ. Drinking water contamination and treatment techniques. Appl Water Sci. 2017; 7: 1043-1067.
6. Anjum M, Miandad R, Waqas M, Gehany F, Barakat MA. Remediation of wastewater using various nano-materials. Arab J Chem. 2019; 12: 4897-4919.

7. Adeleye AS, Conway JR, Garner K, Huang Y, Su Y, Keller AA. Engineered nanomaterials for water treatment and remediation: Costs, benefits, and applicability. Chem Eng J. 2016; 286: 640-662.
8. Gehrke I, Geiser A, Somborn-Schulz A. Innovations in nanotechnology for water treatment. Nanotechnol Sci Appl. 2015; 8: 1-17.
9. McGuinness NB, Garvey M, Whelan A, John H, Zhao C, Zhang G, et al. Nanotechnology solutions for global water challenges. In: Water challenges and solutions on a global scale. Washington, DC: American chemical society; 2015. pp. 375-411.
10. Glangchai LC, Caldorera-Moore M, Shi L, Roy K. Nanoimprint lithography-based fabrication of shape-specific, enzymatically-triggered smart nanoparticles. J Control Release. 2008; 125: 263-272.
11. De Carvalho JF, De Medeiros SN, Morales MA, Dantas AL, Carriço AS. Synthesis of magnetite nanoparticles by high energy ball milling. Appl Surf Sci. 2013; 275: 84-87.
12. Xiong Y, Chen J, Wiley B, Xia Y, Aloni S, Yin Y. Understanding the role of oxidative etching in the polyol synthesis of Pd nanoparticles with uniform shape and size. J Am Chem Soc. 2005; 127: 7332-7333.
13. Mishra YK, Mohapatra S, Kabiraj D, Mohanta B, Lalla NP, Pivin JC, et al. Synthesis and characterization of Ag nanoparticles in silica matrix by atom beam sputtering. Scr Mater. 2007; 56: 629-632.
14. Shah KA, Tali BA. Synthesis of carbon nanotubes by catalytic chemical vapour deposition: A review on carbon sources, catalysts and substrates. Mater Sci Semicond Process. 2016; 41: 67-82.
15. Xu J, Yang H, Fu W, Du K, Sui Y, Chen J, et al. Preparation and magnetic properties of magnetite nanoparticles by sol–gel method. J Magn Magn Mater. 2007; 309: 307-311.
16. Okuyama K, Wuled Lenggoro I. Preparation of nanoparticles via spray route. Chem Eng Sci. 2003; 58: 537-547.
17. Galvez A, Herlin-Boime N, Reynaud C, Clinard C, Rouzaud JN. Carbon nanoparticles from laser pyrolysis. Carbon. 2002; 40: 2775-2789.
18. Abdel-Shafy HI, Mansour MSM. Green synthesis of metallic nanoparticles from natural resources and food waste and their environmental application. In: Green metal nanoparticles. Hoboken, NJ, USA: John Wiley & Sons, Inc.; 2018. pp. 321-385.
19. Jensen CD, Lewinski NA. Nanoparticle synthesis to green informatics frameworks. Curr Opin Green Sustain. 2018; 12: 117-126.
20. Schneider J, Matsuoka M, Takeuchi M, Zhang J, Horiuchi Y, Anpo M, et al. Nanoparticle based photodynamic therapy. Chem Rev. 2014; 19: 9919-9986.
21. Djurišić AB, Leung YH, Ching Ng AM. Strategies for improving the efficiency of semiconductor metal oxide photocatalysis. Mater Horiz. 2014; 1: 400.
22. Kaur M, Mehta SK, Kansal SK. Visible light driven photocatalytic degradation of ofloxacin and malachite green dye using cadmium sulphide nanoparticles. J Environ Chem Eng. 2018; 6: 3631-3639.
23. Kansal SK, Sood S, Umar A, Mehta SK. Photocatalytic degradation of Eriochrome Black T dye using well-crystalline anatase TiO_2 nanoparticles. J Alloys Compd. 2013; 581: 392-397.
24. Jassal V, Shanker U, Kaith BS. Aegle marmelos mediated green synthesis of different nanostructured metal hexacyanoferrates: Activity against photodegradation of harmful organic dyes. Scientifica. 2016; 2016: 2715026.

25. Borhade A, Tope D, Kushare S. Mercenaria shell powder as a cost-effective and eco-friendly photocatalyst for the degradation of Eriochrome Black T Dye. Iran J Sci Technol Trans A. 2020; 44: 75-83.
26. Shah RK. Facile synthesis of novel NiS-Analcime composite for the efficient photocatalytic degradation of Eriochrome Black T dye. Int J Environ Anal Chem. 2022; 102: 8331-8345.
27. Wadhawan S, Jain A, Nayyar J, Mehta SK. Role of nanomaterials as adsorbents in heavy metal ion removal from waste water: A review. J Water Process Eng. 2020; 33: 101038.
28. Ghasemzadeh G, Momenpour M, Omidi F, Hosseini MR, Ahani M, Barzegari A. Applications of nanomaterials in water treatment and environmental remediation. Front Environ Sci Eng. 2014; 8: 471-482.
29. Wang M, Liu Y, Yang L, Tian K, He L, Zhang Z, et al. Bimetallic metal–organic framework derived FeO/TiO_2 embedded in mesoporous carbon nanocomposite for the sensitive electrochemical detection of 4-nitrophenol. Sens Actuators B. 2019; 281: 1063-1072.
30. Palza H, Nuñez M, Bastías R, Delgado K. In situ antimicrobial behavior of materials with copper-based additives in a hospital environment. Int J Antimicrob Agents. 2018; 51: 912-917.
31. Osonga FJ, Yazgan I, Kariuki V, Luther D, Jimenez A, Le P, et al. Greener synthesis and characterization, antimicrobial and cytotoxicity studies of gold nanoparticles of novel shapes and sizes. RSC Adv. 2016; 6: 2302-2313.
32. Rameshkumar A, Ananth DA, Periyasamy S, Garlapati D, Sivasudha T. Role of bioconjugated quantum dots in detection and reduction of pathogenic microbes. In: Green metal nanoparticles. Hoboken, NJ, USA: John Wiley & Sons, Inc.; 2018. pp. 667-688.
33. Ahmaruzzaman M, Mohanta D, Nath A. Environmentally benign fabrication of SnO_2-CNT nanohybrids and their multifunctional efficiency as an adsorbent, catalyst and antimicrobial agent for water decontamination. Sci Rep. 2019; 9: 12935.
34. Anastas P, Warner JC. Green chemistry: Theory and practice. New York: Oxford University Press; 1998.
35. Anastas P, Eghbali N. Green chemistry: Principles and practice. Chem Soc Rev. 2010; 39: 301-312.
36. Albrecht MA, Evans CW, Raston CL. Green chemistry and the health implications of nanoparticles. Green Chem. 2006; 8: 417.
37. Dahl JA, Maddux BLS, Hutchison JE. Toward greener nanosynthesis. Chem Rev. 2007; 107: 2228-2269.
38. Devatha CP, Thalla AK. Green synthesis of nanomaterials, in synthesis of inorganic nanomaterials. In: Synthesis of Inorganic Nanomaterials. Amsterdam, The Netherlands: Elsevier; 2018. pp. 169-184.
39. Mariotti N, Bonomo M, Fagiolari L, Barbero N, Gerbaldi C, Bella F, et al. Recent advances in eco-friendly and cost-effective materials towards sustainable dye-sensitized solar cells. Green Chem. 2020; 22: 7168-7218.
40. Shameli K, Ahmad MB, Yunus WM, Rustaiyan A, Ibrahim NA, Zargar M, et al. Green synthesis of silver/montmorillonite/chitosan bionanocomposites using the UV irradiation method and evaluation of antibacterial activity. Int J Nanomedicine. 2010; 5: 875-887.
41. Bilecka I, Niederberger M. Microwave chemistry for inorganic materials synthesis. Nanoscale. 2010; 2: 1358-1374.

42. Kumar A, Kuang Y, Liang Z, Sun X. Microwave chemistry, recent advancements, and eco-friendly microwave-assisted synthesis of nanoarchitectures and their applications: A review. Mater Today Nano. 2020; 11: 100076.
43. Li J, Huang J, Wu J, Cao L, Li Q, Yanagisawa K. Microwave-assisted growth of $WO_3 \cdot 0.33H_2O$ micro/nanostructures with enhanced visible light photocatalytic properties. CrystEngComm. 2013; 15: 7904-7913.
44. Sun X, He J, Meng Y, Zhang L, Zhang S, Ma X, et al. Microwave-assisted ultrafast and facile synthesis of fluorescent carbon nanoparticles from a single precursor: Preparation, characterization and their application for the highly selective detection of explosive picric acid. J Mater Chem A. 2016; 4: 4161-4171.
45. Manteghain M, Tari F, Bozorgi B. Microwave-assisted synthesis of molybdenum oxide nanoparticles. J Part Sci Technol. 2015; 1: 121-127.
46. Kaur J, Kaur K, Pervaiz N, Mehta SK. Spherical MoO_3 nanoparticles for photocatalytic removal of Eriochrome Black T. ACS Appl Nano Mater. 2021; 4: 12766-12778.
47. Fuentes-García JA, Santoyo-Salzar J, Rangel-Cortes E, Goya GF, Cardozo-Mata V, Pescador-Rojas JA. Effect of ultrasonic irradiation power on sonochemical synthesis of gold nanoparticles. Ultrason Sonochem. 2021; 70: 105274.
48. Xu H, Zeiger BW, Suslick KS. Sonochemical synthesis of nanomaterials. Chem Soc Rev. 2013; 42: 2555-2567.
49. Kamali M, Davarazar M, Aminabhavi TM. Single precursor sonochemical synthesis of mesoporous hexagonal-shape zero-valent copper for effective nitrate reduction. Chem Eng J. 2020; 384: 123359.
50. Yasuda K, Sato T, Asakura Y. Size-controlled synthesis of gold nanoparticles by ultrafine bubbles and pulsed ultrasound. Chem Eng Sci. 2020; 217: 115527.
51. Sharififard H, Rezvanpanah E, Rad SH. A novel natural chitosan/activated carbon/iron bio-nanocomposite: Sonochemical synthesis, characterization, and application for cadmium removal in batch and continuous adsorption process. Bioresour Technol. 2018; 270: 562-569.
52. Altuwirqi RM, Albakri AS, Al-Jawhari H, Ganash EA. Green synthesis of copper oxide nanoparticles by pulsed laser ablation in spinach leaves extract. Optik. 2020; 219: 165280.
53. Rashid RB, Hussain DH, Mahmood RS. Water treatment ability of CuO-ZnO nanocomposites synthesized by laser ablation and anodization techniques. J Southwest Jiaotong Univ. 2020; 55: 53.
54. Al-Antaki AH, Luo X, Duan X, Lamb RN, Hutchison WD, Lawrance W, et al. Continuous flow copper laser ablation synthesis of copper (I and II) oxide nanoparticles in water. ACS Omega. 2019; 4:13577-13584.
55. Luo X, Al-Antaki AH, Alharbi TM, Hutchison WD, Zou YC, Zou J, et al. Laser-ablated vortex fluidic-mediated synthesis of superparamagnetic magnetite nanoparticles in water under flow. ACS Omega. 2018; 3: 11172-11178.
56. Jaleh B. Laser-assisted preparation of Pd nanoparticles on carbon cloth for the degradation of environmental pollutants in aqueous medium. Chemosphere. 2020; 246: 125755.
57. Philippot G, Elissalde C, Maglione M, Aymonier C. Supercritical fluid technology: A reliable process for high quality BaTiO3 based nanomaterials. Adv Powder Technol. 2014; 25: 1415-1429.

58. Liu J, Anand M, Roberts CB. Synthesis and extraction of β-D-Glucose-Stabilized Au nanoparticles processed into low-defect, wide-area thin films and ordered arrays using CO_2-expanded liquids. Langmuir. 2006; 22: 3964-3971.
59. Wang X, Xu X, Zhu A, Li Z, Liu Z. Preparation of nanoparticles in supercritical water: Experiments and molecular dynamics simulations. Mater Today Proc. 2016; 3: 652-656.
60. Corrêa CM, Bizeto MA, Camilo FF. Direct synthesis of silver nanoparticles in ionic liquid. J Nanopart Res. 2016; 18: 132.
61. Meroufel B, Benali O, Benyahia M, Benmoussa Y, Zenasni MA. Adsorptive removal of anionic dye from aqueous solutions by Algerian kaolin: Characteristics, isotherm, kinetic and thermodynamic studies. J Mater Environ Sci. 2013; 4: 482-491.
62. Ahmed F, Arshi N, Anwar MS, Danish R, Koo BH. Quantum-confinement induced enhancement in photocatalytic properties of iron oxide nanoparticles prepared by Ionic liquid. Ceram Int. 2014; 40: 15743-15751.
63. Rizk HE, El-Hefny NE. Synthesis and characterization of magnetite nanoparticles from polyol medium for sorption and selective separation of Pd(II) from aqueous solution. J Alloys Compd. 2020; 812: 152041.
64. Camp JE. Bio-available solvent Cyrene: Synthesis, derivatization, and applications. ChemSusChem. 2018; 11: 3048-3055.
65. Poon R, Zhitomirsky I. Application of Cyrene as a solvent and dispersing agent for fabrication of Mn_3O_4-carbon nanotube supercapacitor electrodes. Colloid Interface Sci Commun. 2020; 34: 100226.
66. Iravani S. Green synthesis of metal nanoparticles using plants. Green Chem. 2011; 13: 2638.
67. Sharma D, Kanchi S, Bisetty K. Biogenic synthesis of nanoparticles: A review. Arab J Chem. 2019; 12: 3576-3600.
68. Gardea-Torresdey JL, Gomez E, Peralta-Videa JR, Parsons JG, Troiani H, Jose-Yacaman M. Alfalfa sprouts: A natural source for the synthesis of silver nanoparticles. Langmuir. 2003; 19: 1357-1361.
69. Nadagouda MN, Varma RS. Green synthesis of silver and palladium nanoparticles at room temperature using coffee and tea extract. Green Chem. 2008; 10: 859.
70. Hatamifard A, Nasrollahzadeh M, Sajadi SM. Biosynthesis, characterization and catalytic activity of an Ag/zeolite nanocomposite for base- and ligand-free oxidative hydroxylation of phenylboronic acid and reduction of a variety of dyes at room temperature. New J Chem. 2016; 40: 2501-2513.
71. Bordbar M. Biosynthesis of Ag/almond shell nanocomposite as a cost-effective and efficient catalyst for degradation of 4-nitrophenol and organic dyes. RSC Adv. 2017; 7: 180-189.
72. Doan VD, Thieu AT, Nguyen TD, Nguyen VC, Cao XT, Nguyen TL, et al. Biosynthesis of gold nanoparticles using litsea cubeba fruit extract for catalytic reduction of 4-nitrophenol. J Nanomater. 2020; 2020: 1-10.
73. Nasrollahzadeh M, Sajadi SM, Maham M, Kohsari I. Biosynthesis, characterization and catalytic activity of the Pd/bentonite nanocomposite for base- and ligand-free oxidative hydroxylation of phenylboronic acid and reduction of chromium (VI) and nitro compounds. Microporous Mesoporous Mater. 2018; 271: 128-137.

74. Ghosh MK, Sahu S, Gupta I, Ghorai TK. Green synthesis of copper nanoparticles from an extract of Jatropha curcas leaves: Characterization, optical properties, CT-DNA binding and photocatalytic activity. RSC Adv. 2020; 10: 22027-22035.
75. Song T, Yang Y. Metal nanoparticles supported on biomass-derived hierarchical porous heteroatom-doped carbon from bamboo shoots: Design, synthesis and applications. Chem Rec. 2019; 19: 1283-1301.
76. Sharma RK, Yadav S, Gupta R, Arora G. Synthesis of magnetic nanoparticles using potato extract for dye degradation: A green chemistry experiment. J Chem Educ. 2019; 96: 3038-3044.
77. Devi TB, Ahmaruzzaman M. Bio-inspired facile and green fabrication of Au@Ag@AgCl core–double shells nanoparticles and their potential applications for elimination of toxic emerging pollutants: A green and efficient approach for wastewater treatment. Chem Eng J. 2017; 317: 726-741.
78. Thi TU, Nguyen TT, Thi YD, Thi KH, Phan BT, Pham KN. Green synthesis of ZnO nanoparticles using orange fruit peel extract for antibacterial activities. RSC Adv. 2020; 10: 23899-23907.
79. Kaur J, Kaur K, Mehta SK, Matharu AS. A novel molybdenum oxide-Starbon catalyst for wastewater remediation. J Mater Chem A. 2020; 8: 14519-14527.
80. Li J, Ma Q, Shao H, Zhou X, Xia H, Xie J. Biosynthesis, characterization, and antibacterial activity of silver nanoparticles produced from rice straw biomass. BioResources. 2017; 12: 4897-4911.
81. Han Z, Dong L, Zhang J, Cui T, Chen S, Ma G, et al. Green synthesis of palladium nanoparticles using lentinan for catalytic activity and biological applications. RSC Adv. 2019; 9: 38265-38270.
82. Zhang Y, Li S, Wang X, Zhang L, Cheung PC. Advances in lentinan: Isolation, structure, chain conformation and bioactivities. Food Hydrocoll. 2011; 25: 196-206.
83. Ren G, Xu L, Lu T, Yin J. Structural characterization and antiviral activity of lentinan from lentinus edodes mycelia against infectious hematopoietic necrosis virus. Int J Biol Macromol. 2018; 115: 1202-1210.
84. Kahrilas GA, Haggren W, Read RL, Wally LM, Fredrick SJ, Hiskey M, et al. Investigation of antibacterial activity by silver nanoparticles prepared by microwave-assisted green syntheses with soluble starch, dextrose, and arabinose. ACS Sustain Chem Eng. 2014; 2: 590-598.
85. Sundar S, Piraman S. Greener saponin induced morphologically controlled various polymorphs of nanostructured iron oxide materials for biosensor applications. RSC Adv. 2015; 5: 74408-74415.
86. Mahal A, Khullar P, Kumar H, Kaur G, Singh N, Jelokhani-Niaraki M, et al. Green chemistry of zein protein toward the synthesis of bioconjugated nanoparticles: Understanding unfolding, fusogenic behavior, and hemolysis. ACS Sustain Chem Eng. 2013; 1: 627-639.
87. Rovani S, Santos JJ, Corio P, Fungaro DA. Highly pure silica nanoparticles with high adsorption capacity obtained from sugarcane waste ash. ACS Omega. 2018; 3: 2618-2627.
88. Peres EC, Slaviero JC, Cunha AM, Hosseini–Bandegharaei A, Dotto GL. Microwave synthesis of silica nanoparticles and its application for methylene blue adsorption. J Environ Chem Eng. 2018; 6: 649-659.
89. Shad S, Belinga-Desaunay-Nault MF, Bashir N, Lynch I. Removal of contaminants from canal water using microwave synthesized zero valent iron nanoparticles. Environ Sci Water Res Technol. 2020; 6: 3057-3065.
90. Deokar GK, Ingale AG. Green synthesis of gold nanoparticles (Elixir of Life) from banana fruit waste extract – an efficient multifunctional agent. RSC Adv. 2016; 6: 74620-74629.

91. García-Gurrola A, Rincón S, Escobar-Puentes AA, Zepeda A, Pérez-Robles JF, Martínez-Bustos F. Synthesis and succinylation of starch nanoparticles by means of a single step using sonochemical energy. Ultrason Sonochem. 2019; 56: 458-465.
92. Maham M, Nasrollahzadeh M, Sajadi SM. Facile synthesis of Ag/ZrO_2 nanocomposite as a recyclable catalyst for the treatment of environmental pollutants. Compos B Eng. 2020; 185: 107783.
93. Demirezen DA, Yıldız YŞ, Yılmaz DD. Amoxicillin degradation using green synthesized iron oxide nanoparticles: Kinetics and mechanism analysis. Environ Nanotechnol Monit Manag. 2019; 11: 100219.
94. Mavaei M, Chahardoli A, Shokoohinia Y, Khoshroo A, Fattahi A. One-step synthesized silver nanoparticles using isoimperatorin: Evaluation of photocatalytic, and electrochemical activities. Sci Rep. 2020; 10: 1762.
95. Karfa P, Madhuri R. Green tiny magnets: An economic and eco-friendly remedy for environmental damage. In: Green metal nanoparticles. Hoboken, NJ, USA: John Wiley & Sons, Inc.; 2018. pp. 245-292.
96. Akpomie KG, Conradie J. Biogenic and chemically synthesized Solanum tuberosum peel–silver nanoparticle hybrid for the ultrasonic aided adsorption of bromophenol blue dye. Sci Rep. 2020; 10: 17094.
97. Jain A, Wadhawan S, Mehta SK. Biogenic synthesis of non-toxic iron oxide NPs via Syzygium aromaticum for the removal of methylene blue. Environ Nanotechnol Monit Manag. 2021; 16: 100464.
98. Jain A, Sharma A, Kapur A, Wadhawan S, Garg M, Pandey SK, et al. Hematite dysprosium oxide nanocoposites biosynthesized via greener route for ciprofloxacin removal and antimicrobial activity. J Nanostructure Chem. 2021; 11: 437.
99. Jain A, Sharma A, Gupta P, Wadhawan S, Mehta SK. Biosynthesis driven dysprosium oxide nanoparticles as a sensor for picric acid. Curr Res Green Sustain Chem. 2021; 4: 100080.
100. Ravi SS, Christena LR, SaiSubramanian N, Anthony SP. Green synthesized silver nanoparticles for selective colorimetric sensing of Hg^{2+} in aqueous solution at wide pH range. Analyst. 2013; 138: 4370-4377.
101. Wicaksono WP, Kadja GT, Amalia D, Uyun L, Rini WP, Hidayat A, et al. A green synthesis of gold–palladium core–shell nanoparticles using orange peel extract through two-step reduction method and its formaldehyde colorimetric sensing performance. Nano-Struct. Nano-Objects. 2020; 24: 100535.
102. Ali K, Ahmed B, Ansari SM, Saquib Q, Al-Khedhairy AA, Dwivedi S, et al. Comparative in situ ROS mediated killing of bacteria with bulk analogue, Eucalyptus leaf extract (ELE)-capped and bare surface copper oxide nanoparticles. Mater Sci Eng C. 2019; 100: 747-758.
103. Haroon M, Zaidi A, Ahmed B, Rizvi A, Khan MS, Musarrat J. Effective inhibition of phytopathogenic microbes by eco-friendly leaf extract mediated silver nanoparticles (AgNPs). Indian J Microbiol. 2019; 59: 273-287.
104. Cherian T, Ali K, Fatima S, Saquib Q, Ansari SM, Alwathnani HA, et al. Myristica fragrans bio-active ester functionalized ZnO nanoparticles exhibit antibacterial and antibiofilm activities in clinical isolates. J Microbiol Methods. 2019; 166: 105716.

105. Virkutyte J, Varma RS. Green synthesis of nanomaterials: Environmental aspects. In: Sustainable nanotechnology and the environment: Advances and achievements. Washington, DC: American chemical society; 2013; pp. 11-39.
106. Gahlawat G, Choudhury AR. A review on the biosynthesis of metal and metal salt nanoparticles by microbes. RSC Adv. 2019; 9: 12944-12967.
107. Faramarzi MA, Sadighi A. Insights into biogenic and chemical production of inorganic nanomaterials and nanostructures. Adv Colloid Interface Sci. 2013; 20.
108. Iravani S. Bacteria in nanoparticle synthesis: Current status and future prospects. Int Sch Res Not. 2014; 2014: 1-18.
109. Beveridge TJ, Murray RG. Sites of metal deposition in the cell wall of Bacillus subtilis. J Bacteriol. 1980; 141: 876-887.
110. Singh Y, Kaushal S, Sodhi RS. Biogenic synthesis of silver nanoparticles using cyanobacterium Leptolyngbya sp. WUC 59 cell-free extract and their effects on bacterial growth and seed germination. Nanoscale Adv. 2020; 2: 3972-3982.
111. Ebadi M, Zolfaghari MR, Aghaei SS, Zargar M, Shafiei M, Zahiri HS, et al. A bio-inspired strategy for the synthesis of zinc oxide nanoparticles (ZnO NPs) using the cell extract of cyanobacterium Nostoc sp. EA03: From biological function to toxicity evaluation. RSC Adv. 2019; 9: 23508-23525.
112. Raj R, Dalei K, Chakraborty J, Das S. Extracellular polymeric substances of a marine bacterium mediated synthesis of CdS nanoparticles for removal of cadmium from aqueous solution. J Colloid Interface Sci. 2016; 462: 166-175.
113. Zonaro E, Piacenza E, Presentato A, Monti F, Dell'Anna R, Lampis S, et al. Ochrobactrum sp. MPV1 from a dump of roasted pyrites can be exploited as bacterial catalyst for the biogenesis of selenium and tellurium nanoparticles. Microb Cell Factories. 2017; 16: 215.
114. Ahmed E, Kalathil S, Shi L, Alharbi O, Wang P. Synthesis of ultra-small platinum, palladium and gold nanoparticles by Shewanella loihica PV-4 electrochemically active biofilms and their enhanced catalytic activities. J Saudi Chem Soc. 2018; 22: 919-929.
115. Buszewski B, Railean-Plugaru V, Pomastowski P, Rafińska K, Szultka-Mlynska M, Golinska P, et al. Antimicrobial activity of biosilver nanoparticles produced by a novel Streptacidiphilus durhamensis strain. J Microbiol Immunol. 2018; 51: 45-54.
116. Hamed AA, Kabary H, Khedr M, Emam AN. Antibiofilm, antimicrobial and cytotoxic activity of extracellular green-synthesized silver nanoparticles by two marine-derived actinomycete. RSC Adv. 2020; 10: 10361-10367.
117. Saad EL, Salem SS, Fouda A, Awad MA, El-Gamal MS, Abdo AM. New approach for antimicrobial activity and bio-control of various pathogens by biosynthesized copper nanoparticles using endophytic actinomycetes. J Radiat. 2018; 11: 262-270.
118. Salem SS, Fouda A. Green synthesis of metallic nanoparticles and their prospective biotechnological applications: An overview. Biol Trace Elem Res. 2021; 199: 344-370.
119. Singh P, Kim YJ, Zhang D, Yang DC. Biological synthesis of nanoparticles from plants and microorganisms. Trends Biotechnol. 2016; 34: 588-599.
120. Venkatesh KS, Gopinath K, Palani NS, Arumugam A, Jose SP, Bahadur SA, et al. Plant pathogenic fungus F. solani mediated biosynthesis of nanoceria: Antibacterial and antibiofilm activity. RSC Adv. 2016; 6: 42720-42729.

121. Bhargava A, Jain N, Khan MA, Pareek V, Dilip RV, Panwar J. Utilizing metal tolerance potential of soil fungus for efficient synthesis of gold nanoparticles with superior catalytic activity for degradation of rhodamine B. J Environ Manage. 2016; 183: 22-32.
122. Mishra A, Kumari M, Pandey S, Chaudhry V, Gupta KC, Nautiyal CS. Biocatalytic and antimicrobial activities of gold nanoparticles synthesized by Trichoderma sp. Bioresour Technol. 2014; 166: 235-242.
123. Gudikandula K, Vadapally P, Singara Charya MA. Biogenic synthesis of silver nanoparticles from white rot fungi: Their characterization and antibacterial studies. OpenNano. 2017; 2: 64-78.
124. Tyagi S, Tyagi PK, Gola D, Chauhan N, Bharti RK. Extracellular synthesis of silver nanoparticles using entomopathogenic fungus: Characterization and antibacterial potential. SN Appl Sci. 2019; 1: 1545.
125. Kanaujiya D, Kumar V, Dwivedi SK, Prasad G. Photobiosynthesis of silver nanoparticle using extract of aspergillus flavus CR500: Its characterization, antifungal activity and mechanism against sclerotium rolfsii and rhizoctonia solani. J Clust Sci. 2020; 31: 1041-1050.
126. Bhadwal AS, Tripathi RM, Gupta RK, Kumar N, Singh RP, Shrivastav A. Biogenic synthesis and photocatalytic activity of CdS nanoparticles. RSC Adv. 2014; 4: 9484.
127. Baskar G, Chandhuru J, Sheraz Fahad K, Praveen AS, Chamundeeswari M, Muthukumar T. Anticancer activity of fungal l-asparaginase conjugated with zinc oxide nanoparticles. J Mater Sci Mater Med. 2015; 26: 43.
128. Shah M, Fawcett D, Sharma S, Tripathy SK, Poinern GE. Green synthesis of metallic nanoparticles via biological entities. Materials. 2015; 8: 7278-7308.
129. Seshadri S, Saranya K, Kowshik M. Green synthesis of lead sulfide nanoparticles by the lead resistant marine yeast, Rhodosporidium diobovatum. Biotechnol Prog. 2011; 27: 1464-1469.
130. Elahian F, Reiisi S, Shahidi A, Mirzaei SA. High-throughput bioaccumulation, biotransformation, and production of silver and selenium nanoparticles using genetically engineered Pichia pastoris. Nanomedicine. 2017; 13: 853-861.
131. Dahoumane SA, Mechouet M, Wijesekera K, Filipe CD, Sicard C, Bazylinski DA, et al. Algae-mediated biosynthesis of inorganic nanomaterials as a promising route in nanobiotechnology – a review. Green Chem. 2017; 19: 552-587.
132. Momeni S, Nabipour I. A simple green synthesis of palladium nanoparticles with Sargassum alga and their electrocatalytic activities towards hydrogen peroxide. Appl Biochem Biotechnol. 2015; 176: 1937-1949.
133. Ramakrishna M, Rajesh Babu D, Gengan RM, Chandra S, Nageswara Rao G. Green synthesis of gold nanoparticles using marine algae and evaluation of their catalytic activity. J Nanostruct Chem. 2016; 6: 1-13.
134. Pugazhendhi A, Prabakar D, Jacob JM, Karuppusamy I, Saratale RG. Synthesis and characterization of silver nanoparticles using Gelidium amansii and its antimicrobial property against various pathogenic bacteria. Microb Pathog. 2018; 114: 41-45.
135. Narayana A, Bhat SA, Fathima A, Lokesh SV, Surya SG, Yelamaggad CV. Green and low-cost synthesis of zinc oxide nanoparticles and their application in transistor-based carbon monoxide sensing. RSC Adv. 2020; 10: 13532-13542.
136. Shenton W, Douglas T, Young M, Stubbs G, Mann S. Inorganic–organic nanotube composites from template mineralization of tobacco mosaic virus. Adv Mater. 1999; 11: 253-256.

137. Lee SW, Mao C, Flynn CE, Belcher AM. Ordering of quantum dots using genetically engineered viruses. Science. 2002; 296: 892-895.
138. Mao C, Flynn CE, Hayhurst A, Sweeney R, Qi J, Georgiou G, et al. Viral assembly of oriented quantum dot nanowires. Proc Natl Acad Sci. 2003; 100: 6946-6951.
139. Losada-García N, Rodríguez-Otero A, Palomo JM. Tailorable synthesis of heterogeneous enzyme–copper nanobiohybrids and their application in the selective oxidation of benzene to phenol. Catal Sci Technol. 2020; 10: 196-206.
140. Shi H, Tan L, Du Q, Chen X, Li L, Liu T, et al. Green synthesis of Fe_3O_4 nanoparticles with controlled morphologies using urease and their application in dye adsorption. Dalton Trans. 2014; 43: 12474-12479.
141. Khan SA, Ahmad A. Enzyme mediated synthesis of water-dispersible, naturally protein capped, monodispersed gold nanoparticles; their characterization and mechanistic aspects. RSC Adv. 2014; 4: 7729-7734.
142. Jayaseelan C, Ramkumar R, Rahuman AA, Perumal P. Green synthesis of gold nanoparticles using seed aqueous extract of Abelmoschus esculentus and its antifungal activity. Ind Crops Prod. 2013; 45: 423-429.
143. Vo TT, Nguyen TT, Huynh TT, Vo TT, Nguyen TT, Nguyen DT, et al. Biosynthesis of silver and gold nanoparticles using aqueous extract from Crinum latifolium leaf and their applications forward antibacterial effect and wastewater treatment. J Nanomater. 2019; 2019: 1-14.
144. Boomi P, Poorani GP, Selvam S, Palanisamy S, Jegatheeswaran S, Anand K, et al. Green biosynthesis of gold nanoparticles using Croton sparsiflorus leaves extract and evaluation of UV protection, antibacterial and anticancer applications. Appl Organomet Chem. 2020; 34: e5574.
145. Yu J, Xu D, Guan HN, Wang C, Huang LK. Facile one-step green synthesis of gold nanoparticles using Citrus maxima aqueous extracts and its catalytic activity. Mater Lett. 2016; 166: 110-112.
146. Bennur T, Khan Z, Kshirsagar R, Javdekar V, Zinjarde S. Biogenic gold nanoparticles from the Actinomycete Gordonia amarae: Application in rapid sensing of copper ions. Sens Actuators B. 2016; 233: 684-690.
147. Meysam SN, Hosein SBG, Naimeh K. Biosynthesis of gold nanoparticles using Streptomyces fulvissimus isolate. Nanomed J. 2015; 4: 153-159.
148. Srinath BS, Rai VR. Rapid biosynthesis of gold nanoparticles by Staphylococcus epidermidis: Its characterisation and catalytic activity. Mater Lett. 2015; 146: 23-25.
149. Manivasagan P, Alam MS, Kang KH, Kwak M, Kim SK. Extracellular synthesis of gold bionanoparticles by Nocardiopsis sp. and evaluation of its antimicrobial, antioxidant and cytotoxic activities. Bioprocess Biosyst Eng. 2015; 38: 1167-1177.
150. Ranjitha VR, Rai VR. Actinomycetes mediated synthesis of gold nanoparticles from the culture supernatant of Streptomyces griseoruber with special reference to catalytic activity. 3 Biotech. 2017; 7: 299.
151. Krishnan S, Patel PN, Balasubramanian KK, Chadha A. Yeast supported gold nanoparticles: An efficient catalyst for the synthesis of commercially important aryl amines. New J Chem. 2021; 45: 1915-1923.
152. Qu Y, You S, Zhang X, Pei X, Shen W, Li Z, et al. Biosynthesis of gold nanoparticles using cell-free extracts of Magnusiomyces ingens LH-F1 for nitrophenols reduction. Bioprocess Biosyst Eng. 2018; 41: 359-367.

153. Abdel-Raouf N, Al-Enazi NM, Ibraheem IB. Green biosynthesis of gold nanoparticles using Galaxaura elongata and characterization of their antibacterial activity. Arab J Chem. 2017; 10: S3029-S3039.
154. Suganya KU, Govindaraju K, Kumar VG, Dhas TS, Karthick V, Singaravelu G, et al. Blue green alga mediated synthesis of gold nanoparticles and its antibacterial efficacy against Gram positive organisms. Mater Sci Eng C. 2015; 47: 351-356.
155. Ahiwale SS, Bankar AV, Tagunde S, Kapadnis BP. A bacteriophage mediated gold nanoparticles synthesis and their anti-biofilm activity. Indian J Microbiol. 2017; 57: 188-194.
156. Joshi CG, Danagoudar A, Poyya J, Kudva AK, Dhananjaya BL. Biogenic synthesis of gold nanoparticles by marine endophytic fungus-Cladosporium cladosporioides isolated from seaweed and evaluation of their antioxidant and antimicrobial properties. Process Biochem. 2017; 63: 137-144.
157. Priyadarshini E, Pradhan N, Sukla LB, Panda PK. Controlled synthesis of gold nanoparticles using Aspergillus terreus IF0 and its antibacterial potential against gram negative pathogenic bacteria. J Nanotechnol. 2014; 2014: 653198.
158. Nabikhan A, Kandasamy K, Raj A, Alikunhi NM. Synthesis of antimicrobial silver nanoparticles by callus and leaf extracts from saltmarsh plant, Sesuvium portulacastrum L. Colloids Surf B. 2010; 79: 488-493.
159. Vanaja M, Paulkumar K, Baburaja M, Rajeshkumar S, Gnanajobitha G, Malarkodi C, et al. Degradation of methylene blue using biologically synthesized silver nanoparticles. Bioinorg Chem Appl. 2014; 2014: 1-8.
160. Jyoti K, Singh A. Green synthesis of nanostructured silver particles and their catalytic application in dye degradation. J Genet Eng Biotechnol. 2016; 14: 311-317.
161. Kaviya S, Santhanalakshmi J, Viswanathan B, Muthumary J, Srinivasan K. Biosynthesis of silver nanoparticles using citrus sinensis peel extract and its antibacterial activity. Spectrochim Acta A. 2011; 79: 594-598.
162. Satapathy MK, Banerjee P, Das P. Plant-mediated synthesis of silver-nanocomposite as novel effective azo dye adsorbent. Appl Nanosci. 2015; 5: 1-9.
163. San Keskin NO, Kılıç NK, Dönmez G, Tekinay T. Green synthesis of silver nanoparticles using cyanobacteria and evaluation of their photocatalytic and antimicrobial activity. J Nano Res. 2016; 40: 120-127.
164. Saravanan C, Rajesh R, Kaviarasan T, Muthukumar K, Kavitake D, Shetty PH. Synthesis of silver nanoparticles using bacterial exopolysaccharide and its application for degradation of azo-dyes. Biotechnol Rep. 2017; 15: 33-40.
165. Shanthi S, Jayaseelan BD, Velusamy P, Vijayakumar S, Chih CT, Vaseeharan B. Biosynthesis of silver nanoparticles using a probiotic Bacillus licheniformis Dahb1 and their antibiofilm activity and toxicity effects in Ceriodaphnia cornuta. Microb Pathog. 2016; 93: 70-77.
166. Shu M, He F, Li Z, Zhu X, Ma Y, Zhou Z, et al. Biosynthesis and antibacterial activity of silver nanoparticles using yeast extract as reducing and capping agents. Nanoscale Res Lett. 2020; 15: 14.
167. Roy K, Sarkar CK, Ghosh CK. Photocatalytic activity of biogenic silver nanoparticles synthesized using yeast (Saccharomyces cerevisiae) extract. Appl Nanosci. 2015; 5: 953-959.

168. Salari Z, Danafar F, Dabaghi S, Ataei SA. Sustainable synthesis of silver nanoparticles using macroalgae Spirogyra varians and analysis of their antibacterial activity. J Saudi Chem Soc. 2016; 20: 459-464.
169. Poornima S, Valivittan K. Degradation of malachite green (dye) by using photo-catalytic biogenic silver nanoparticles synthesized using red algae (Gracilaria corticata) aqueous extract. Int J Curr Microbiol App Sci. 2017; 6: 62-70.
170. Sinha SN, Paul D, Halder N, Sengupta D, Patra SK. Green synthesis of silver nanoparticles using fresh water green alga Pithophora oedogonia (Mont.) Wittrock and evaluation of their antibacterial activity. Appl Nanosci. 2015; 5: 703-709.
171. Ganapathy Selvam G, Sivakumar K. Phycosynthesis of silver nanoparticles and photocatalytic degradation of methyl orange dye using silver (Ag) nanoparticles synthesized from Hypnea musciformis (Wulfen) J.V. Lamouroux. Appl Nanosci. 2015; 5: 617-622.
172. Xue B, He D, Gao S, Wang D, Yokoyama K, Wang L. Biosynthesis of silver nanoparticles by the fungus Arthroderma fulvum and its antifungal activity against genera of Candida, Aspergillus and Fusarium. Int J Nanomedicine. 2016; 11: 1899.
173. Kavish R, Shruti A, Jyoti S, Agrawal PK. Mycosynthesis of silver nanoparticles using endophytic fungus and investigation of its antibacterial and azo dye degradation efficacy. Kavaka. 2018; 49: 65-71.
174. Hamedi S, Ghaseminezhad M, Shokrollahzadeh S, Shojaosadati SA. Controlled biosynthesis of silver nanoparticles using nitrate reductase enzyme induction of filamentous fungus and their antibacterial evaluation. Artif Cell Nanomed Biotechnol. 2017; 45: 1588-1596.
175. Cunha FA, Cunha MD, da Frota SM, Mallmann EJ, Freire TM, Costa LS, et al. Biogenic synthesis of multifunctional silver nanoparticles from Rhodotorula glutinis and Rhodotorula mucilaginosa: Antifungal, catalytic and cytotoxicity activities. World J Microbiol Biotechnol. 2018; 34: 127.
176. Ramos MM, dos S. Morais E, da S. Sena I, Lima AL, de Oliveira FR, de Freitas CM, et al. Silver nanoparticle from whole cells of the fungi Trichoderma spp. isolated from Brazilian Amazon. Biotechnol Lett. 2020; 42: 833-843.
177. Karthik R. Green synthesis of platinum nanoparticles using quercus glauca extract and its electrochemical oxidation of hydrazine in water samples. Int J Electrochem Sci. 2016; 11: 8245-8255.
178. Coccia F, Tonucci L, Bosco D, Bressan M, d'Alessandro N. One-pot synthesis of lignin-stabilised platinum and palladium nanoparticles and their catalytic behaviour in oxidation and reduction reactions. Green Chem. 2012; 14: 1073.
179. Bogireddy NK, Pal U, Kumar MK, Domínguez JM, Gomez LM, Agarwal V. Green fabrication of 2D platinum superstructures and their high catalytic activity for mitigation of organic pollutants. Catal Today. 2021; 360: 185-193.
180. Tahir K, Nazir S, Ahmad A, Li B, Khan AU, Khan ZU, et al. Facile and green synthesis of phytochemicals capped platinum nanoparticles and in vitro their superior antibacterial activity. J Photochem Photobiol B. 2017; 166: 246-251.
181. Kora AJ, Rastogi L. Peroxidase activity of biogenic platinum nanoparticles: A colorimetric probe towards selective detection of mercuric ions in water samples. Sens Actuators B. 2018; 254: 690-700.

182. Martins M, Mourato C, Sanches S, Noronha JP, Crespo MB, Pereira IA. Biogenic platinum and palladium nanoparticles as new catalysts for the removal of pharmaceutical compounds. Water Res. 2017; 108: 160-168.
183. Gupta K, Chundawat TS. Bio-inspired synthesis of platinum nanoparticles from fungus Fusarium oxysporum: Its characteristics, potential antimicrobial, antioxidant and photocatalytic activities. Mater Res Express. 2019; 6: 1050d6.
184. Du L, Xu Q, Huang M, Xian L, Feng JX. Synthesis of small silver nanoparticles under light radiation by fungus Penicillium oxalicum and its application for the catalytic reduction of methylene blue. Mater Chem Phys. 2015; 160: 40-47.
185. Tahir K, Nazir S, Li B, Ahmad A, Nasir T, Khan AU, et al. Sapium sebiferum leaf extract mediated synthesis of palladium nanoparticles and in vitro investigation of their bacterial and photocatalytic activities. J Photochem Photobiol B. 2016; 164: 164-173.
186. Narasaiah BP, Mandal BK. Remediation of azo-dyes based toxicity by agro-waste cotton boll peels mediated palladium nanoparticles. J Saudi Chem Soc. 2020; 24: 267-281.
187. Narasaiah P, Mandal BK, Sarada NC. Green synthesis of Pd NPs from Pimpinella tirupatiensis plant extract and their application in photocatalytic activity dye degradation. IOP Conf Ser Mater Sci Eng. 2017; 263: 022013.
188. Velmurugan P, Shim J, Kim K, Oh BT. Prunus × yedoensis tree gum mediated synthesis of platinum nanoparticles with antifungal activity against phytopathogens. Mater Lett. 2016; 174: 61-65.
189. Wang W, Zhang B, He Z. Bioelectrochemical deposition of palladium nanoparticles as catalysts by Shewanella oneidensis MR-1 towards enhanced hydrogen production in microbial electrolysis cells. Electrochim Acta. 2019; 318: 794-800.
190. Sriramulu M, Sumathi S. Biosynthesis of palladium nanoparticles using Saccharomyces cerevisiae extract and its photocatalytic degradation behaviour. Adv Nat Sci. 2018; 9: 025018.
191. Anju AR, Gupta K, Chundawat TS. In Vitro antimicrobial and antioxidant activity of biogenically synthesized palladium and platinum nanoparticles using Botryococcus braunii. Turkish J Pharm Sci. 2020; 17: 299-306.
192. Sikiru S, Ayodele OA, Sanusi YK, Adebukola SY, Soleimani H, Yekeen N, et al. A comprehensive review on nanotechnology application in wastewater treatment a case study of metal-based using green synthesis. J Environ Chem Eng. 2022; 10: 108065.
193. Sikiru S, Rostami A, Soleimani H, Yahya N, Afeez Y, Aliu O, et al. Graphene: Outlook in the enhance oil recovery (EOR). J Mol Liq. 2021; 321: 114519.
194. Deepika S, Kumar RH, Selvaraj CI, Roopan SM. Toxicity of metal/metal oxide nanoparticles and their future prospects. In: Green metal nanoparticles. Hoboken, NJ, USA: John Wiley & Sons, Inc.; 2018. pp. 141-164.
195. Chaudhary S, Sharma P, Kumar S, Alex SA, Kumar R, Mehta SK, et al. A comparative multi-assay approach to study the toxicity behaviour of Eu_2O_3 nanoparticles. J Mol Liq. 2018; 269: 783-795.
196. Kakakhel MA, Wu F, Sajjad W, Zhang Q, Khan I, Ullah K, et al. Long-term exposure to high-concentration silver nanoparticles induced toxicity, fatality, bioaccumulation, and histological alteration in fish (Cyprinus carpio). Environ Sci Eur. 2021; 33: 14.
197. Janani B, Raju LL, Thomas AM, Alyemeni MN, Dudin GA, Wijaya L, et al. Impact of bovine serum albumin – A protein corona on toxicity of ZnO NPs in environmental model systems of plant, bacteria, algae and crustaceans. Chemosphere. 2021; 270: 128629.

198. Chaudhary S, Kumari M, Chauhan P, Chaudhary GR. Upcycling of plastic waste into fluorescent carbon dots: An environmentally viable transformation to biocompatible C-dots with potential prospective in analytical applications. Waste Manage. 2021; 120: 675-686.
199. Roy S, Maji PK, Goh KL. Sustainable design of flexible 3D aerogel from waste PET bottle for wastewater treatment to energy harvesting device. Chem Eng J. 2021; 413: 127409.
200. El-Nasr RS, Abdelbasir SM, Kamel AH, Hassan SS. Environmentally friendly synthesis of copper nanoparticles from waste printed circuit boards. Sep Purif Technol. 2020; 230: 115860.
201. Mohan H, Lim JM, Lee SW, Jang JS, Park YJ, Seralathan KK, et al. Enhanced visible light photocatalysis with E-waste-based V_2O_5/zinc-ferrite: BTEX degradation and mechanism. J Chem Technol Biotechnol. 2020; 95: 2842-2852.